

Chapter 3

Finite Difference Methods

“Those who know others are clever; those who know themselves have discernment; those who overcome others have force; those who overcome themselves are strong; those who know contentment are rich; those who persevere are people of purpose.”

Paraphrase of Lao Tzu

3.1 Introduction

It is rare for real-life EM problems to fall neatly into a class that can be solved by the analytical methods presented in the preceding chapter. Classical approaches may fail if [1]:

- the PDE is not linear and cannot be linearized without seriously affecting the result
- the solution region is complex
- the boundary conditions are of mixed types
- the boundary conditions are time-dependent
- the medium is inhomogeneous or anisotropic

Whenever a problem with such complexity arises, numerical solutions must be employed. Of the numerical methods available for solving PDEs, those employing finite differences are more easily understood, more frequently used, and more universally applicable than any other.

The finite difference method (FDM) was first developed by A. Thom [2] in the 1920s under the title “the method of squares” to solve nonlinear hydrodynamic equations. Since then, the method has found applications in solving different field problems. The finite difference techniques are based upon approximations which permit replacing differential equations by finite difference equations. These finite difference approximations are algebraic in form; they relate the value of the dependent variable at a

point in the solution region to the values at some neighboring points. Thus a finite difference solution basically involves three steps:

- (1) dividing the solution region into a grid of nodes
- (2) approximating the given differential equation by finite difference equivalent that relates the dependent variable at a point in the solution region to its values at the neighboring points
- (3) solving the difference equations subject to the prescribed boundary conditions and/or initial conditions

The course of action taken in three steps is dictated by the nature of the problem being solved, the solution region, and the boundary conditions. The most commonly used grid patterns for two-dimensional problems are shown in Fig. 3.1. A three-dimensional grid pattern will be considered later in the chapter.

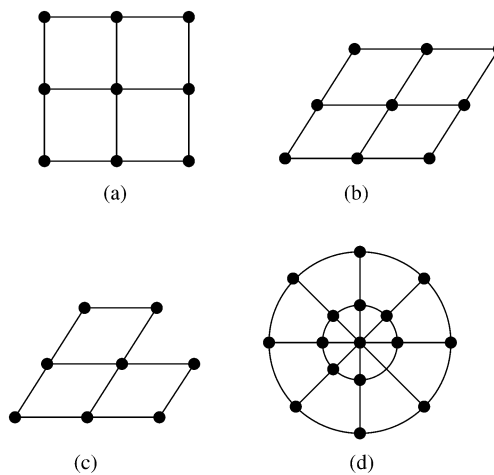


Figure 3.1
Common grid patterns: (a) rectangular grid, (b) skew grid, (c) triangular grid, (d) circular grid.

3.2 Finite Difference Schemes

Before finding the finite difference solutions to specific PDEs, we will look at how one constructs finite difference approximations from a given differential equation. This essentially involves estimating derivatives numerically.

Given a function $f(x)$ shown in Fig. 3.2, we can approximate its derivative, slope or the tangent at P by the slope of the arc PB, giving the *forward-difference* formula,

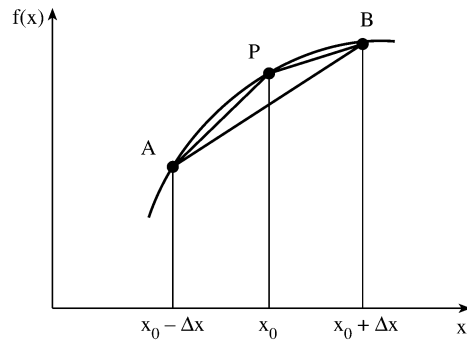


Figure 3.2
Estimates for the derivative of $f(x)$ at P using forward, backward, and central differences.

$$f'(x_0) \simeq \frac{f(x_0 + \Delta x) - f(x_0)}{\Delta x} \quad (3.1)$$

or the slope of the arc AP, yielding the *backward-difference* formula,

$$f'(x_0) \simeq \frac{f(x_0) - f(x_0 - \Delta x)}{\Delta x} \quad (3.2)$$

or the slope of the arc AB, resulting in the *central-difference* formula,

$$f'(x_0) \simeq \frac{f(x_0 + \Delta x) - f(x_0 - \Delta x)}{2\Delta x} \quad (3.3)$$

We can also estimate the second derivative of $f(x)$ at P as

$$\begin{aligned} f''(x_0) &\simeq \frac{f'(x_0 + \Delta x/2) - f'(x_0 - \Delta x/2)}{\Delta x} \\ &= \frac{1}{\Delta x} \left[\frac{f(x_0 + \Delta x) - f(x_0)}{\Delta x} - \frac{f(x_0) - f(x_0 - \Delta x)}{\Delta x} \right] \end{aligned}$$

or

$$f''(x_0) \simeq \frac{f(x_0 + \Delta x) - 2f(x_0) + f(x_0 - \Delta x)}{(\Delta x)^2} \quad (3.4)$$

Any approximation of a derivative in terms of values at a discrete set of points is called *finite difference* approximation.

The approach used above in obtaining finite difference approximations is rather intuitive. A more general approach is using Taylor's series. According to the well-known expansion,

$$f(x_o + \Delta x) = f(x_o) + \Delta x f'(x_o) + \frac{1}{2!}(\Delta x)^2 f''(x_o) + \frac{1}{3!}(\Delta x)^3 f'''(x_o) + \dots \quad (3.5)$$

and

$$f(x_o - \Delta x) = f(x_o) - \Delta x f'(x_o) + \frac{1}{2!}(\Delta x)^2 f''(x_o) - \frac{1}{3!}(\Delta x)^3 f'''(x_o) + \dots \quad (3.6)$$

Upon adding these expansions,

$$f(x_o + \Delta x) + f(x_o - \Delta x) = 2f(x_o) + (\Delta x)^2 f''(x_o) + O(\Delta x)^4 \quad (3.7)$$

where $O(\Delta x)^4$ is the error introduced by truncating the series. We say that this error is of the order $(\Delta x)^4$ or simply $O(\Delta x)^4$. Therefore, $O(\Delta x)^4$ represents terms that are not greater than $(\Delta x)^4$. Assuming that these terms are negligible,

$$f''(x_o) \simeq \frac{f(x_o + \Delta x) - 2f(x_o) + f(x_o - \Delta x)}{(\Delta x)^2}$$

which is Eq. (3.4). Subtracting Eq. (3.6) from Eq. (3.5) and neglecting terms of the order $(\Delta x)^3$ yields

$$f'(x_o) \simeq \frac{f(x_o + \Delta x) - f(x_o - \Delta x)}{2\Delta x}$$

which is Eq. (3.3). This shows that the leading errors in Eqs. (3.3) and (3.4) are of the order $(\Delta x)^2$. Similarly, the difference formula in Eqs. (3.1) and (3.2) have truncation errors of $O(\Delta x)$. Higher order finite difference approximations can be obtained by taking more terms in Taylor series expansion. If the infinite Taylor series were retained, an exact solution would be realized for the problem. However, for practical reasons, the infinite series is usually truncated after the second-order term. This imposes an error which exists in all finite difference solutions.

To apply the difference method to find the solution of a function $\Phi(x, t)$, we divide the solution region in the $x - t$ plane into equal rectangles or meshes of sides Δx and Δt as in Fig. 3.3. We let the coordinates (x, t) of a typical grid point or node be

$$\begin{aligned} x &= i\Delta x, & i &= 0, 1, 2, \dots \\ t &= j\Delta t, & j &= 0, 1, 2, \dots \end{aligned} \quad (3.8a)$$

and the value of Φ at P be

$$\Phi_P = \Phi(i\Delta x, j\Delta t) = \Phi(i, j) \quad (3.8b)$$

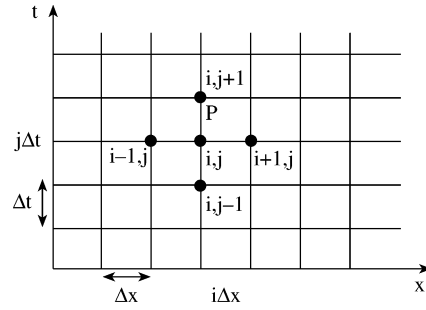


Figure 3.3
Finite difference mesh for two independent variables x and t .

With this notation, the central difference approximations of the derivatives of Φ at the (i, j) th node are

$\Phi_x _{i,j} \simeq \frac{\Phi(i+1, j) - \Phi(i-1, j)}{2\Delta x},$	(3.9a)
$\Phi_t _{i,j} \simeq \frac{\Phi(i, j+1) - \Phi(i, j-1)}{2\Delta t},$	(3.9b)
$\Phi_{xx} _{i,j} \simeq \frac{\Phi(i+1, j) - 2\Phi(i, j) + \Phi(i-1, j)}{(\Delta x)^2},$	(3.9c)
$\Phi_{tt} _{i,j} \simeq \frac{\Phi(i, j+1) - 2\Phi(i, j) + \Phi(i, j-1)}{(\Delta t)^2}$	(3.9d)

Table 3.1 gives some useful finite difference approximations for Φ_x and Φ_{xx} .

3.3 Finite Differencing of Parabolic PDEs

Consider a simple example of a parabolic (or diffusion) partial differential equation with one spatial independent variable

$$k \frac{\partial \Phi}{\partial t} = \frac{\partial^2 \Phi}{\partial x^2} \quad (3.10)$$

where k is a constant. The equivalent finite difference approximation is

$$k \frac{\Phi(i, j+1) - \Phi(i, j)}{\Delta t} = \frac{\Phi(i+1, j) - 2\Phi(i, j) + \Phi(i-1, j)}{(\Delta x)^2} \quad (3.11)$$

where $x = i\Delta x$, $i = 0, 1, 2, \dots, n$, $t = j\Delta t$, $j = 0, 1, 2, \dots$. In Eq. (3.11), we have used the forward difference formula for the derivative with respect to t and

Table 3.1 Finite Difference Approximations for Φ_x and Φ_{xx}

Derivative	Finite Difference Approximation	Type	Error
Φ_x	$\frac{\Phi_{i+1}-\Phi_i}{\Delta x}$	FD	$O(\Delta x)$
	$\frac{\Phi_i-\Phi_{i-1}}{\Delta x}$	BD	$O(\Delta x)$
	$\frac{\Phi_{i+1}-\Phi_{i-1}}{\Delta x}$	CD	$O(\Delta x)^2$
	$\frac{-\Phi_{i+2}+4\Phi_{i+1}-3\Phi_i}{2\Delta x}$	FD	$O(\Delta x)^2$
	$\frac{3\Phi_i-4\Phi_{i-1}+\Phi_{i-2}}{2\Delta x}$	BD	$O(\Delta x)^2$
	$\frac{-\Phi_{i+2}+8\Phi_{i+1}-8\Phi_i+\Phi_{i-2}}{12\Delta x}$	CD	$O(\Delta x)^4$
Φ_{xx}	$\frac{\Phi_{i+2}-2\Phi_{i+1}+\Phi_i}{(\Delta x)^2}$	FD	$O(\Delta x)^2$
	$\frac{\Phi_i-2\Phi_{i-1}+\Phi_{i-2}}{(\Delta x)^2}$	BD	$O(\Delta x)^2$
	$\frac{\Phi_{i+1}-2\Phi_i+\Phi_{i-1}}{(\Delta x)^2}$	CD	$O(\Delta x)^2$
	$\frac{-\Phi_{i+2}+16\Phi_{i+1}-30\Phi_i+16\Phi_{i-1}-\Phi_{i-2}}{(\Delta x)^2}$	CD	$O(\Delta x)^4$

where FD = Forward Difference, BD = Backward Difference, and CD = Central Difference.

central difference formula for that with respect to x . If we let

$$r = \frac{\Delta t}{k(\Delta x)^2}, \quad (3.12)$$

Eq. (3.11) can be written as

$$\Phi(i, j+1) = r\Phi(i+1, j) + (1-2r)\Phi(i, j) + r\Phi(i-1, j) \quad (3.13)$$

This *explicit formula* can be used to compute $\Phi(x, t + \Delta t)$ explicitly in terms of $\Phi(x, t)$. Thus the values of Φ along the first time row (see Fig. 3.3), $t = \Delta t$, can be calculated in terms of the boundary and initial conditions, then the values of Φ along the second time row, $t = 2\Delta t$, are calculated in terms of the first time row, and so on.

A graphic way of describing the difference formula of Eq. (3.13) is through the *computational molecule* of Fig. 3.4(a), where the square is used to represent the grid point where Φ is presumed known and a circle where Φ is unknown.

In order to ensure a stable solution or reduce errors, care must be exercised in selecting the value of r in Eqs. (3.12) and (3.13). It will be shown in Section 3.6 that Eq. (3.13) is valid only if the coefficient $(1-2r)$ in Eq. (3.13) is nonnegative or $0 < r \leq 1/2$. If we choose $r = 1/2$, Eq. (3.13) becomes

$$\Phi(i, j+1) = \frac{1}{2}[\Phi(i+1, j) + \Phi(i-1, j)] \quad (3.14)$$

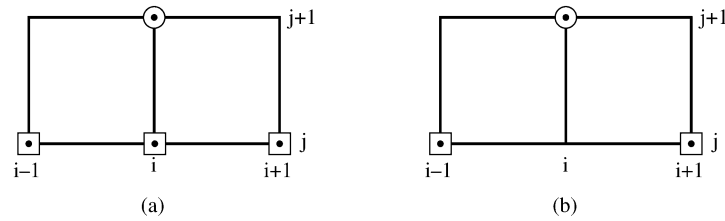


Figure 3.4
Computational molecule for parabolic PDE: (a) for $0 < r \leq 1/2$, (b) for $r = 1/2$.

so that the computational molecule becomes that shown in Fig. 3.4(b).

The fact that obtaining stable solutions depends on r or the size of the time step Δt renders the explicit formula of Eq. (3.13) inefficient. Although the formula is simple to implement, its computation is slow. An *implicit formula*, proposed by Crank and Nicholson in 1974, is valid for all finite values of r . We replace $\partial^2 \Phi / \partial x^2$ in Eq. (3.10) by the average of the central difference formulas on the j th and $(j + 1)$ th time rows so that

$$k \frac{\Phi(i, j + 1) - \Phi(i, j)}{\Delta t} = \frac{1}{2} \left[\frac{\Phi(i + 1, j) - 2\Phi(i, j) + \Phi(i - 1, j)}{(\Delta x)^2} + \frac{\Phi(i + 1, j + 1) - 2\Phi(i, j + 1) + \Phi(i - 1, j + 1)}{(\Delta x)^2} \right]$$

This can be rewritten as

$$\begin{aligned} -r\Phi(i - 1, j + 1) + 2(1 + r)\Phi(i, j + 1) - r\Phi(i + 1, j + 1) \\ = r\Phi(i - 1, j) + 2(1 - r)\Phi(i, j) + r\Phi(i + 1, j) \end{aligned} \quad (3.15)$$

where r is given by Eq. (3.12). The right side of Eq. (3.15) consists of three known values, while the left side has the three unknown values of Φ . This is illustrated in the computational molecule of Fig. 3.5(a). Thus if there are n free nodes along each time row, then for $j = 0$, applying Eq. (3.15) to nodes $i = 1, 2, \dots, n$ results in n

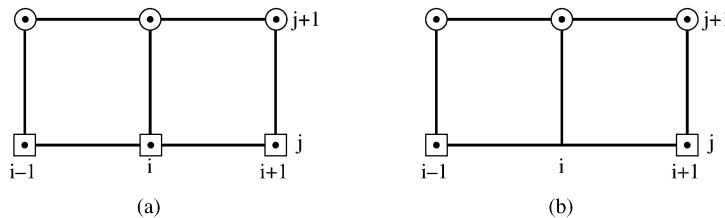


Figure 3.5
Computational molecule for Crank-Nicholson method: (a) for finite values of r , (b) for $r = 1$.

simultaneous equations with n unknown values of Φ and known initial and boundary values of Φ . Similarly, for $j = 1$, we obtain n simultaneous equations for n unknown values of Φ in terms of the known values $j = 0$, and so on. The combination of accuracy and unconditional stability allows the use of a much larger time step with Crank-Nicholson method than is possible with the explicit formula. Although the method is valid for all finite values of r , a convenient choice of $r = 1$ reduces Eq. (3.15) to

$$-\Phi(i-1, j+1) + 4\Phi(i, j+1) - \Phi(i+1, j+1) = \Phi(i-1, j) + \Phi(i+1, j) \quad (3.16)$$

with the computational molecule of Fig. 3.5(b).

More complex finite difference schemes can be developed by applying the same principles discussed above. Two of such schemes are the Leapfrog method and the Dufort-Frankel method [3, 4]. These and those discussed earlier are summarized in Table 3.2. Notice that the last two methods are two-step finite difference schemes in that finding Φ at time $j + 1$ requires knowing Φ at two previous time steps j and $j - 1$, whereas the first two methods are one-step schemes. For further treatment on the finite difference solution of parabolic PDEs, see Smith [5] and Ferziger [6].

Example 3.1

Solve the diffusion equation

$$\frac{\partial^2 \Phi}{\partial x^2} = \frac{\partial \Phi}{\partial t}, \quad 0 \leq x \leq 1 \quad (3.17)$$

subject to the boundary conditions

$$\Phi(0, t) = 0 = \Phi(1, t) = 0, \quad t > 0 \quad (3.18a)$$

and initial condition

$$\Phi(x, 0) = 100 \quad (3.18b)$$

Solution

This problem may be regarded as a mathematical model of the temperature distribution in a rod of length $L = 1$ m with its end in contacts with ice blocks (or held at 0°C) and the rod initially at 100°C . With that physical interpretation, our problem is finding the internal temperature Φ as a function of position and time. We will solve this problem using both explicit and implicit methods.

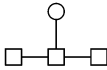
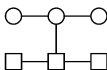
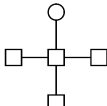
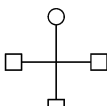
(a) Explicit Method

For easy hand calculations, let us choose $\Delta x = 0.1$, $r = 1/2$ so that

$$\Delta t = \frac{r(\Delta x)^2}{k} = 0.05$$

Table 3.2 Finite Difference Approximation to the Parabolic Equation:

$$\frac{\partial \Phi}{\partial t} = \frac{1}{k} \frac{\partial^2 \Phi}{\partial x^2}, \quad k > 0$$

Method	Algorithm	Molecule
1. First order (Euler)	$\frac{\Phi_i^{j+1} - \Phi_i^j}{\Delta t} = \frac{\Phi_{i+1}^j - 2\Phi_i^j + \Phi_{i-1}^j}{k(\Delta x)^2}$ <p>explicit, stable for $r = \Delta t / k(\Delta x)^2 \leq 0.5$</p>	
2. Crank-Nicholson	$\frac{\Phi_i^{j+1} - \Phi_i^j}{\Delta t} = \frac{\Phi_{i+1}^{j+1} - 2\Phi_i^{j+1} + \Phi_{i-1}^{j+1}}{2k(\Delta x)^2} + \frac{\Phi_{i+1}^j - 2\Phi_i^j + \Phi_{i-1}^j}{2k(\Delta x)^2}$ <p>implicit, always stable</p>	
3. Leapfrog	$\frac{\Phi_i^{j+1} - \Phi_i^{j-1}}{2\Delta t} = \frac{\Phi_{i+1}^j - 2\Phi_i^j + \Phi_{i-1}^j}{k(\Delta x)^2}$ <p>explicit, always unstable</p>	
4. Dufort-Frankel	$\frac{\Phi_i^{j+1} - \Phi_i^{j-1}}{2\Delta t} = \frac{\Phi_{i+1}^j - \Phi_{i-1}^j}{k(\Delta x)^2}$ <p>explicit, unconditionally stable</p>	

since $k = 1$. We need the solution for only $0 \leq x \leq 0.5$ due to the fact that the problem is symmetric with respect to $x = 0.5$. First we calculate the initial and boundary values using Eq. (3.18). These values of Φ at the fixed nodes are shown in Table 3.3 for $x = 0, x = 1$, and $t = 0$. Notice that the values of $\Phi(0, 0)$ and $\Phi(1, 0)$ are taken as the average of 0 and 100. We now calculate Φ at the free nodes using Eq. (3.14) or the molecule of Fig. 3.4(b). The result is shown in Table 3.3. The analytic solution to Eq. (3.17) subject to Eq. (3.18) is

$$\Phi(x, t) = \frac{400}{\pi} \sum_{k=0}^{\infty} \frac{1}{n} \sin n\pi x \exp(-n^2 \pi^2 t), \quad n = 2k + 1$$

Comparison of the explicit finite difference solution with the analytic solution at $x = 0.4$ is shown in Table 3.4. The table shows that the finite difference solution is

reasonably accurate. Greater accuracy can be achieved by choosing smaller values of Δx and Δt .

Table 3.3 Result for Example 3.1

x	0	0.1	0.2	0.3	0.4	0.5	0.6	...	1.0
t									
0	50	100	100	100	100	100	100		50
0.005	0	75.0	100	100	100	100	100		0
0.01	0	50	87.5	100	100	100	100		0
0.015	0	43.75	75	93.75	100	100	100		0
0.02	0	37.5	68.75	87.5	96.87	100	96.87		0
0.025	0	34.37	62.5	82.81	93.75	96.87	93.75		0
0.03	0	31.25	58.59	78.21	89.84	93.75	89.84		0
⋮									
0.1	0	14.66	27.92	38.39	45.18	47.44	45.18		0

Table 3.4 Comparison of Explicit Finite Difference Solution with Analytic Solution; for Example 3.1

t	Finite difference solution at $x = 0.4$	Analytic solution at $x = 0.4$	Percentage error
0.005	100	99.99	0.01
0.01	100	99.53	0.47
0.015	100	97.85	2.2
0.02	96.87	95.18	1.8
0.025	93.75	91.91	2.0
0.03	89.84	88.32	1.7
0.035	85.94	84.61	1.6
0.04	82.03	80.88	1.4
⋮			
0.10	45.18	45.13	0.11

(b) Implicit Method

Let us choose $\Delta x = 0.2$, $r = 1$ so that $\Delta t = 0.04$. The values of Φ at the fixed nodes are calculated as in part (a) (see Table 3.3). For the free nodes, we apply Eq. (3.16) or the molecule of Fig. 3.5(b). If we denote $\Phi(i, j + 1)$ by Φ_i ($i = 1, 2, 3, 4$), the values of Φ for the first time step (Fig. 3.6) can be obtained by solving the following simultaneous equations

$$\begin{aligned}
 -0 + 4\Phi_1 - \Phi_2 &= 50 + 100 \\
 -\Phi_1 + 4\Phi_2 + \Phi_3 &= 100 + 100 \\
 -\Phi_2 + 4\Phi_3 - \Phi_4 &= 100 + 100 \\
 -\Phi_3 + 4\Phi_4 - 0 &= 100 + 50
 \end{aligned}$$

We obtain

$$\Phi_1 = 58.13, \quad \Phi_2 = 82.54, \quad \Phi_3 = 72, \quad \Phi_4 = 55.5$$

at $t = 0.04$. Using these values of Φ , we apply Eq. (3.16) to obtain another set of simultaneous equations for $t = 0.08$ as

$$\begin{aligned} -0 + 4\Phi_1 - \Phi_2 &= 0 + 82.54 \\ -\Phi_1 + 4\Phi_2 - \Phi_3 &= 58.13 + 72 \\ -\Phi_2 + 4\Phi_3 - \Phi_4 &= 82.54 + 55.5 \\ -\Phi_3 + 4\Phi_4 - 0 &= 72 + 0 \end{aligned}$$

which results in

$$\Phi_1 = 34.44, \quad \Phi_2 = 55.23, \quad \Phi_3 = 56.33, \quad \Phi_4 = 32.08$$

This procedure can be programmed and accuracy can be increased by choosing more points for each time step. ■

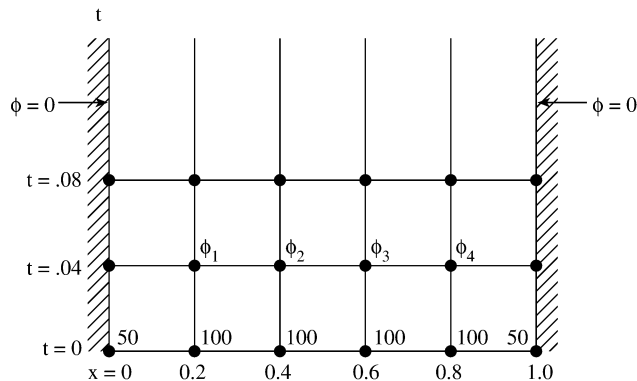


Figure 3.6
For Example 3.1, part (b).

3.4 Finite Differencing of Hyperbolic PDEs

The simplest hyperbolic partial differential equation is the wave equation of the form

$$u^2 \frac{\partial^2 \Phi}{\partial x^2} = \frac{\partial^2 \Phi}{\partial t^2} \quad (3.19)$$

where u is the speed of the wave. An equivalent finite difference formula is

$$u^2 \frac{\Phi(i+1, j) - 2\Phi(i, j) + \Phi(i-1, j))}{(\Delta x)^2} = \frac{\Phi(i, j+1) - 2\Phi(i, j) + \Phi(i, j-1)}{(\Delta t)^2}$$

where $x = i\Delta x, t = j\Delta t, i, j = 0, 1, 2, \dots$. This equation can be written as

$$\boxed{\Phi(i, j+1) = 2(1-r)\Phi(i, j) + r[\Phi(i+1, j) + \Phi(i-1, j)] - \Phi(i, j-1)}$$
(3.20)

where $\Phi(i, j)$ is an approximation to $\Phi(x, t)$ and r is the “aspect ratio” given by

$$r = \left(\frac{u\Delta t}{\Delta x}\right)^2$$
(3.21)

Equation (3.20) is an explicit formula for the wave equation. The corresponding computational molecule is shown in Fig. 3.7(a). For the solution algorithm in Eq. (3.20)

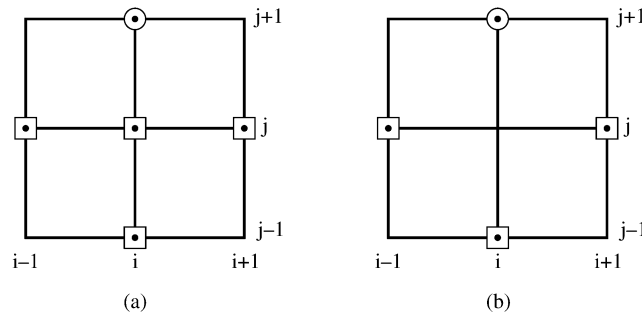


Figure 3.7

Computational molecule for wave equation: (a) for arbitrary $r \leq 1$, (b) for $r = 1$.

to be stable, the aspect ratio $r \leq 1$, as will be shown in Example 3.5. If we choose $r = 1$, Eq. (3.20) becomes

$$\Phi(i, j+1) = \Phi(i+1, j) + \Phi(i-1, j) - \Phi(i, j-1)$$
(3.22)

with the computational molecule in Fig. 3.7(b). Unlike the single-step schemes of Eqs. (3.13) and (3.15), the two-step schemes of Eqs. (3.20) and (3.22) require that the values of Φ at times j and $j-1$ be known to get Φ at time $j+1$. Thus, we must derive a separate algorithm to “start” the solution of Eq. (3.20) or (3.22); that is, we must compute $\Phi(i, 1)$ and $\Phi(i, 2)$. To do this, we utilize the prescribed initial condition. For example, suppose the initial condition on the PDE in Eq. (3.19) is

$$\left. \frac{\partial \Phi}{\partial t} \right|_{t=0} = 0$$

We use the backward-difference formula

$$\frac{\partial \Phi(x, 0)}{\partial t} \simeq \frac{\Phi(i, 1) - \Phi(i, -1)}{2\Delta t} = 0$$

or

$$\Phi(i, 1) = \Phi(i, -1) \quad (3.23)$$

Substituting Eq. (3.23) into Eq. (3.20) and taking $j = 0$ (i.e., at $t = 0$), we get

$$\Phi(i, 1) = 2(1 - r)\Phi(i, 0) + r[\Phi(i - 1, 0) + \Phi(i + 1, 0)] - \Phi(i, 1)$$

or

$$\Phi(i, 1) = (1 - r)\Phi(i, 0) + \frac{r}{2}[\Phi(i - 1, 0) + \Phi(i + 1, 0)] \quad (3.24)$$

Using the starting formula in Eq. (3.24) together with the prescribed boundary and initial conditions, the value of Φ at any grid point (i, j) can be obtained directly from Eq. (3.20).

There are implicit methods for solving hyperbolic PDEs just as we have implicit methods for parabolic PDEs. However, for hyperbolic PDEs, implicit methods result in an infinite number of simultaneous equations to be solved and therefore cannot be used without making some simplifying assumptions. Interested readers are referred to Smith [5] or Ferziger [6].

Example 3.2

Solve the wave equation

$$\Phi_{tt} = \Phi_{xx}, \quad 0 < x < 1, \quad t \geq 0$$

subject to the boundary conditions

$$\Phi(0, t) = 0 = \Phi(1, t), \quad t \geq 0$$

and the initial conditions

$$\begin{aligned} \Phi(x, 0) &= \sin \pi x, & 0 < x < 1, \\ \Phi_t(x, 0) &= 0, & 0 < x < 1 \quad \square \end{aligned}$$

Solution

The analytical solution is easily obtained as

$$\Phi(x, t) = \sin \pi x \cos \pi t \quad (3.25)$$

Using the explicit finite difference scheme of Eq. (3.20) with $r = 1$, we obtain

$$\Phi(i, j + 1) = \Phi(i - 1, j) + \Phi(i + 1, j) - \Phi(i, j - 1), \quad j \geq 1 \quad (3.26)$$

For $j = 0$, substituting

$$\Phi_t = \frac{\Phi(i, 1) - \Phi(i, -1)}{2\Delta t} = 0$$

or

$$\Phi(i, 1) = \Phi(i, -1)$$

into Eq. (3.26) gives the starting formula

$$\Phi(i, 1) = \frac{1}{2}[\Phi(i - 1, 0) + \Phi(i + 1, 0)] \quad (3.27)$$

Since $u = 1$, and $r = 1$, $\Delta t = \Delta x$. Also, since the problem is symmetric with respect to $x = 0.5$, we solve for Φ using Eqs. (3.26) and (3.27) within $0 < x < 0.5$, $t \geq 0$. We can either calculate the values by hand or write a simple computer program. With the FORTRAN code in Fig. 3.8, the result shown in Table 3.5 is obtained for $\Delta t = \Delta x = 0.1$. The finite difference solution agrees with the exact solution in Eq. (3.25) to six decimal places. The accuracy of the FD solution can be increased by choosing a smaller spatial increment Δx and a smaller time increment Δt . ■

Table 3.5 Solution of the Wave Equation in Example 3.2

x	0	0.1	0.2	0.3	0.4	0.5	0.6	...
t								
0.0	0	0.3090	0.5879	0.8990	0.9511	1.0	0.9511	
0.1	0	0.2939	0.5590	0.7694	0.9045	0.9511	0.9045	
0.2	0	0.2500	0.4755	0.6545	0.7694	0.8090	0.7694	
0.3	0	0.1816	0.3455	0.4755	0.5590	0.5878	0.5590	
0.4	0	0.0955	0.1816	0.2500	0.2939	0.3090	0.2939	
0.5	0	0	0	0	0	0	0	
0.6	0	-0.0955	-0.1816	-0.2500	-0.2939	-0.3090	-0.2939	
0.7	0	-0.1816	-0.3455	-0.4755	-0.5590	-0.5878	-0.5590	
	⋮	⋮	⋮	⋮	⋮	⋮	⋮	⋮

3.5 Finite Differencing of Elliptic PDEs

A typical elliptic PDE is Poisson's equation, which in two dimensions is given by

$$\nabla^2 \Phi = \frac{\partial^2 \Phi}{\partial x^2} + \frac{\partial^2 \Phi}{\partial y^2} = g(x, y) \quad (3.28)$$

```

0001
0002 C *****
0003 C FORTRAN CODE FOR EXAMPLE 3.2
0004 C ON ONE-DIMENSIONAL WAVE EQUATION
0005 C SOLVED USING AN EXPLICIT FINITE DIFFERENCE SCHEME
0006 C *****
0007
0008     DIMENSION PHI(0:50,0:200), PHIEX(0:50,0:200)
0009     DATA PIE/3.141592654/
0010 C SET SPATIAL AND TIME INCREMENTS
0011     DX = 0.1
0012     DT = 0.1
0013 C INITIALIZE - THIS ALSO TAKES CARE OF BOUNDARY CONDITIONS
0014     DO 10 I = 0,10
0015     DO 10 J = 0,200
0016     PHI(I,J) = 0.0
0017 10 CONTINUE
0018 C INSERT THE INITIAL CONDITIONS
0019     DO 20 I = 0,10
0020     X = DX*FLOAT(I)
0021     PHI(I,0) = SIN(PIE*X)
0022 20 CONTINUE
0023     DO 30 I=1,9
0024     PHI(I,1) = ( PHI(I-1,0) + PHI(I+1,0) )/2.0
0025 30 CONTINUE
0026 C NOW APPLY THE EXPLICIT FD SCHEME
0027     DO 40 J = 1,10
0028     DO 40 I = 1,9
0029     PHI(I,J+1) = PHI(I-1,J) + PHI(I+1,J) - PHI(I,J-1)
0030 40 CONTINUE
0031 C CALCULATE EXACT RESULT
0032     DO 50 J = 0,10
0033     T = DT*FLOAT(J)
0034     CT = COS(PIE*T)
0035     DO 50 I=0,10
0036     X = DX*FLOAT(I)
0037     PHIEX(I,J) = SIN(PIE*X)*CT
0038 50 CONTINUE
0039 C OUTPUT THE FD APPROXIMATE AND EXACT RESULTS
0040     DO 70 J = 0,7
0041     DO 70 I = 0,7
0042     WRITE(6,60) J,I,PHI(I,J),PHIEX(I,J)
0043 60 FORMAT(3X,'J=',I3,3X,'I=',I3,3X,2(F14.10,3X),/)
0044 70 CONTINUE
0045     STOP
0046     END

```

Figure 3.8
FORTRAN code for Example 3.2.

We can use the central difference approximation for the partial derivatives of which the simplest forms are

$$\frac{\partial^2 \Phi}{\partial x^2} = \frac{\Phi(i+1, j) - 2\Phi(i, j) + \Phi(i-1, j)}{(\Delta x)^2} + O(\Delta x)^2 \quad (3.29a)$$

$$\frac{\partial^2 \Phi}{\partial y^2} = \frac{\Phi(i, j+1) - 2\Phi(i, j) + \Phi(i, j-1)}{(\Delta y)^2} + O(\Delta y)^2 \quad (3.29b)$$

where $x = i\Delta x$, $y = j\Delta y$, and $i, j = 0, 1, 2, \dots$. If we assume that $\Delta x = \Delta y = h$, to simplify calculations, substituting Eq. (3.29) into Eq. (3.28) gives

$$\left[\Phi(i+1, j) + \Phi(i-1, j) + \Phi(i, j+1) + \Phi(i, j-1) \right] - 4\Phi(i, j) = h^2 g(i, j)$$

or

$$\Phi(i, j) = \frac{1}{4} \left[\Phi(i+1, j) + \Phi(i-1, j) + \Phi(i, j+1) + \Phi(i, j-1) - h^2 g(i, j) \right] \quad (3.30)$$

at every point (i, j) in the mesh for Poisson's equation. The spatial increment h is called the *mesh size*. A special case of Eq. (3.28) is when the source term vanishes, i.e., $g(x, y) = 0$. This leads to Laplace's equation. Thus for Laplace's equation, Eq. (3.30) becomes

$$\Phi(i, j) = \frac{1}{4} [\Phi(i+1, j) + \Phi(i-1, j) + \Phi(i, j+1) + \Phi(i, j-1)] \quad (3.31)$$

It is worth noting that Eq. (3.31) states that the value of Φ for each point is the average of those at the four surrounding points. The five-point computational molecule for the difference scheme in Eq. (3.31) is illustrated in Fig. 3.9(a) where values of the coefficients are shown. This is a convenient way of displaying finite difference algorithms

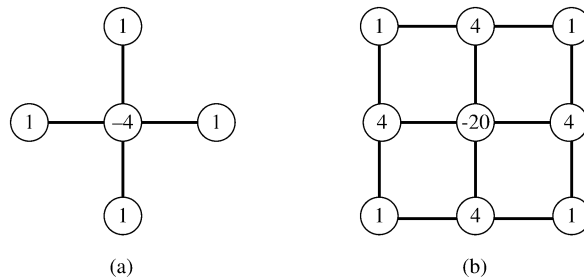


Figure 3.9
Computational molecules for Laplace's equation based on: (a) second order approximation, (b) fourth order approximation.

for elliptic PDEs. The molecule in Fig. 3.9(a) is the second order approximation of Laplace's equation. This is obviously not the only way to approximate Laplace's equation, but it is the most popular choice. An alternative fourth order difference is

$$\begin{aligned} & -20\Phi(i, j) + 4[\Phi(i+1, j) + \Phi(i-1, j) + \Phi(i, j+1) + \Phi(i, j-1)] \\ & + \Phi(i+1, j-1) + \Phi(i-1, j-1) + \Phi(i-1, j+1) \\ & + \Phi(i+1, j+1) = 0 \end{aligned} \quad (3.32)$$

The corresponding computational molecule is shown in Fig. 3.9(b).

The application of the finite difference method to elliptic PDEs often leads to a large system of algebraic equations, and their solution is a major problem in itself. Two commonly used methods of solving the system of equations are band matrix and iterative methods.

3.5.1 Band Matrix Method

From Eqs. (3.30) to (3.32), we notice that only nearest neighboring nodes affect the value of Φ at each node. Hence application of any of Eqs. (3.30) to (3.32) to all free nodes in the solution region results in a set of simultaneous equations of the form

$$[A][X] = [B] \quad (3.33)$$

where $[A]$ is a *sparse* matrix (it has many zero elements), $[X]$ is a column matrix consisting of the unknown values of Φ at the free nodes, and $[B]$ is a column matrix containing the known values of Φ at fixed nodes. Matrix $[A]$ is also banded in that its nonzero terms appear clustered near the main diagonal. Matrix $[X]$, containing the unknown elements, can be obtained from

$$[X] = [A]^{-1}[B] \quad (3.34)$$

or by solving Eq. (3.33) using the Gauss elimination discussed in Appendix D.1.

3.5.2 Iterative Methods

The iterative methods are generally used to solve a large system of simultaneous equations. An iterative method for solving equations is one in which a first approximation is used to calculate a second approximation, which in turn is used to calculate the third approximation, and so on. The three common iterative methods (Jacobi, Gauss-Seidel, and successive over-relaxation (SOR)) are discussed in Appendix D.2. We will apply only SOR here.

To apply the method of SOR to Eq. (3.30), for example, we first define the *residual* $R(i, j)$ at node (i, j) as the amount by which the value of $\Phi(i, j)$ does not satisfy Eq. (3.30), i.e.,

$$\begin{aligned} R(i, j) = & \Phi(i + 1, j) + \Phi(i - 1, j) + \Phi(i, j + 1) \\ & + \Phi(i, j - 1) - 4\Phi(i, j) - h^2g(i, j) \end{aligned} \quad (3.35)$$

The value of the residual at k th iteration, denoted by $R^k(i, j)$, may be regarded as a correction which must be added to $\Phi(i, j)$ to make it nearer to the correct value. As convergence to the correct value is approached, $R^k(i, j)$ tends to zero. Hence to improve the rate of convergence, we multiply the residual by a number ω and add that to $\Phi(i, j)$ at the k th iteration to get $\Phi(i, j)$ at $(k + 1)$ th iteration. Thus

$$\Phi^{k+1}(i, j) = \Phi^k(i, j) + \frac{\omega}{4}R^k(i, j)$$

or

$$\begin{aligned} \Phi^{k+1}(i, j) = & \Phi^k(i, j) + \frac{\omega}{4} \left[\Phi^k(i+1, j) + \Phi^{k+1}(i-1, j) + \Phi^{k+1}(i, j-1) \right. \\ & \left. + \Phi^k(i, j+1) - 4\Phi^k(i, j) - h^2 g(i, j) \right] \end{aligned} \quad (3.36)$$

The parameter ω is called the *relaxation factor* while the technique is known as the method of *successive over-relaxation* (SOR). The value of ω lies between 1 and 2. (When $\omega = 1$, the method is simply called successive relaxation.) Its optimum value ω_{opt} must be found by trial-and-error. In order to start Eq. (3.36), an initial guess, $\Phi^0(i, j)$, is made at every free node. Typically, we may choose $\Phi^0(i, j) = 0$ or the average of Φ at the fixed nodes.

Example 3.3

Solve Laplace's equation

$$\nabla^2 V = 0, \quad 0 \leq x, y \leq 1$$

with $V(x, 1) = 45x(1-x)$, $V(x, 0) = 0 = V(0, y) = V(1, y)$. \square

Solution

Let $h = 1/3$ so that the solution region is as in Fig. 3.10. Applying Eq. (3.31) to each

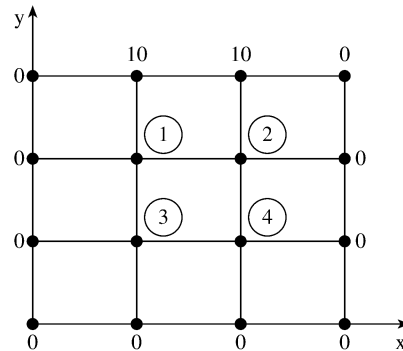


Figure 3.10
Finite difference grid for Example 3.3.

of the four points leads to

$$\begin{aligned} 4V_1 - V_2 - V_3 - 0 &= 10 \\ -V_1 + 4V_2 - 0 - V_4 &= 10 \\ -V_1 - 0 + 4V_3 - V_4 &= 0 \\ -0 - V_2 - V_3 + 4V_4 &= 0 \end{aligned}$$

This can be written as

$$\begin{bmatrix} 4 & -1 & -1 & 0 \\ -1 & 4 & 0 & -1 \\ -1 & 0 & 4 & -1 \\ 0 & -1 & -1 & 4 \end{bmatrix} \begin{bmatrix} V_1 \\ V_2 \\ V_3 \\ V_4 \end{bmatrix} = \begin{bmatrix} 10 \\ 10 \\ 0 \\ 0 \end{bmatrix}$$

or

$$[A][V] = [B]$$

where $[A]$ is the band matrix, $[V]$ is the column matrix containing the unknown potentials at the free nodes, and $[B]$ is the column matrix of potentials at the fixed nodes. Solving the equations either by matrix inversion or by Gauss elimination, we obtain

$$V_1 = 3.75, \quad V_2 = 3.75, \quad V_3 = 1.25, \quad V_4 = 1.25 \quad \blacksquare$$

Example 3.4

Solve Poisson's equation

$$\nabla^2 V = -\frac{\rho_S}{\epsilon}, \quad 0 \leq x, y \leq 1$$

and obtain the potential at the grid points shown in Fig. 3.11. Assume $\rho_S = x(y - 1)$ nC/m² and $\epsilon_r = 1.0$. Use the method of successive over-relaxation. \square

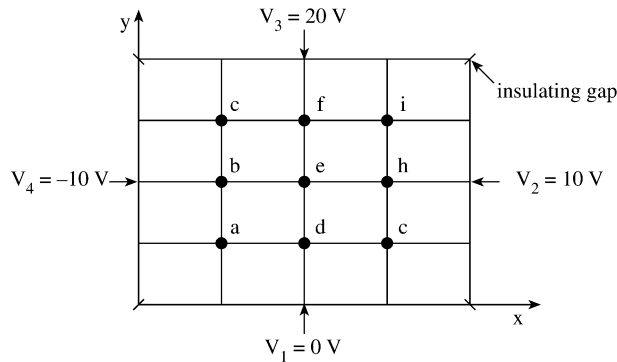


Figure 3.11
Solution region for the problem in Example 3.4.

Solution

This problem has an exact analytical solution and is deliberately chosen so that we can verify the numerical results with exact ones, and we can also see how a problem

with a complicated analytical solution is easily solved using finite difference method. For the exact solution, we use the superposition theorem and let

$$V = V_1 + V_2$$

where V_1 is the solution to Laplace's equation $\nabla^2 V_1 = 0$ with the inhomogeneous boundary conditions shown in Fig. 3.11 and V_2 is the solution to Poisson's equation $\nabla^2 V_2 = g = -\rho_S/\epsilon$ subject to homogeneous boundary conditions. From Example 2.1, it is evident that

$$V_1 = V_I + V_{II} + V_{III} + V_{IV}$$

where V_I to V_{IV} are defined by Eqs. (2.53) to (2.56). V_2 can be obtained by the series expansion method of Section 2.7. From example 2.12,

$$V_2 = \sum_{m=1}^{\infty} \sum_{n=1}^{\infty} A_{mn} \sin \frac{m\pi x}{a} \sin \frac{n\pi y}{b}$$

where

$$\begin{aligned} A_{mn} &= \int_0^a \int_0^b g(x, y) \sin \frac{m\pi x}{a} \sin \frac{n\pi y}{b} dx dy \\ &= \frac{\left[1.0 - \frac{1}{b}[1 - (-1)^n]\right]}{[(m\pi/a)^2 + (n\pi/b)^2]} \cdot \frac{(-1)^{m+n} 144ab}{mn\pi}, \end{aligned}$$

$a = b = 1$, and $g(x, y) = -x(y - 1) \cdot 10^{-9}/\epsilon_0$.

For the finite difference solution, it can be shown that in a rectangular region, the optimum over-relaxation factor is given by the smaller root of the quadratic equation [10]

$$t^2 \omega^2 - 16\omega + 16 = 0$$

where $t = \cos(\pi/N_x) + \cos(\pi/N_y)$ and N_x and N_y are the number of intervals along x and y axes, respectively. Hence

$$\omega = \frac{8 - \sqrt{64 - 16t^2}}{t^2}$$

We try three cases of $N_x = N_y = 4, 12$ and 20 so that $\Delta x = \Delta y = h = 1/4, 1/12$, and $1/20$, respectively. Also we set

$$g(x, y) = -\frac{\rho_S}{\epsilon} = -\frac{x(y - 1) \cdot 10^{-9}}{10^{-9}/36\pi} = -36\pi x(y - 1)$$

Figure 3.12 presents the FORTRAN code for the solution of this problem. The potentials at the free nodes for the different cases of h are shown in Table 3.6. Notice that as the mesh size h reduces, the solution becomes more accurate, but it takes more iterations for the same tolerance. ■

```

0001 C*****
0002 C FINITE DIFFERENCE SOLUTION OF POISSON'S EQUATION
0003 C  $V_{xx} + V_{yy} = G$ 
0004 C USING THE METHOD OF SUCCESSIVE OVER-RELAXATION
0005 C
0006 C NX : NO. OF INTERVALS ALONG X-AXIS
0007 C NY : NO. OF INTERVALS ALONG Y-AXIS
0008 C A X B : DIMENSION OF THE SOLUTION REGION
0009 C V(I,J) : POTENTIAL AT GRID POINT (X,Y) = H*(I,J)
0010 C WHERE 1 = 0,1,...,NX, J = 0,1,...,NY
0011 C H : MESH SIZE
0012 C *****
0013
0014 DIMENSION V(0:20,0:20)
0015 DATA PIE/3.14159/
0016 DATA A,B/1.0,1.0/
0017 DATA V1,V2,V3,V4/0.0,10.0,20.0,-10.0/
0018
0019 C SPECIFY BOUNDARY VALUES AND NECESSARY PARAMETERS
0020 NX= 4
0021 NY= 4
0022 H = A/FLOAT(NX)
0023 C SET INITIAL GUESS EQUAL TO ZEROS OR TO AVERAGE OF
0024 C FIXED VALUES
0025 DO 10 I=1,NX-1
0026 DO 10 J=1,NY-1
0027 V(I,J)=(V1 + V2 + V3 + V4)/4.0
0028 10 CONTINUE
0029 C SET POTENTIALS AT FIXED NODES
0030 DO 20 I = 1, NX-1
0031 V(I,0)=V1
0032 V(I,NY)=V3
0033 20 CONTINUE
0034 DO 30 J=1,NY-1
0035 V(0,J)=V4
0036 V(NX,J)=V2
0037 30 CONTINUE
0038 V(0,0)=(V1 + V4)/2.0
0039 V(NX,0)=(V1 + V2)/2.0
0040 V(0,NY)=(V3 + V4)/2.0
0041 V(NX,NY)=(V2 + V3)/2.0
0042 C FIND THE OPTIMUM OVER-RELAXATION FACTOR
0043 T = COS(PIE/NX) + COS(PIE/NY)
0044 W = ( 8.0 - SQRT(64.0 - 16.0*T*T))/(T*T)
0045 WRITE(6,40) W
0046 40 FORMAT(2X,'SOR FACTOR OMEGA=',F10.6)
0047 W4 = W/4.0
0048 C ITERATION BEGINS
0049 NCOUNT = 0
0050 50 RMIN = 0.0
0051 DO 70 I =1,NX-1
0052 X = H*FLOAT(I)
0053 DO 70 J = 1,NY-1
0054 Y = H*FLOAT(J)
0055 G = -36.0*PIE*X*(Y - 1.0)
0056 R = W4*( V(I+1,J) + V(I-1,J) + V(I,J+1) + V(I,J-1)
0057 1 -4.0*V(I,J) - G*H*H )
0058 RMIN = RMIN + ABS(R)
0059 V(I,J) = V(I,J) + R
0060 70 CONTINUE

```

Figure 3.12
FORTRAN code for Example 3.4 (Continued).

```

0061         RMIN = RMIN/LOAT(NX*NY)
0062         IF(RMIN.GE.0.0001) THEN
0063 C SOLUTION HAS CONVERGED
0064         NCOUNT = NCOUNT + 1
0065         IF(NCOUNT.LT.100) THEN
0066             GO TO 50
0067         ELSE
0068             WRITE(6,80)
0069 80 FORMAT(2X,'SOLUTION DOES NOT CONVERGE IN 100 ITERATIONS')
0070             GO TO 100
0071         ENDIF
0072     ENDIF
0073 C SOLUTION HAS CONVERGED
0074     WRITE(6,90) NCOUNT
0075 90 FORMAT(2X,'SOLUTION CONVERGES IN',2X,I3,2X,'ITERATIONS',/)
0076 100 CONTINUE
0077 C OUTPUT THE FINITE DIFFERENCE APPROX. RESULTS
0078     DO 120 I = 1,NX-1
0079     DO 120 J = 1,NY-1
0080     WRITE(6,110) I,J,V(I,J)
0081 110 FORMAT(2X,'I=',I3,2X,'J=',I3,2X,'V =',E12.6,/)
0082 120 CONTINUE
0083 C -----
0084 C CALCULATE THE EXACT SOLUTION
0085 C
0086 C POISSON'S EQUATION WITH HOMOGENEOUS BOUNDARY CONDITIONS
0087 C SOLVED BY SERIES EXPANSION
0088 C
0089     DO 150 I =1,NX-1
0090     X = H*FLOAT(I)
0091     DO 150 J = 1,NY-1
0092     Y = H*FLOAT(J)
0093     SUM = 0.0
0094     DO 130 M = 1,10 ! TAKE ONLY 10 TERMS OF THE SERIES
0095     FM = FLOAT(M)
0096     DO 130 N = 1,10
0097     FN = FLOAT(N)
0098     FACTOR1 = (FM*PIE/A)**2 + (FN*PIE/B)**2
0099     FACTOR2 = ( (-1.0)**(M+N) ) *144.0*A*B/(PIE*FM*FN)
0100     FACTOR3 = 1.0 - (1.0 - (-1.0)**N)/B
0101     FACTOR = FACTOR2*FACTOR3/FACTOR1
0102     SUM = SUM + FACTOR*SIN(FM*PIE*X/A)*SIN(FN*PIE*Y/B)
0103 130 CONTINUE
0104     VH = SUM
0105 C
0106 C LAPLACE'S EQUATION WITH INHOMOGENEOUS BOUNDARY CONDITIONS
0107 C SOLVED USING THE METHOD OF SEPARATION OF VARIABLES
0108 C
0109     C1=4.0*V1/PIE
0110     C2=4.0*V2/PIE
0111     C3=4.0*V3/PIE
0112     C4=4.0*V4/PIE
0113     SUM=0.0
0114     DO 140 K =1,10 ! TAKE ONLY 10 TERMS OF THE SERIES
0115     N=2*K-1
0116     AN=FLOAT(N)
0117     A1=SIN(AN*PIE*X/B)
0118     A2=SIHH(AN*PIE*(A-Y)/B)
0119     A3=AN*SIHH(AN*PIE*A/B)
0120     TERM1=C1*A1*A2/A3

```

Figure 3.12

(Cont.) FORTRAN code for Example 3.4 (Continued).

```

0121      B1=SIHH(AH*PIE*X/A)
0122      B2=SIN(AH*PIE*Y/A)
0123      B3=AH*SIHH(AH*PIE*B/A)
0124      TERM2=C2*B1*B2/B3
0125      D1=SIN(AH*PIE*X/B)
0126      D2=SIHH(AH*PIE*Y/B)
0127      D3=AH*SIHH(AH*PIE*A/B)
0128      TERM3=C3*D1*D2/D3
0129      E1=SIHH(AH*PIE*(B-X)/A)
0130      E2=SIN(AH*PIE*Y/A)
0131      E3=AH*SIHH(AH*PIE*B/A)
0132      TERM4=C4*E1*E2/E3
0133      TERM = TERM1 + TERM2 + TERM3 + TERM4
0134      SUM=SUM + TERM
0135      140  CONTINUE
0136      VI = SUM
0137      V(I,J) = VH + VI
0138      150  CONTINUE
0139      C
0140      C  OUTPUT EXACT RESULTS
0141      C
0142      DO 160 I = 1, NX-1
0143      DO 160 J = 1, NY-1
0144      WRITE(6,110) I,J,V(I,J)
0145      160  CONTINUE
0146      STOP
0147      END

```

Figure 3.12
(Cont.) FORTRAN code for Example 3.4.

Table 3.6 Successive Over-relaxation Solution of Example 3.4

Node	$h = 1/4$	$h = 1/2$	$h = 1/20$	Exact Solution
	$\omega_{opt} = 1.171$	$\omega_{opt} = 1.729$	$\omega_{opt} = 1.729$	
	8 iterations	26 iterations	43 iterations	
a	-3.247	-3.409	-3.424	-3.429
b	-1.703	-1.982	-2.012	-2.029
c	4.305	4.279	4.277	4.277
d	-0.0393	-0.0961	-0.1087	-0.1182
e	3.012	2.928	2.921	2.913
f	9.368	9.556	9.578	9.593
g	3.044	2.921	2.909	2.902
h	6.111	6.072	6.069	6.065
i	11.04	11.12	11.23	11.13

3.6 Accuracy and Stability of FD Solutions

The question of accuracy and stability of numerical methods is extremely important if our solution is to be reliable and useful. Accuracy has to do with the closeness of the approximate solution to exact solutions (assuming they exist). Stability is the

requirement that the scheme does not increase the magnitude of the solution with increase in time.

There are three sources of errors that are nearly unavoidable in numerical solution of physical problems [8]:

- modeling errors,
- truncation (or discretization) errors, and
- roundoff errors.

Each of these error types will affect accuracy and therefore degrade the solution.

The modeling errors are due to several assumptions made in arriving at the mathematical model. For example, a nonlinear system may be represented by a linear PDE. Truncation errors arise from the fact that in numerical analysis, we can deal only with a finite number of terms from processes which are usually described by infinite series. For example, in deriving finite difference schemes, some higher-order terms in the Taylor series expansion were neglected, thereby introducing truncation error. Truncation errors may be reduced by using finer meshes, that is, by reducing the mesh size h and time increment Δt . Alternatively, truncation errors may be reduced by using a large number of terms in the series expansion of derivatives, that is, by using higher-order approximations. However, care must be exercised in applying higher-order approximations. Instability may result if we apply a difference equation of an order higher than the PDE being examined. These higher-order difference equations may introduce “spurious solutions.”

Roundoff errors reflect the fact that computations can be done only with a finite precision on a computer. This unavoidable source of errors is due to the limited size of registers in the arithmetic unit of the computer. Roundoff errors can be minimized by the use of double-precision arithmetic. The only way to avoid roundoff errors completely is to code all operations using integer arithmetic. This is hardly possible in most practical situations.

Although it has been noted that reducing the mesh size h will increase accuracy, it is not possible to indefinitely reduce h . Decreasing the truncation error by using a finer mesh may result in increasing the roundoff error due to the increased number of arithmetic operations. A point is reached where the minimum total error occurs for any particular algorithm using any given word length [9]. This is illustrated in [Fig. 3.13](#). The concern about accuracy leads us to question whether the finite difference solution can grow unbounded, a property termed the instability of the difference scheme. A numerical algorithm is said to be stable if a small error at any stage produces a smaller cumulative error. It is unstable otherwise. The consequence of instability (producing unbounded solution) is disastrous. To determine whether a finite difference scheme is stable, we define an error, ϵ^n , which occurs at time step n , assuming that there is one independent variable. We define the amplification of this error at time step $n + 1$ as

$$\epsilon^{n+1} = g\epsilon^n \quad (3.37)$$

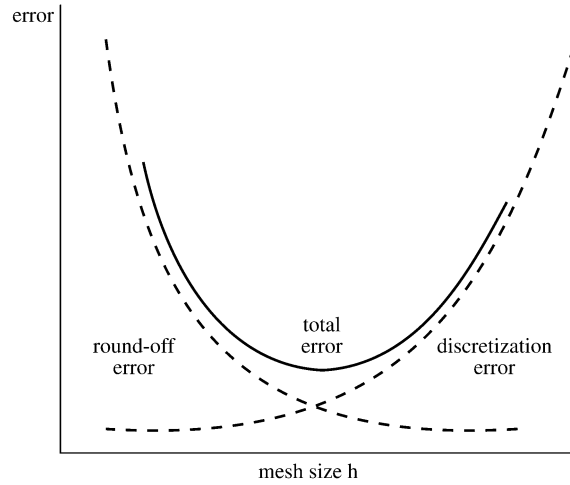


Figure 3.13
Error as a function of the mesh size.

where g is known as the *amplification factor*. In more complex situations, we have two or more independent variables, and Eq. (3.37) becomes

$$[\epsilon]^{n+1} = [G][\epsilon]^n \quad (3.38)$$

where $[G]$ is the amplification matrix. For the stability of the difference scheme, it is required that Eq. (3.37) satisfy

$$|\epsilon^{n+1}| \leq |\epsilon^n|$$

or

$$|g| \leq 1 \quad (3.39a)$$

For the case in Eq. (3.38),

$$\|G\| \leq 1 \quad (3.39b)$$

One useful and simple method of finding a stability criterion for a difference scheme is to construct a Fourier analysis of the difference equation and thereby derive the amplification factor. We illustrate this technique, known as *von Neumann's method* [4, 5, 7, 10], by considering the explicit scheme of Eq. (3.13):

$$\Phi_i^{n+1} = (1 - 2r)\Phi_i^n + r(\Phi_{i+1}^n + \Phi_{i-1}^n) \quad (3.40)$$

where $r = \Delta t / k(\Delta x)^2$. We have changed our usual notation so that we can use $j = \sqrt{-1}$ in the Fourier series. Let the solution be

$$\Phi_i^n = \sum A_n(t) e^{jkix}, \quad 0 \leq x \leq 1 \quad (3.41a)$$

where k is the wave number. Since the differential equation (3.10) approximated by Eq. (3.13) is linear, we need consider only a Fourier mode, i.e.,

$$\Phi_i^n = A(t)e^{jkix} \quad (3.41b)$$

Substituting Eq. (3.41b) into Eq. (3.40) gives

$$A^{n+1}e^{jkix} = (1 - 2r)A^n e^{jkix} + r(e^{jkx} + e^{-jkx})A^n e^{jkix}$$

or

$$A^{n+1} = A^n[1 - 2r + 2 \cos kx] \quad (3.42)$$

Hence the amplification factor is

$$\begin{aligned} g &= \frac{A^{n+1}}{A^n} = 1 - 2r + 2 \cos kx \\ &= 1 - 4r \sin^2 \frac{kx}{2} \end{aligned} \quad (3.43)$$

In order to satisfy Eq. (3.39a),

$$\left| 1 - 4r \sin^2 \frac{kx}{2} \right| \leq 1$$

Since this condition must hold for every wave number k , we take the maximum value of the sine function so that

$$1 - 4r \geq -1 \quad \text{and} \quad r \geq 0$$

or

$$r \leq \frac{1}{2} \quad \text{and} \quad r \geq 0$$

Of course, $r = 0$ implies $\Delta t = 0$, which is impractical. Thus

$$0 < r \leq \frac{1}{2} \quad (3.44)$$

Example 3.5

For the finite difference scheme of Eq. (3.20), use the von Neumann approach to determine the stability condition. \square

Solution

We assume a trial solution of the form

$$\Phi_i^n = A^n e^{jkix}$$

Substituting this into Eq. (3.20) results in

$$A^{n+1}e^{jkix} = 2(1-r)A^n e^{jkix} + r(e^{jkx} + e^{-jkx})A^n e^{jkix} - A^{n-1}e^{jkix}$$

or

$$A^{n+1} = A^n [2(1-r) + 2r \cos kx] - A^{n-1} \quad (3.45)$$

In terms of $g = A^{n+1}/A^n$, Eq. (3.45) becomes

$$g^2 - 2pg + 1 = 0 \quad (3.46)$$

where $p = 1 - 2r \sin^2 \frac{kx}{2}$. The quadratic equation (3.46) has solutions

$$g_1 = p + [p^2 - 1]^{1/2}, \quad g_2 = p - [p^2 - 1]^{1/2}$$

For $|g_j| \leq 1$, where $i = 1, 2$, p must lie between 1 and -1 , i.e., $-1 \leq p \leq 1$ or

$$-1 \leq 1 - 2r \sin^2 \frac{kx}{2} \leq 1$$

which implies that $r \leq 1$ or $u\Delta t \leq \Delta x$ for stability. This idea can be extended to show that the stability condition for two-dimensional wave equation is $u\Delta t/h < \frac{1}{\sqrt{2}}$,

where $h = \Delta x = \Delta y$. ■

3.7 Practical Applications I — Guided Structures

The finite difference method has been applied successfully to solve many EM-related problems. Besides those simple examples we have considered earlier in this chapter, the method has been applied to diverse problems [11] including:

- Transmission-line problems [12]–[21],
- Waveguides [21]–[26],
- Microwave circuit [27]–[30],
- EM penetration and scattering problems [31, 32],
- EM pulse (EMP) problems [33],
- EM exploration of minerals [34], and
- EM energy deposition in human bodies [35, 36].

It is practically impossible to cover all those applications within the limited scope of this text. In this section, we consider the relatively easier problems of transmission lines and waveguides while the problems of penetration and scattering of EM waves will be treated in the next section. Other applications utilize basically similar techniques.

3.7.1 Transmission Lines

The finite difference techniques are suited for computing the characteristic impedance, phase velocity, and attenuation of several transmission lines—polygonal lines, shielded strip lines, coupled strip lines, microstrip lines, coaxial lines, and rectangular lines [12]–[19]. The knowledge of the basic parameters of these lines is of paramount importance in the design of microwave circuits.

For concreteness, consider the microstrip line shown in Fig. 3.14(a). The geometry in Fig. 3.14(a) is deliberately selected to be able to illustrate how one accounts for discrete inhomogeneities (i.e., homogeneous media separated by interfaces) and lines of symmetry using a finite difference technique. The techniques presented are equally applicable to other lines. Assuming that the mode is TEM, having components of neither \mathbf{E} nor \mathbf{H} fields in the direction of propagation, the fields obey Laplace's equation over the line cross section. The TEM mode assumption provides good approximations if the line dimensions are much smaller than half a wavelength, which means that the operating frequency is far below cutoff frequency for all higher order modes [16]. Also owing to biaxial symmetry about the two axes only one quarter of the cross section need to be considered as shown in Fig. 3.14(b).

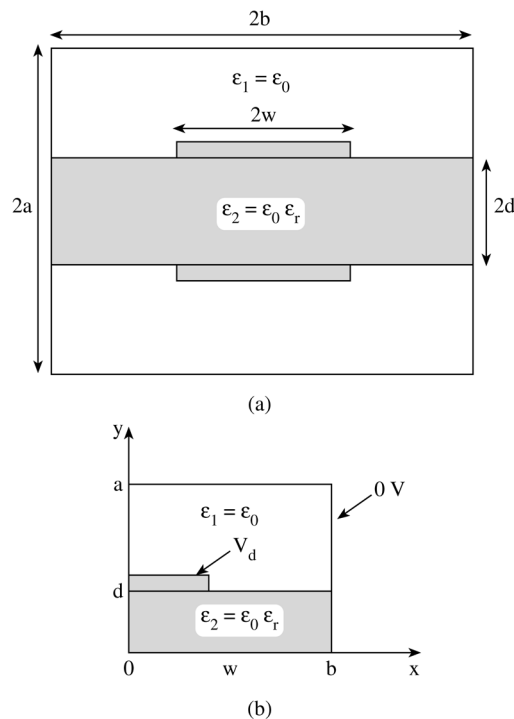


Figure 3.14
(a) Shielded double strip line with partial dielectric support; (b) problem in (a) simplified by making full use of symmetry.

The finite difference approximation of Laplace's equation, $\nabla^2 V = 0$, has been derived in Eq. (3.31), namely,

$$V(i, j) = \frac{1}{4} [V(i + 1, j) + V(i - 1, j) + V(i, j + 1) + V(i, j - 1)] \quad (3.47)$$

For the sake of conciseness, let us denote

$$\begin{aligned} V_o &= V(i, j) \\ V_1 &= V(i, j + 1) \\ V_2 &= V(i - 1, j) \\ V_3 &= V(i, j - 1) \\ V_4 &= V(i + 1, j) \end{aligned} \quad (3.48)$$

so that Eq. (3.47) becomes

$$V_o = \frac{1}{4} [V_1 + V_2 + V_3 + V_4] \quad (3.49)$$

with the computation molecule shown in Fig. 3.15. Equation (3.49) is the general formula to be applied to all free nodes in the free space and dielectric region of Fig. 3.14(b).

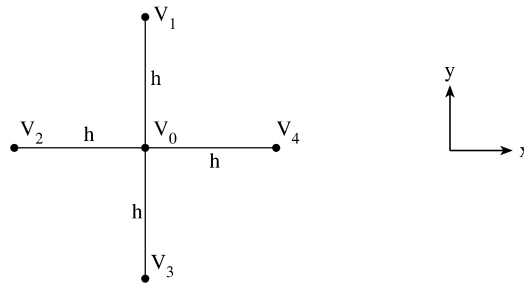


Figure 3.15
Computation molecule for Laplace's equation.

On the dielectric boundary, the boundary condition,

$$D_{1n} = D_{2n} , \quad (3.50)$$

must be imposed. We recall that this condition is based on Gauss's law for the electric field, i.e.,

$$\oint_{\ell} \mathbf{D} \cdot d\mathbf{l} = \oint_{\ell} \epsilon \mathbf{E} \cdot d\mathbf{l} = Q_{\text{enc}} = 0 \quad (3.51)$$

since no free charge is deliberately placed on the dielectric boundary. Substituting $\mathbf{E} = -\nabla V$ in Eq. (3.51) gives

$$0 = \oint_{\ell} \epsilon \nabla V \cdot d\mathbf{l} = \oint_{\ell} \epsilon \frac{\partial V}{\partial n} dl \quad (3.52)$$

where $\partial V/\partial n$ denotes the derivative of V normal to the contour ℓ . Applying Eq. (3.52) to the interface in Fig. 3.16 yields

$$0 = \epsilon_1 \frac{(V_1 - V_0)h}{h} + \epsilon_1 \frac{(V_2 - V_0)h}{h} \frac{1}{2} + \epsilon_2 \frac{(V_2 - V_0)h}{h} \frac{1}{2} \\ + \epsilon_2 \frac{(V_3 - V_0)h}{h} + \epsilon_2 \frac{(V_4 - V_0)h}{h} \frac{1}{2} + \epsilon_1 \frac{(V_4 - V_0)h}{h} \frac{1}{2}$$

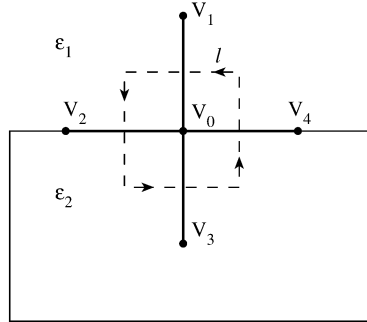


Figure 3.16
Interface between media of dielectric permittivities ϵ_1 and ϵ_2 .

Rearranging the terms,

$$2(\epsilon_1 + \epsilon_2)V_0 = \epsilon_1 V_1 + \epsilon_2 V_3 + \frac{(\epsilon_1 + \epsilon_2)}{2}(V_2 + V_4)$$

or

$$V_0 = \frac{\epsilon_1}{2(\epsilon_1 + \epsilon_2)} V_1 + \frac{\epsilon_2}{2(\epsilon_1 + \epsilon_2)} V_3 + \frac{1}{4} V_2 + \frac{1}{4} V_4 \quad (3.53)$$

This is the finite difference equivalent of the boundary condition in Eq. (3.50). Notice that the discrete inhomogeneity does not affect points 2 and 4 on the boundary but affects points 1 and 3 in proportion to their corresponding permittivities. Also note that when $\epsilon_1 = \epsilon_2$, Eq. (3.53) reduces to Eq. (3.49).

On the line of symmetry, we impose the condition

$$\frac{\partial V}{\partial n} = 0 \quad (3.54)$$

This implies that on the line of symmetry along the y -axis, ($x = 0$ or $i = 0$) $\frac{\partial V}{\partial x} = (V_4 - V_2)/h = 0$ or $V_2 = V_4$ so that Eq. (3.49) becomes

$$V_o = \frac{1}{4} [V_1 + V_3 + 2V_4] \quad (3.55a)$$

or

$$V(0, j) = \frac{1}{4} [V(0, j + 1) + V(0, j - 1) + 2V(1, j)] \quad (3.55b)$$

On the line of symmetry along the x -axis ($y = 0$ or $j = 0$), $\frac{\partial V}{\partial y} = (V_1 - V_3)/h = 0$ or $V_3 = V_1$ so that

$$V_o = \frac{1}{4} [2V_1 + V_2 + V_4] \quad (3.56a)$$

or

$$V(i, 0) = \frac{1}{4} [2V(i, 1) + V(i - 1, 0) + V(i + 1, 0)] \quad (3.56b)$$

The computation molecules for Eqs. (3.55) and (3.56) are displayed in Fig. 3.17.

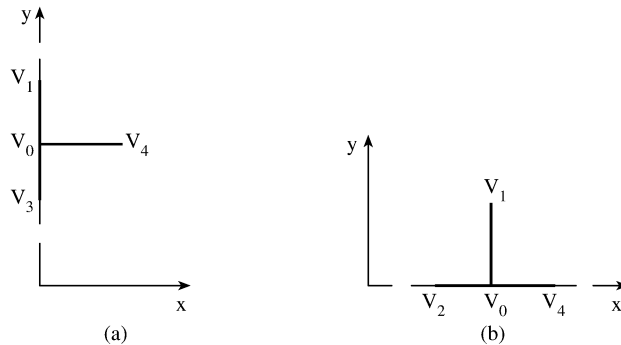


Figure 3.17

Computation molecule used for satisfying symmetry conditions: (a) $\partial V/\partial x = 0$, (b) $\partial V/\partial y = 0$.

By setting the potential at the fixed nodes equal to their prescribed values and applying Eqs. (3.49), (3.53), (3.55), and (3.56) to the free nodes according to the band matrix or iterative methods discussed in Section 3.5, the potential at the free nodes can be determined. Once this is accomplished, the quantities of interest can be calculated.

The characteristic impedance Z_o and phase velocity u of the line are defined as

$$Z_o = \sqrt{\frac{L}{C}} \quad (3.57a)$$

$$u = \frac{1}{\sqrt{LC}} \quad (3.57b)$$

where L and C are the inductance and capacitance per unit length, respectively. If the dielectric medium is nonmagnetic ($\mu = \mu_o$), the characteristic impedance Z_{oo} and phase velocity u_o with the dielectric removed (i.e., the line is air-filled) are given by

$$Z_{oo} = \sqrt{\frac{L}{C_o}} \quad (3.58a)$$

$$u_o = \frac{1}{\sqrt{LC_o}} \quad (3.58b)$$

where C_o is the capacitance per unit length without the dielectric. Combining Eqs. (3.57) and (3.58) yields

$$Z_o = \frac{1}{u_o \sqrt{CC_o}} = \frac{1}{uC} \quad (3.59a)$$

$$u = u_o \sqrt{\frac{C_o}{C}} = \frac{u_o}{\sqrt{\epsilon_{\text{eff}}}} \quad (3.59b)$$

$$\epsilon_{\text{eff}} = \frac{C}{C_o} \quad (3.59c)$$

where $u_o = c = 3 \times 10^8$ m/s, the speed of light in free space, and ϵ_{eff} is the effective dielectric constant. Thus to find Z_o and u for an inhomogeneous medium requires calculating the capacitance per unit length of the structure, with and without the dielectric substrate.

If V_d is the potential difference between the inner and the outer conductors,

$$C = \frac{4Q}{V_d}, \quad (3.60)$$

so that the problem is reduced to finding the charge per unit length Q . (The factor 4 is needed since we are working on only one quarter of the cross section.) To find Q , we apply Gauss's law to a closed path ℓ enclosing the inner conductor. We may select ℓ as the rectangular path between two adjacent rectangles as shown in Fig. 3.18.

$$\begin{aligned} Q &= \oint_{\ell} \mathbf{D} \cdot d\mathbf{l} = \oint_{\ell} \epsilon \frac{\partial V}{\partial n} d\ell \\ &= \epsilon \left(\frac{V_P - V_N}{\Delta x} \right) \Delta y + \epsilon \left(\frac{V_M - V_L}{\Delta x} \right) \Delta y + \epsilon \left(\frac{V_H - V_L}{\Delta y} \right) \Delta x \\ &\quad + \epsilon \left(\frac{V_G - V_K}{\Delta y} \right) \Delta x + \dots \end{aligned} \quad (3.61)$$

(3) Find $C_o = \frac{4Q}{V_d}$.

(4) Repeat steps (1) and (2) (with the dielectric space) and find $C = \frac{4Q}{V_d}$.

(5) Finally, calculate $Z_o = \frac{1}{c\sqrt{CC_o}}$, $c = 3 \times 10^8$ m/s

The attenuation of the line can be calculated by following similar procedure outlined in [14, 20, 21]. The procedure for handling boundaries at infinity and that for boundary singularities in finite difference analysis are discussed in [37, 38].

3.7.2 Waveguides

The solution of waveguide problems is well suited for finite difference schemes because the solution region is closed. This amounts to solving the Helmholtz or wave equation

$$\nabla^2\Phi + k^2\Phi = 0 \quad (3.64)$$

where $\Phi = E_z$ for TM modes or $\Phi = H_z$ for TE modes, while k is the wave number given by

$$k^2 = \omega^2\mu\epsilon - \beta^2 \quad (3.65)$$

The permittivity ϵ of the dielectric medium can be real for a lossless medium or complex for a lossy medium. We consider all fields to vary with time and axial distance as $\exp j(\omega t - \beta z)$. In the eigenvalue problem of Eq. (3.64), both k and Φ are to be determined. The cutoff wavelength is $\lambda_c = 2\pi/k_c$. For each value of the cutoff wave number k_c , there is a solution for the eigenfunction Φ_i , which represents the field configuration of a propagating mode.

To apply the finite difference method, we discretize the cross section of the waveguide by a suitable square mesh. Applying Eq. (3.29) to Eq. (3.64) gives

$$\Phi(i+1, j) + \Phi(i-1, j) + \Phi(i, j+1) + \Phi(i, j-1) - (4 - h^2k^2)\Phi(i, j) = 0 \quad (3.66)$$

where $\Delta x = \Delta y = h$ is the mesh size. Equation (3.66) applies to all the free or interior nodes. At the boundary points, we apply Dirichlet condition ($\Phi = 0$) for the TM modes and Neumann condition ($\partial\Phi/\partial n = 0$) for the TE modes. This implies that at point A in Fig. 3.19, for example,

$$\Phi_A = 0 \quad (3.67)$$

for TM modes. At point A, $\partial\Phi/\partial n = 0$ implies that $\Phi_D = \Phi_E$ so that Eq. (3.64) becomes

$$\Phi_B + \Phi_C + 2\Phi_D - (4 - h^2k^2)\Phi_A = 0 \quad (3.68)$$

for TE modes. By applying Eq. (3.66) and either Eq. (3.67) or (3.68) to all mesh points in the waveguide cross section, we obtain m simultaneous equations involving the m unknowns $(\Phi_1, \Phi_2, \dots, \Phi_m)$. These simultaneous equations may be conveniently

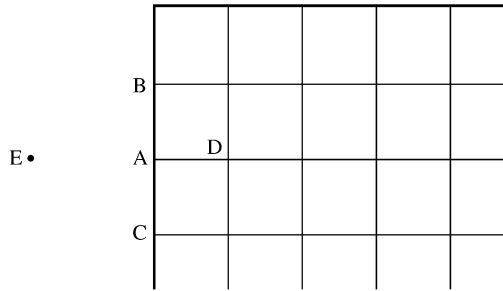


Figure 3.19
Finite difference mesh for a waveguide.

cast into the matrix equation

$$(A - \lambda I)\Phi = 0 \quad (3.69a)$$

or

$$A\Phi = \lambda\Phi \quad (3.69b)$$

where A is an $m \times m$ band matrix of known integer elements, I is an identity matrix, $\Phi = (\Phi_1, \Phi_2, \dots, \Phi_m)$ is the eigenvector, and

$$\lambda = (kh)^2 = \left(\frac{2\pi h}{\lambda_c}\right)^2 \quad (3.70)$$

is the eigenvalue. There are several ways of determining λ and the corresponding Φ . We consider two of these options.

The first option is the *direct method*. Equation (3.69) can be satisfied only if the determinant of $(A - \lambda I)$ vanishes, i.e.,

$$|A - \lambda I| = 0 \quad (3.71)$$

This results in a polynomial in λ , which can be solved [39] for the various eigenvalues λ . For each λ , we obtain the corresponding Φ from Eq. (3.66). This method requires storing the relevant matrix elements and does not take advantage of the fact that matrix A is sparse. In favor of the method is the fact that a computer subroutine usually exists (see [40] or Appendix D.4) that solves the eigenvalue problem in Eq. (3.71) and that determines all the eigenvalues of the matrix. These eigenvalues give the dominant and higher modes of the waveguide, although accuracy deteriorates rapidly with mode number.

The second option is the *iterative method*. In this case, the matrix elements are usually generated rather than stored. We begin with $\Phi_1 = \Phi_2 = \dots = \Phi_m = 1$ and a guessed value for k . The field Φ_{ij}^{k+1} at the (i, j) th node in the $(k + 1)$ th iteration is obtained from its known value in the k th iteration using

$$\Phi^{k+1}(i, j) = \Phi^k(i, j) + \frac{\omega R_{ij}}{(4 - h^2 k^2)} \quad (3.72)$$

where ω is the acceleration factor, $1 < \omega < 2$, and R_{ij} is the residual at the (i, j) th node given by

$$\begin{aligned} R_{ij} = & \Phi(i, j + 1) + \Phi(i, j - 1) + \Phi(i + 1, j) \\ & + \Phi(i - 1, j) - (4 - h^2 k^2) \Phi(i, j) \end{aligned} \quad (3.73)$$

After three or four scans of the complete mesh using Eq. (3.73), the value of $\lambda = h^2 k^2$ should be updated using Raleigh formula

$$k^2 = \frac{-\int_S \Phi \nabla^2 \Phi dS}{\int_S \Phi^2 dS} \quad (3.74)$$

The finite difference equivalent of Eq. (3.74) is

$$k^2 = \frac{-\sum_{i=1} \sum_{j=1} \Phi(i, j) [\Phi(i+1, j) + \Phi(i-1, j) + \Phi(i, j+1) + \Phi(i, j-1) - 4\Phi(i, j)]}{h^2 \sum_{i=1} \sum_{j=1} \Phi^2(i, j)} \quad (3.75)$$

where Φ s are the latest field values after three or four scans of the mesh and the summation is carried out over all points in the mesh. The new value of k obtained from Eq. (3.75) is now used in applying Eq. (3.72) over the mesh for another three or four times to give more accurate field values, which are again substituted into Eq. (3.75) to update k . This process is continued until the difference between consecutive values of k is within a specified acceptable tolerance.

If the first option is to be applied, matrix A must first be found. To obtain matrix A is not easy. Assuming TM modes, one way of calculating A is to number the free nodes from left to right, bottom to top, starting from the left-hand corner as shown typically in Fig. 3.20. If there are n_x and n_y divisions along the x and y directions, the number of free nodes is

$$n_f = (n_x - 1)(n_y - 1) \quad (3.76)$$

Each free node must be assigned two sets of numbers, one to correspond to m in Φ_m and the other to correspond to (i, j) in $\Phi(i, j)$. An array $NL(i, j) = m$, $i = 1, 2, \dots, n_x - 1$, $j = 1, 2, \dots, n_y - 1$ is easily developed to relate the two numbering schemes. To determine the value of element A_{mn} , we search $NL(i, j)$ to find (i_m, j_m) and (i_n, j_n) , which are the values of (i, j) corresponding to nodes m

and n , respectively. With these ideas, we obtain

$$A_{mn} = \begin{cases} 4, & m = n \\ -1, & i_m = i_n, \quad j_m = j_n + 1 \\ -1, & i_m = i_n, \quad j_m = j_n - 1 \\ -1, & i_m = i_n + 1, \quad j_m = j_n \\ -1, & i_m = i_n - 1, \quad j_m = j_n \\ 0, & \text{otherwise} \end{cases} \quad (3.77)$$

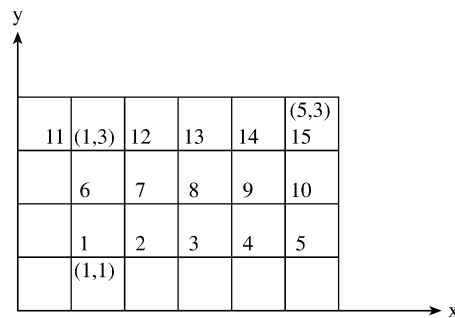


Figure 3.20
Relating node numbering schemes for $n_x = 6, n_y = 4$.

Example 3.6

Calculate Z_o for the microstrip transmission line in Fig. 3.14 with

$$\begin{aligned} a = b = 2.5 \text{ cm}, & \quad d = 0.5 \text{ cm}, & \quad \omega = 1 \text{ cm} \\ t = 0.001 \text{ cm}, & \quad \epsilon_1 = \epsilon_o, & \quad \epsilon_2 = 2.35\epsilon_o \end{aligned} \quad \square$$

Solution

This problem is representative of the various types of problems that can be solved using the concepts developed in Section 3.7.1. The computer program in Fig. 3.21 was developed based on the five-step procedure outlined above. By specifying the step size h and the number of iterations, the program first sets the potential at all nodes equal to zero. The potential on the outer conductor is set equal to zero, while that on the inner conductor is set to 100 volts so that $V_d = 100$. The program finds C_o when the dielectric slab is removed and C when the slab is in place and finally determines Z_o . For a selected h , the number of iterations must be large enough and greater than the number of divisions along x or y direction. Table 3.7 shows some typical results. ■

```

0001 C*****
0002 C USING THE FINITE DIFFERENCE METHOD
0003 C THIS PROGRAM CALCULATES THE CHARACTERISTIC IMPEDANCE
0004 C OF A MICROSTRIP LINE
0005 C*****
0006
0007 DIMENSION V(-1:200,-1:200), SV(2),Q(2)
0008 DATA A,B,D,W/2.5,2.5,0.5,1.0/ ! line data
0009 DATA ER,E0,U/2.35,8.81E-12,3.0E+8/
0010
0011 H = 0.025
0012 NT = 1000 ! NO. OF ITERATIONS
0013 NX = A/H
0014 NY = B/H
0015 ND = D/H
0016 NW = W/H
0017 VD = 100.0
0018 C
0019 C CALCULATE CHARGE WITH AND WITHOUT DIELECTRIC
0020 C
0021 ERR = 1.0
0022 DO 90 L=1,2
0023 E1 = E0
0024 E2 = E0*ERR
0025 C
0026 C INITIALIZATION
0027 C
0028 DO 10 I=0,NX
0029 DO 10 J=0,NY
0030 V(I,J) = 0.0
0031 10 CONTINUE
0032 C
0033 C SET POTENTIAL ON INNER CONDUCTOR (FIXED NODES) EQUAL
    TO VD
0034 C
0035 DO 20 I=0,NW
0036 V(I,ND) = VD
0037 20 CONTINUE
0038 C
0039 C CALCULATE POTENTIAL AT FREE NODES
0040 C
0041 P1 = E1/(2.0*(E1 + E2))
0042 P2 = E2/(2.0*(E1 + E2))
0043 DO 50 K=1,NT
0044 DO 40 I=0,NX-1
0045 DO 40 J=0,NY-1
0046 IF( (J.EQ.ND).AND.(I.LE.NW) ) GO TO 40
0047 IF(J.EQ.ND) THEN
0048 C IMPOSE BOUNDARY CONDITION AT THE INTERFACE
0049 V(I,J) = 0.25*(V(I+1,J) + V(I-1,J)) +
0050 1 P1*V(I,J+1) + P2*V(I,J-1)
0051 GO TO 40
0052 ENDIF
0053 IF(I.EQ.0) THEN
0054 C IMPOSE SYMMETRY CONDITION ALONG Y-AXIS
0055 V(I,J) = (2.0*V(I+1,J) + V(I,J+1) + V(I,J-1) )/4.0
0056 GO TO 40
0057 ENDIF
0058 IF(J.EQ.0) THEN
0059 C IMPOSE SYMMETRY CONDITION ALONG X-AXIS
0060 V(I,J) = (V(I+1,J) + V(I-1,J) + 2.0*V(I,J+1) )/4.0

```

Figure 3.21
Computer program for Example 3.6 (Continued).

```

0061          GO TO 40
0062          ENDDIF
0063      30      V(I,J) =(V(I+1,J)+V(I-1,J)+V(I,J+1)+V(I,J-1))/4.0
0064      40      CONTINUE
0065      50      CONTINUE
0066      C
0067      C NOW, CALCULATE THE TOTAL CHARGE ENCLOSED IN A
0068      C RECTANGULAR PATH SURROUNDING THE INNER CONDUCTOR
0069      C
0070          IOUT = (NX + NW)/2
0071          JOUT = (NY + ND)/2
0072      C SUM POTENTIAL ON INNER AND OUTER LOOPS
0073          DO 80 K=1,2
0074              SUM = 0.0
0075              DO 60 I=1,IOUT-1
0076                  SUM = SUM + E1*V(I,JOUT)
0077      60      CONTINUE
0078                  SUM = SUM + E1*V(0,JOUT)/2.0 ! SYMMETRY POINT
0079                  DO 70 J=1,JOUT-1
0080                      IF(J.LT.ND) SUM = SUM + E2*V(IOUT,J)
0081                      IF(J.EQ.ND) SUM = SUM + (E1+E2)*V(IOUT,J)/2.0
0082                      IF(J.GT.ND) SUM = SUM + E1*V(IOUT,J)
0083      70      CONTINUE
0084                  SUM = SUM + E2*V(IOUT,0)/2.0 ! SYMMETRY POINT
0085                  IF(K.EQ.1) SV(1) = SUM
0086                  IOUT = IOUT -1 ! FOR INNER LOOP
0087                  JOUT = JOUT -1
0088      80      CONTINUE
0089                  SUM = SUM + 2.0*E1*V(IOUT,JOUT) ! CORNER POINT
0090                  SV(2) = SUM
0091                  Q(L) = ABS( SV(1) - SV(2) )
0092                  ERR = ER
0093      90      CONTINUE
0094      C
0095      C FINALLY, CALCULATE Zo
0096      C
0097          CO = 4.0*Q(1)/VD
0098          C1 = 4.0*Q(2)/VD
0099          ZO = 1.0/( U*SQRT(CO*C1) )
0100          WRITE(6,*) H,NT,ZO
0101          PRINT *,H,NT,ZO
0102          STOP
0103          END

```

Figure 3.21

(Cont.) Computer program for Example 3.6.

3.8 Practical Applications II — Wave Scattering (FDTD)

The finite-difference time-domain (FDTD) formulation of EM field problems is a convenient tool for solving scattering problems. The FDTD method, first introduced by Yee [42] in 1966 and later developed by Taflove and others [31, 32, 35], [43]–[46], is a direct solution of Maxwell’s time-dependent curl equations. The scheme treats the irradiation of the scatterer as an initial value problem. Our discussion on the FD-TD method will cover:

- Yee’s finite difference algorithm,
- accuracy and stability,

Table 3.7 Characteristic Impedance of a Microstrip Line for Example 3.6

h	Number of iterations	Z_o
0.25	700	49.05
0.1	500	57.85
0.05	500	65.82
0.05	700	63.10
0.05	1000	61.53
Other method [41]: $Z_o = 62.50$		

- absorbing boundary conditions,
- initial fields, and
- programming aspects.

Some model examples with FORTRAN codes will be provided to illustrate the method.

3.8.1 Yee's Finite Difference Algorithm

In an isotropic medium, Maxwell's equations can be written as

$$\nabla \times \mathbf{E} = -\mu \frac{\partial \mathbf{H}}{\partial t} \quad (3.78a)$$

$$\nabla \times \mathbf{H} = \sigma \mathbf{E} + \epsilon \frac{\partial \mathbf{E}}{\partial t} \quad (3.78b)$$

The vector Eq. (3.78) represents a system of six scalar equations, which can be expressed in rectangular coordinate system as:

$$\frac{\partial H_x}{\partial t} = \frac{1}{\mu} \left(\frac{\partial E_y}{\partial z} - \frac{\partial E_z}{\partial y} \right), \quad (3.79a)$$

$$\frac{\partial H_y}{\partial t} = \frac{1}{\mu} \left(\frac{\partial E_z}{\partial x} - \frac{\partial E_x}{\partial z} \right), \quad (3.79b)$$

$$\frac{\partial H_z}{\partial t} = \frac{1}{\mu} \left(\frac{\partial E_x}{\partial y} - \frac{\partial E_y}{\partial x} \right), \quad (3.79c)$$

$$\frac{\partial E_x}{\partial t} = \frac{1}{\epsilon} \left(\frac{\partial H_z}{\partial y} - \frac{\partial H_y}{\partial z} - \sigma E_x \right), \quad (3.79d)$$

$$\frac{\partial E_y}{\partial t} = \frac{1}{\epsilon} \left(\frac{\partial H_x}{\partial z} - \frac{\partial H_z}{\partial x} - \sigma E_y \right), \quad (3.79e)$$

$$\frac{\partial E_z}{\partial t} = \frac{1}{\epsilon} \left(\frac{\partial H_y}{\partial x} - \frac{\partial H_x}{\partial y} - \sigma E_z \right) \quad (3.79f)$$

Following Yee's notation, we define a grid point in the solution region as

$$(i, j, k) \equiv (i \Delta x, j \Delta y, k \Delta z) \quad (3.80)$$

and any function of space and time as

$$F^n(i, j, k) \equiv F(i\delta, j\delta, k\delta, n\Delta t) \quad (3.81)$$

where $\delta = \Delta x = \Delta y = \Delta z$ is the space increment, Δt is the time increment, while i, j, k , and n are integers. Using central finite difference approximation for space and time derivatives that are second-order accurate,

$$\frac{\partial F^n(i, j, k)}{\partial x} = \frac{F^n(i + 1/2, j, k) - F^n(i - 1/2, j, k)}{\delta} + O(\delta^2) \quad (3.82)$$

$$\frac{\partial F^n(i, j, k)}{\partial t} = \frac{F^{n+1/2}(i, j, k) - F^{n-1/2}(i, j, k)}{\Delta t} + O(\Delta t^2) \quad (3.83)$$

In applying Eq. (3.82) to all the space derivatives in Eq. (3.79), Yee positions the components of \mathbf{E} and \mathbf{H} about a unit cell of the lattice as shown in Fig. 3.22. To

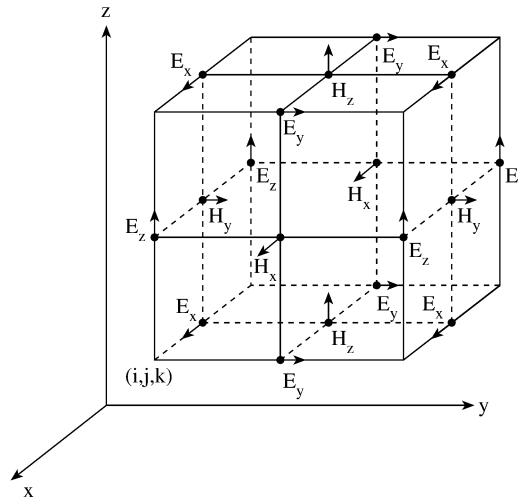


Figure 3.22
Positions of the field components in a unit cell of the Yee's lattice.

incorporate Eq. (3.83), the components of \mathbf{E} and \mathbf{H} are evaluated at alternate half-time steps. Thus we obtain the explicit finite difference approximation of Eq. (3.79) as:

$$\begin{aligned}
H_x^{n+1/2}(i, j + 1/2, k + 1/2) &= H_x^{n-1/2}(i, j + 1/2, k + 1/2) \\
&+ \frac{\delta t}{\mu(i, j + 1/2, k + 1/2)\delta} \left[E_y^n(i, j + 1/2, k + 1) \right. \\
&- E_y^n(i, j + 1/2, k) \\
&\left. + E_z^n(i, j, k + 1/2) - E_z^n(i, j + 1, k + 1/2) \right],
\end{aligned} \tag{3.84a}$$

$$\begin{aligned}
H_y^{n+1/2}(i + 1/2, j, k + 1/2) &= H_y^{n-1/2}(i + 1/2, j, k + 1/2) \\
&+ \frac{\delta t}{\mu(i + 1/2, j, k + 1/2)\delta} \left[E_z^n(i + 1, j, k + 1/2) \right. \\
&- E_z^n(i, j, k + 1/2) \\
&\left. + E_x^n(i + 1/2, j, k) - E_x^n(i + 1/2, j, k + 1) \right],
\end{aligned} \tag{3.84b}$$

$$\begin{aligned}
H_z^{n+1/2}(i + 1/2, j + 1/2, k) &= H_z^{n-1/2}(i + 1/2, j + 1/2, k) \\
&+ \frac{\delta t}{\mu(i + 1/2, j + 1/2, k)\delta} \left[E_x^n(i + 1/2, j + 1, k) \right. \\
&- E_x^n(i + 1/2, j, k) \\
&\left. + E_y^n(i, j + 1/2, k) - E_y^n(i + 1, j + 1/2, k) \right],
\end{aligned} \tag{3.84c}$$

$$\begin{aligned}
E_x^{n+1}(i + 1/2, j, k) &= \left(1 - \frac{\sigma(i + 1/2, j, k)\delta t}{\epsilon(i + 1/2, j, k)} \right) \cdot \\
&E_x^n(i + 1/2, j, k) \\
&+ \frac{\delta t}{\epsilon(i + 1/2, j, k)\delta} \left[H_z^{n+1/2}(i + 1/2, j + 1/2, k) \right. \\
&- H_z^{n+1/2}(i + 1/2, j - 1/2, k) \\
&+ H_y^{n+1/2}(i + 1/2, j, k - 1/2) \\
&\left. - H_y^{n+1/2}(i + 1/2, j, k + 1/2) \right],
\end{aligned} \tag{3.84d}$$

$$\begin{aligned}
E_y^{n+1}(i, j + 1/2, k) &= \left(1 - \frac{\sigma(i, j + 1/2, k)\delta t}{\epsilon(i, j + 1/2, k)}\right) \cdot \\
&E_y^n(i, j + 1/2, k) \\
&+ \frac{\delta t}{\epsilon(i, j + 1/2, k)\delta} \left[H_x^{n+1/2}(i, j + 1/2, k + 1/2) \right. \\
&- H_x^{n+1/2}(i, j + 1/2, k - 1/2) \\
&+ H_z^{n+1/2}(i - 1/2, j + 1/2, k) \\
&\left. - H_z^{n+1/2}(i + 1/2, j + 1/2, k) \right], \tag{3.84e}
\end{aligned}$$

$$\begin{aligned}
E_z^{n+1}(i, j, k + 1/2) &= \left(1 - \frac{\sigma(i, j, k + 1/2)\delta t}{\epsilon(i, j, k + 1/2)}\right) \cdot \\
&E_z^n(i, j, k + 1/2) \\
&+ \frac{\delta t}{\epsilon(i, j, k + 1/2)\delta} \left[H_y^{n+1/2}(i + 1/2, j, k + 1/2) \right. \\
&- H_y^{n+1/2}(i - 1/2, j, k + 1/2) \\
&+ H_x^{n+1/2}(i, j - 1/2, k + 1/2) \\
&\left. - H_x^{n+1/2}(i, j + 1/2, k + 1/2) \right] \tag{3.84f}
\end{aligned}$$

Notice from Eqs. (3.84a)–(3.84f) and Fig. 3.22 that the components of \mathbf{E} and \mathbf{H} are interlaced within the unit cell and are evaluated at alternate half-time steps. All the field components are present in a quarter of a unit cell as shown typically in Fig. 3.23(a). Figure 3.23(b) illustrates typical relations between field components on a plane; this is particularly useful when incorporating boundary conditions. The figure can be inferred from Eq. (3.79d) or Eq. (3.84d). In translating the hyperbolic system of Eqs. (3.84a)–(3.84f) into a computer code, one must make sure that, within the same time loop, one type of field components is calculated first and the results obtained are used in calculating another type.

3.8.2 Accuracy and Stability

To ensure the accuracy of the computed results, the spatial increment δ must be small compared to the wavelength (usually $\leq \lambda/10$) or minimum dimension of the scatterer. This amounts to having 10 or more cells per wavelength. To ensure the stability of the finite difference scheme of Eqs. (3.84a)–(3.84f), the time increment Δt must satisfy the following stability condition [43, 47]:

$$u_{\max} \Delta t \leq \left[\frac{1}{\Delta x^2} + \frac{1}{\Delta y^2} + \frac{1}{\Delta z^2} \right]^{-1/2} \tag{3.85}$$

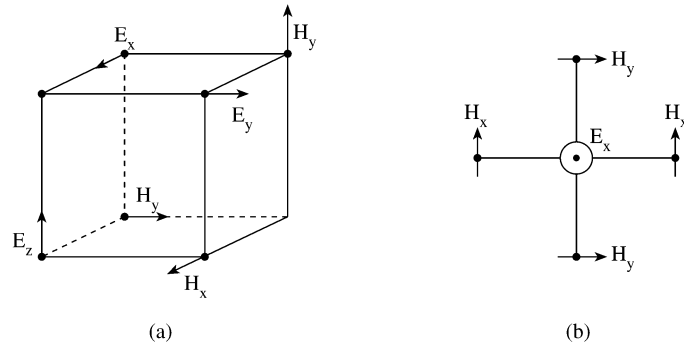


Figure 3.23
Typical relations between field components: (a) within a quarter of a unit cell, (b) in a plane.

where u_{\max} is the maximum wave phase velocity within the model. Since we are using a cubic cell with $\Delta x = \Delta y = \Delta z = \delta$, Eq. (3.85) becomes

$$\frac{u_{\max} \Delta t}{\delta} \leq \frac{1}{\sqrt{n}} \quad (3.86)$$

where n is the number of space dimensions. For practical reasons, it is best to choose the ratio of the time increment to spatial increment as large as possible yet satisfying Eq. (3.86).

3.8.3 Lattice Truncation Conditions

A basic difficulty encountered in applying the FD-TD method to scattering problems is that the domain in which the field is to be computed is open or unbounded (see Fig. 1.3). Since no computer can store an unlimited amount of data, a finite difference scheme over the whole domain is impractical. We must limit the extent of our solution region. In other words, an artificial boundary must be enforced, as in Fig. 3.24, to create the numerical illusion of an infinite space. The solution region must be large enough to enclose the scatterer, and suitable boundary conditions on the artificial boundary must be used to simulate the extension of the solution region to infinity. Outer boundary conditions of this type have been called either *radiation conditions*, *absorbing boundary conditions*, or *lattice truncation conditions*. Although several types of boundary conditions have been proposed [48, 49], we will only consider those developed by Taflove et al. [43, 44].

The lattice truncation conditions developed by Taflove et al. allow excellent overall accuracy and numerical stability even when the lattice truncation planes are positioned no more than 5δ from the surface of the scatterer. The conditions relate in a simple way the values of the field components at the truncation planes to the field components at points one or more δ within the lattice (or solution region).

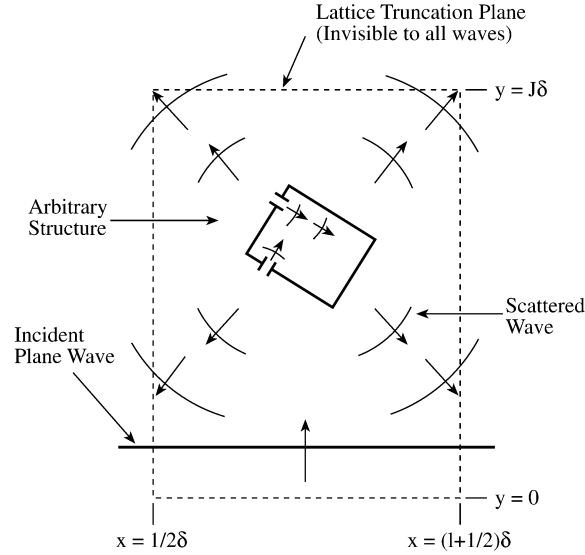


Figure 3.24
Solution region with lattice truncation.

For simplicity, we first consider one-dimensional wave propagation. Assume waves have only E_z and H_x components and propagate in the $\pm y$ directions. Also assume a time step of $\delta t = \delta y/c$, the maximum allowed by the stability condition of Eq. (3.86). If the lattice extends from $y = 0$ to $y = J\Delta y$, with E_z component at the end points, the truncation conditions are:

$$E_z^n(0) = E_z^{n-1}(1) \quad (3.87a)$$

$$E_z^n(J) = E_z^{n-1}(J-1) \quad (3.87b)$$

With these lattice conditions, all possible $\pm y$ -directed waves are absorbed at $y = 0$ and $J\Delta y$ without reflection. Equation (3.87) assumes free-space propagation. If we wish to simulate the lattice truncation in a dielectric medium of refractive index m , Eq. (3.87) is modified to

$$E_z^n(0) = E_z^{n-m}(1) \quad (3.88a)$$

$$E_z^n(J) = E_z^{n-m}(J-1) \quad (3.88b)$$

For the three-dimensional case, we consider scattered waves having all six field components and propagating in all possible directions. Assume a time-step of $\delta t = \delta/2c$, a value which is about 13% lower than the maximum allowed ($\delta t = \delta/\sqrt{3}c$) by Eq. (3.86). If the lattice occupies $\frac{1}{2}\delta < x < (I_{\max} + \frac{1}{2})\delta$, $0 < y < J_{\max}\delta$, $0 < z < K_{\max}\delta$, the truncation conditions are [36, 44]:

(a) plane $i = 1/2$

$$H_y^n(1/2, j, k + 1/2) = \frac{1}{3} \left[H_y^{n-2}(3/2, j, k - 1/2) + H_y^{n-2}(3/2, j, k + 1/2) + H_y^{n-2}(3/2, j, k + 3/2) \right], \quad (3.89a)$$

$$H_z^n(1/2, j + 1/2, k) = \frac{1}{3} \left[H_z^{n-2}(3/2, j + 1/2, k - 1) + H_z^{n-2}(3/2, j + 1/2, k) + H_z^{n-2}(3/2, j + 1/2, k + 1) \right], \quad (3.89b)$$

(b) plane $i = I_{\max} + 1/2$

$$H_y^n(I_{\max} + 1/2, j, k + 1/2) = \frac{1}{3} \left[H_y^{n-2}(I_{\max} - 1/2, j, k - 1/2) + H_y^{n-2}(I_{\max} - 1/2, j, k + 1/2) + H_y^{n-2}(I_{\max} - 1/2, j, k + 3/2) \right], \quad (3.89c)$$

$$H_z^n(I_{\max} + 1/2, j + 1/2, k) = \frac{1}{3} \left[H_z^{n-2}(I_{\max} - 1/2, j + 1/2, k - 1) + H_z^{n-2}(I_{\max} - 1/2, j + 1/2, k) + H_z^{n-2}(I_{\max} - 1/2, j + 1/2, k + 1) \right], \quad (3.89d)$$

(c) plane $j = 0$,

$$E_x^n(i + 1/2, 0, k) = E_x^{n-2}(i + 1/2, 1, k), \quad (3.89e)$$

$$E_z^n(i, 0, k + 1/2) = E_z^{n-2}(i, 1, k + 1/2), \quad (3.89f)$$

(d) plane $j = J_{\max}$

$$E_x^n(i + 1/2, J_{\max}, k) = E_x^{n-2}(i + 1/2, J_{\max} - 1, k) \quad (3.89g)$$

$$E_z^n(i, J_{\max}, k + 1/2) = E_z^{n-2}(i, J_{\max} - 1, k + 1/2), \quad (3.89h)$$

(e) plane $k = 0$,

$$E_x^n(i + 1/2, j, 0) = \frac{1}{3} \left[E_x^{n-2}(i - 1/2, j, 1) + E_x^{n-2}(i + 1/2, j, 1) + E_x^{n-2}(i + 3/2, j, 1) \right], \quad (3.89i)$$

$$E_y^n(i, j + 1/2, 0) = \frac{1}{3} \left[E_y^{n-2}(i - 1, j + 1/2, 1) + E_y^{n-2}(i, j + 1/2, 1) + E_y^{n-2}(i + 1, j + 1/2, 1) \right], \quad (3.89j)$$

(f) plane $k = K_{\max}$,

$$E_x^n(i + 1/2, j, K_{\max}) = \frac{1}{3} \left[E_x^{n-2}(i - 1/2, j, K_{\max} - 1) + E_x^{n-2}(i + 1/2, j, K_{\max} - 1) + E_x^{n-2}(i + 3/2, j, K_{\max} - 1) \right], \quad (3.89k)$$

$$E_y^n(i, j + 1/2, K_{\max}) = \frac{1}{3} \left[E_y^{n-2}(i - 1, j + 1/2, K_{\max} - 1) + E_y^{n-2}(i, j + 1/2, K_{\max} - 1) + E_y^{n-2}(i + 1, j + 1/2, K_{\max} - 1) \right] \quad (3.89l)$$

These boundary conditions minimize the reflection of any outgoing waves by simulating the propagation of the wave from the lattice plane adjacent to the lattice truncation plane in a number of time steps corresponding to the propagation delay. The averaging process is used to take into account all possible local angles of incidence of the outgoing wave at the lattice boundary and possible multiple incidences [43]. If the solution region is a dielectric medium of refractive index m rather than free space, we replace the superscript $n - 2$ in Eqs. (3.89a)–(3.89l) by $n - m$.

3.8.4 Initial Fields

The initial field components are obtained by simulating either an incident plane wave pulse or single-frequency plane wave. The simulation should not take excessive storage nor cause spurious wave-reflections. A desirable plane wave source condition takes into account the scattered fields at the source plane. For the three-dimensional case, a typical wave source condition at plane $y = j_s$ (near $y = 0$) is

$$E_z^n(i, j_s, k + 1/2) \leftarrow 1000 \sin(2\pi f n \delta t) + E_z^n(i, j_s, k + 1/2) \quad (3.90)$$

where f is the irradiation frequency. Equation (3.90) is a modification of the algorithm for all points on plane $y = j_s$; the value of the sinusoid is added to the value of E_z^n obtained from Eqs. (3.84a)–(3.84f).

At $t = 0$, the plane wave source of frequency f is assumed to be turned on. The propagation of waves from this source is simulated by time stepping, that is, repeatedly implementing Yee's finite difference algorithm on a lattice of points. The incident wave is tracked as it first propagates to the scatterer and then interacts with it via surface-current excitation, diffusion, penetration, and diffraction. Time stepping is continued until the sinusoidal steady state is achieved at each point. The field envelope, or maximum absolute value, during the final half-wave cycle of time stepping is taken as the magnitude of the phasor of the steady-state field [32, 43].

From experience, the number of time steps needed to reach the sinusoidal steady state can be greatly reduced by introducing a small isotropic conductivity σ_{ext} within the solution region exterior to the scatterer. This causes the fields to converge more rapidly to the expected steady state condition.

3.8.5 Programming Aspects

Since most EM scattering problems involve nonmagnetic media ($\mu_r = 1$), the quantity $\delta t/\mu(i, j, k)\delta$ can be assumed constant for all (i, j, k) . The nine multiplications per unit cell per time required by Yee's algorithm of Eqs. (3.84a)–(3.84f) can be reduced to six multiplications, thereby reducing computer time. Following Taflove et al. [31, 35, 44], we define the following constants:

$$R = \delta t/2\epsilon_o, \quad (3.91a)$$

$$R_a = (c\delta t/\delta)^2, \quad (3.91b)$$

$$R_b = \delta t/\mu_o\delta, \quad (3.91c)$$

$$C_a = \frac{1 - R\sigma(m)/\epsilon_r(m)}{1 + R\sigma(m)/\epsilon_r(m)}, \quad (3.91d)$$

$$C_b = \frac{R_a}{\epsilon_r(m) + R\sigma(m)} \quad (3.91e)$$

where $m = \text{MEDIA}(i, j, k)$ is an integer referring to the dielectric or conducting medium type at location (i, j, k) . For example, for a solution region comprising of three different homogeneous media shown in Fig. 3.25, m is assumed to be 1 to 3.

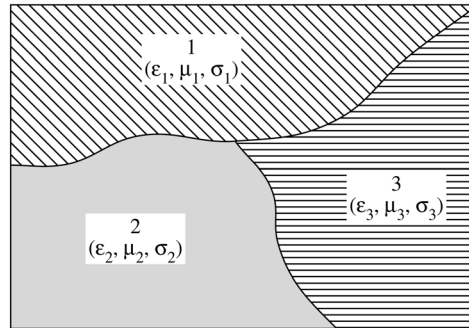


Figure 3.25

A typical inhomogeneous solution region with integer m assigned to each medium.

(This m should not be confused with the refractive index of the medium, mentioned earlier.) In addition to the constants in Eq. (3.91), we define proportional electric field

$$\tilde{\mathbf{E}} = R_b \mathbf{E} \quad (3.92)$$

Thus Yee's algorithm is modified and simplified for easy programming as [50, 51]:

$$H_x^n(i, j, k) = H_x^{n-1}(i, j, k) + \tilde{E}_y^{n-1}(i, j, k+1) - \tilde{E}_y^{n-1}(i, j, k) - \tilde{E}_z^{n-1}(i, j+1, k) + \tilde{E}_z^{n-1}(i, j, k), \quad (3.93a)$$

$$H_y^n(i, j, k) = H_y^{n-1}(i, j, k) + \tilde{E}_z^{n-1}(i+1, j, k) - \tilde{E}_z^{n-1}(i, j, k) - \tilde{E}_x^{n-1}(i, j, k+1) + \tilde{E}_x^{n-1}(i, j, k), \quad (3.93b)$$

$$H_z^n(i, j, k) = H_z^{n-1}(i, j, k) + \tilde{E}_x^{n-1}(i, j+1, k) - \tilde{E}_x^{n-1}(i, j, k) - \tilde{E}_y^{n-1}(i+1, j, k) + \tilde{E}_y^{n-1}(i, j, k), \quad (3.93c)$$

$$\begin{aligned} \tilde{E}_x^n(i, j, k) &= C_a(m)\tilde{E}_x^{n-1}(i, j, k) \\ &\quad + C_b(m) \left[H_z^{n-1}(i, j, k) - H_z^{n-1}(i, j-1, k) \right. \\ &\quad \left. - H_y^{n-1}(i, j, k) + H_y^{n-1}(i, j, k-1) \right], \end{aligned} \quad (3.93d)$$

$$\begin{aligned} \tilde{E}_y^n(i, j, k) &= C_a(m)\tilde{E}_y^{n-1}(i, j, k) \\ &\quad + C_b(m) \left[H_x^{n-1}(i, j, k) - H_x^{n-1}(i, j, k-1) \right. \\ &\quad \left. - H_z^{n-1}(i, j, k) + H_z^{n-1}(i-1, j, k) \right], \end{aligned} \quad (3.93e)$$

$$\begin{aligned} \tilde{E}_z^n(i, j, k) &= C_a(m)\tilde{E}_z^{n-1}(i, j, k) \\ &\quad + C_b(m) \left[H_y^{n-1}(i, j, k) - H_y^{n-1}(i-1, j, k) \right. \\ &\quad \left. - H_x^{n-1}(i, j, k) + H_x^{n-1}(i, j-1, k) \right] \end{aligned} \quad (3.93f)$$

The relationship between the original and modified algorithms is illustrated in Fig. 3.26 and shown in Table 3.8. Needless to say, the truncation conditions in Eqs. (3.89a)–(3.89l) must be modified accordingly. This modification eliminates the need for computer storage of separate ϵ and σ arrays; only a MEDIA array which specifies the type-integer of the dielectric or conducting medium at the location of each electric field component in the lattice need be stored. Also the programming problem of handling half integral values of i, j, k has been eliminated.

With the modified algorithm, we determine the scattered fields as follows. Let the solution region, completely enclosing the scatterer, be defined by $0 < i < I_{max}$, $0 < j < J_{max}$, $0 < k < K_{max}$. At $t \leq 0$, the program is started by setting all field components at the grip points equal to zero:

$$\tilde{E}_x^0(i, j, k) = \tilde{E}_y^0(i, j, k) = \tilde{E}_z^0(i, j, k) = 0 \quad (3.94a)$$

$$H_x^0(i, j, k) = H_y^0(i, j, k) = H_z^0(i, j, k) = 0 \quad (3.94b)$$

for $0 < i < I_{max}$, $0 < j < J_{max}$, $0 < k < K_{max}$. If we know

$$H_x^{n-1}(i, j, k), E_z^{n-1}(i, j, k),$$

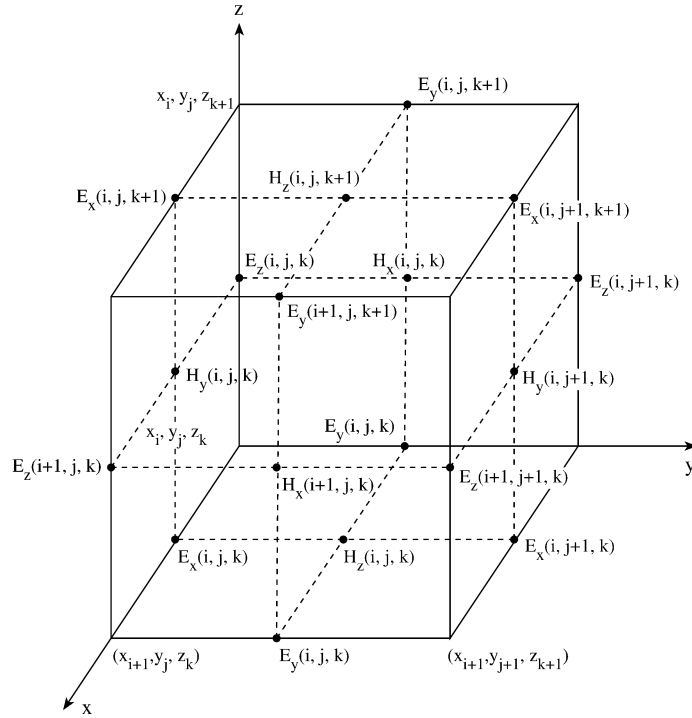


Figure 3.26
Modified node numbering.

and

$$E_y^{n-1}(i, j, k)$$

at all grid points in the solution region, we can determine new $H_x^n(i, j, k)$ everywhere from Eq. (3.93a). The same applies for finding other field components except that the lattice truncation conditions of Eqs. (3.89a)–(3.89l) must be applied when necessary. The plane wave source is activated at $t = \delta t$, the first time step, and left on during the entire run. The field components are advanced by Yee's finite difference formulas in Eqs. (3.93a)–(3.93f) and by the lattice truncation condition in Eqs. (3.89a)–(3.89l). The time stepping is continued for $t = N_{\max} \delta t$, where N_{\max} is chosen large enough that the sinusoidal steady state is achieved. In obtaining the steady state solutions, the program must not be left for too long (i.e., N_{\max} should not be too large), otherwise the imperfection of the boundary conditions causes the model to become unstable.

The FD-TD method has the following inherent advantages over other modeling techniques, such as the moment method and transmission-line modeling:

- It is conceptually simple.

Table 3.8 Relationship Between Original and Modified Field Components (lattice size = $I_{\max}\delta \times J_{\max}\delta \times K_{\max}\delta$)

Original	Modified	Limits on modified (i, j, k)
$H_x^{n+1/2}(x_i, y_{j+1/2}, z_{k+1/2})$	$H_x^n(i, j, k)$	$i = 0, \dots, I_{\max}$ $j = 0, \dots, J_{\max} - 1$ $k = 0, \dots, K_{\max} - 1$
$H_y^{n+1/2}(x_{i+1/2}, y_j, z_{k+1/2})$	$H_y^n(i, j, k)$	$i = 0, \dots, I_{\max} - 1$ $j = 0, \dots, J_{\max}$ $k = 0, \dots, K_{\max} - 1$
$H_z^{n+1/2}(x_{i+1/2}, y_{j+1/2}, z_k)$	$H_z^n(i, j, k)$	$i = 0, \dots, I_{\max} - 1$ $j = 0, \dots, J_{\max} - 1$ $k = 0, \dots, K_{\max}$
$E_x^n(x_{i+1/2}, y_j, z_k)$	$E_x^n(i, j, k)$	$i = 0, \dots, I_{\max} - 1$ $j = 0, \dots, J_{\max}$ $k = 0, \dots, K_{\max}$
$E_y^n(x_i, y_{j+1/2}, z_k)$	$E_y^n(i, j, k)$	$i = 0, \dots, I_{\max}$ $j = 0, \dots, J_{\max} - 1$ $k = 0, \dots, K_{\max}$
$E_z^n(x_i, y_j, z_{k+1/2})$	$E_z^n(i, j, k)$	$i = 0, \dots, I_{\max}$ $j = 0, \dots, J_{\max}$ $k = 0, \dots, K_{\max} - 1$

- The algorithm does not require the formulation of integral equations, and relatively complex scatterers can be treated without the inversion of large matrices.
- It is simple to implement for complicated, inhomogeneous conducting or dielectric structures because constitutive parameters (σ, μ, ϵ) can be assigned to each lattice point.
- Its computer memory requirement is not prohibitive for many complex structures of interest.
- The algorithm makes use of the memory in a simple sequential order.
- It is much easier to obtain frequency domain data from time domain results than the converse. Thus, it is more convenient to obtain frequency domain results via time domain when many frequencies are involved.

The method has the following disadvantages:

- Its implementation necessitates modeling object as well as its surroundings. Thus, the required program execution time may be excessive.
- Its accuracy is at least one order of magnitude worse than that of the method of moments, for example.

- Since the computational meshes are rectangular in shape, they do not conform to scatterers with curved surfaces, as is the case of the cylindrical or spherical boundary.
- As in all finite difference algorithms, the field quantities are only known at grid nodes.

Time-domain modeling in three dimensions involves a number of issues which are yet to be resolved even for frequency-domain modeling. Among these are whether it is best to reduce Maxwell's equations to a second-order equation for the electric (or magnetic) field or to work directly with the coupled first-order equation. The former approach is used in [35], for example, for solving the problem of EM exploration for minerals. The latter approach has been used with great success in computing EM scattering from objects as demonstrated in this section. In spite of these unresolved issues, the FD-TD algorithm has been applied to solve scattering and other problems including:

- aperture penetration [44, 52, 53],
- antenna/radiation problems [54]–[60],
- microwave circuits [63]–[68],
- eigenvalue problems [69],
- EM absorption in human tissues (bioelectromagnetics) [35, 36],[70]–[74], and
- other areas [75]–[79].

The following two examples are taken from the work of Taflove et al. [32, 43, 44]. The problems whose exact solutions are known will be used to illustrate the applications and accuracy of FD-TD algorithm.

Example 3.7

Consider the scattering of a $x + y$ -directed plane wave of frequency 2.5 GHz by a uniform, circular, dielectric cylinder of radius 6 cm. We assume that the cylinder is infinite in the z direction and that the incident fields do not vary along z . Thus $\partial/\partial z = 0$ and the problem is reduced to the two-dimensional scattering of the incident wave with only E_z , H_x , and H_y components. Our objective is to compute one of the components, say E_z , at points within the cylinder. \square

Solution

Assuming a lossless dielectric with

$$\epsilon_d = 4\epsilon_o, \quad \mu_d = \mu_o, \quad \sigma_d = 0, \quad (3.95)$$

the speed of the wave in the cylinder is

$$u_d = \frac{c}{\sqrt{\epsilon_r}} = 1.5 \times 10^8 \text{ m/s} \quad (3.96)$$

Hence $\lambda_d = u_d/f = 6 \text{ cm}$. We may select $\delta = \Delta x = \Delta y = \Delta z = \lambda_d/20 = 0.3 \text{ cm}$ and $\delta t = \delta/2c = 5 \text{ ps}$. Thus we use the two-dimensional grid of Fig. 3.27 as the solution domain. Due to the symmetry of the scatterer, the domain can be reduced relative to Fig. 3.27 to the 25×49 subdomain of Fig. 3.28. Choosing the cylinder

Assumptions:

$$E_x = E_y = 0; \quad H_z = 0$$

$$\frac{\partial}{\partial z} = 0$$

Maxwell's Equations:

$$\frac{\partial H_x}{\partial t} = -\frac{1}{\mu} \frac{\partial E_z}{\partial y}$$

$$\frac{\partial H_y}{\partial t} = \frac{1}{\mu} \frac{\partial E_z}{\partial x}$$

$$\frac{\partial E_z}{\partial t} =$$

$$\frac{1}{\epsilon} \left(\frac{\partial H_y}{\partial x} - \frac{\partial H_x}{\partial y} - \sigma E_x \right)$$

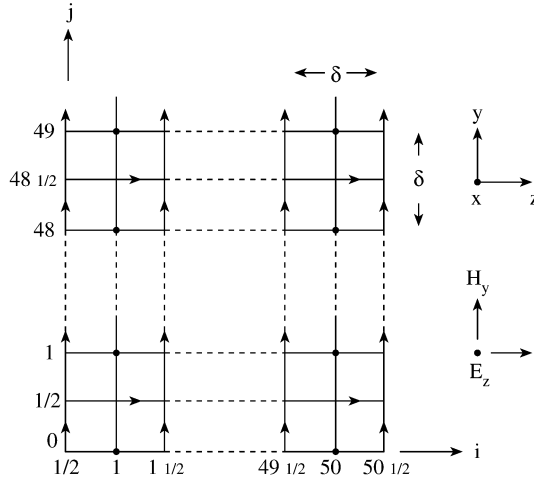


Figure 3.27
Two-dimensional lattice for Example 3.7.

axis as passing through point $(i, j) = (25.5, 24.5)$ allows the *symmetry condition* to be imposed at line $i = 26$, i.e.,

$$\tilde{E}_z^n(26, j) = \tilde{E}_z^n(25, j) \quad (3.97)$$

Soft grid truncation conditions are applied at $j = 0, 49$ and $i = 1/2$, i.e.,

$$\tilde{E}_z^n(i, 0) = \frac{1}{3} \left[\tilde{E}_z^{n-2}(i-1, 1) + \tilde{E}_z^{n-2}(i, 1) + \tilde{E}_z^{n-2}(i+1, 1) \right], \quad (3.98)$$

$$\tilde{E}_z^n(i, 49) = \frac{1}{3} \left[\tilde{E}_z^{n-2}(i-1, 48) + \tilde{E}_z^{n-2}(i, 48) + \tilde{E}_z^{n-2}(i+1, 48) \right], \quad (3.99)$$

$$H_y^n(0.5, 49) = \frac{1}{3} \left[H_y^{n-2}(1.5, j) + H_y^{n-2}(1.5, j-1) + H_y^{n-2}(1.5, j+1) \right] \quad (3.100)$$

where $n-2$ is due to the fact that $\delta = 2c\delta t$ is selected. Notice that the actual values of (i, j, k) are used here, while the modified values for easy programming are used in the program; the relationship between the two types of values is in Table 3.8.

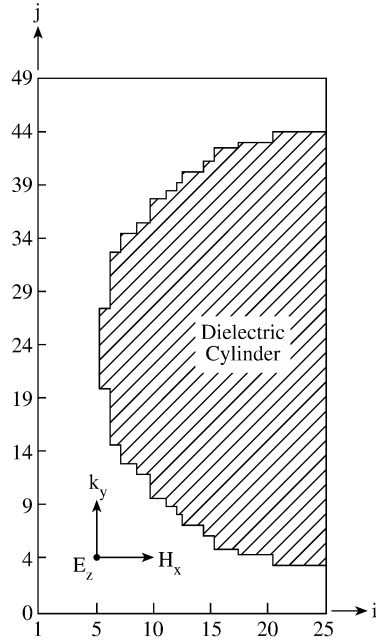


Figure 3.28
Finite difference model of cylindrical dielectric scatterer relative to the grid of Figure 3.27.

Grid points (i, j) internal to the cylinder, determined by

$$\left[(i - 25.5)^2 + (j - 24.5)^2 \right]^{1/2} \leq 20, \quad (3.101)$$

are assigned the constitutive parameters ϵ_d , μ_o , and ϵ_d , while grid points external to the cylinder are assigned parameters of free space ($\epsilon = \epsilon_o$, $\mu = \mu_o$, $\sigma = 0$).

A FORTRAN program has been developed by Bommel [80] based on the ideas expounded above. A similar but more general code is THREDE developed by Holland [50]. The program starts by setting all field components at grid points equal to zero. A plane wave source

$$\tilde{E}_z^n(i, 2) \leftarrow 1000 \sin(2\pi f n \delta t) + \tilde{E}_z^n(i, 2) \quad (3.102)$$

is used to generate the incident wave at $j = 2$ and $n = 1$, the first time step, and left on during the entire run. The program is time stepped to $t = N_{\max} \delta t$, where N_{\max} is large enough that sinusoidal steady state is achieved. Since $f = 2.5$ GHz, the wave period $T = 1/f = 400$ ps $= 80\delta t$. Hence $N_{\max} = 500 = 6.25T/\delta t$ is sufficient to reach steady state. Thus the process is terminated after 500 timesteps. Typical results are portrayed in Fig. 3.29 for the envelope of $E_z^n(15, j)$ for $460 \leq n \leq 500$. Figure 3.29 also shows the exact solution using series expansion [81]. Bommel's code has both

the numerical and exact solutions. By simply changing the constitutive parameters of the media and specifying the boundary of the scatterer (through a look-up table for complex objects), the program can be applied to almost any two-dimensional scattering or penetration problem. ■

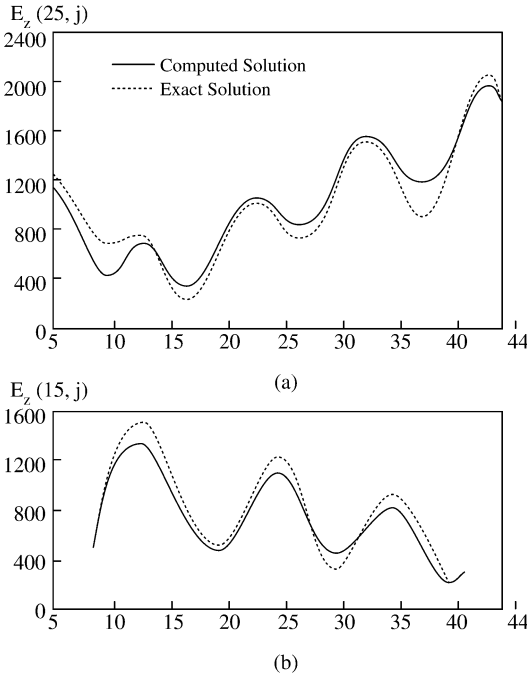


Figure 3.29
Computed internal E_z on line: (a) $i = 25$, (b) $i = 15$.

Example 3.8

Consider the penetration of a $+y$ -directed plane wave of frequency 2.5 GHz by a uniform, dielectric sphere of radius 4.5 cm. The problem is similar to the previous example except that it is three-dimensional and more general. We assume that the incident wave has only E_z and H_x components. □

Solution

Like in the previous example, we assume that internal to the lossless dielectric sphere,

$$\epsilon_d = 4\epsilon_o, \quad \mu_d = \mu_o, \quad \sigma_d = 0 \tag{3.103}$$

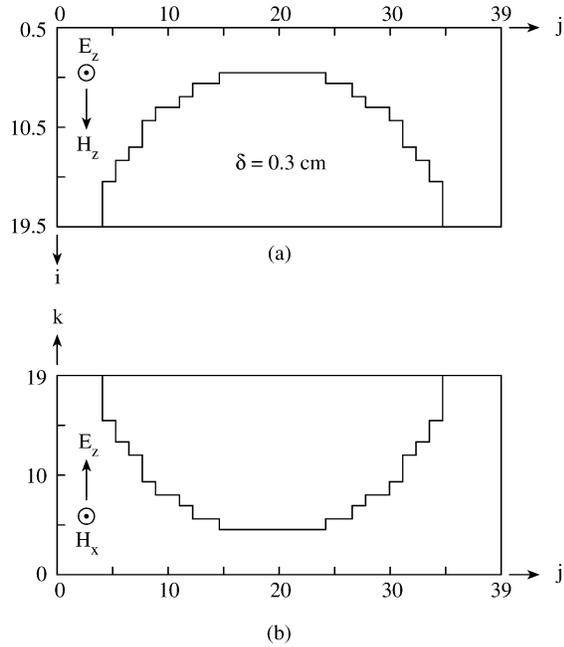


Figure 3.30
FD-TD model of dielectric sphere.

We select

$$\delta = \lambda_d/20 = 0.3 \text{ cm} \quad (3.104)$$

and

$$\delta t = \delta/2c = 5 \text{ ps} \quad (3.105)$$

This choice of the grid size implies that the radius of the sphere is $4.5/0.3 = 15$ units. The sphere model centered at grid point $(19.5, 20, 19)$ in a $19 \times 39 \times 19$ lattice is portrayed in Fig. 3.30 at two lattice symmetry planes $k = 19$ and $i = 19.5$. Grid points (i, j, k) internal to the sphere are determined by

$$\left[(i - 19.5)^2 + (j - 20)^2 + (k - 19)^2 \right]^{1/2} \leq 15 \quad (3.106)$$

Rather than assigning $\sigma = 0$ to points external to the sphere, a value $\sigma = 0.1 \text{ mho/m}$ is assumed to reduce spurious wave reflections. The FORTRAN code shown in Fig. 3.31, a modified version of Bommel's [80], is used to generate field components E_y and E_z near the sphere irradiation axis. With the dimensions and constitutive parameters of the sphere specified as input data, the program is developed based on the following steps:

1. Compute the parameters of each medium using Eq. (3.91) where $m = 1, 2$.
2. Initialize field components.
3. Use the FD-TD algorithm in Eqs. (3.93a)–(3.93f) to generate field components. This is the heart of the program. It entails taking the following steps:
 - (i) Calculate actual values of grid point (x, y, z) using the relationship in Table 3.8. This will be needed later to identify the constitutive parameters of the medium at that point using subroutine MEDIA.
 - (ii) Apply soft lattice truncation conditions in Eqs. (3.89a)–(3.89l) at appropriate boundaries, i.e., at $x = \delta/2, y = 0, y_{\max}$, and $z = 0$. Notice that some of the conditions in Eqs. (3.89a)–(3.89l) are not necessary in this case because we restrict the solution to one-fourth of the sphere due to geometrical symmetry. At other boundaries ($x = x_{\max}$ and $z = z_{\max}$), the symmetry conditions are imposed. For example, at $k = 19$,

$$\tilde{E}_x^n(i, j, 20) = \tilde{E}_x^n(i, j, 18)$$

- (iii) Apply FD-TD algorithm in Eqs. (3.93a)–(3.93f).
- (iv) Activate the plane wave source, i.e.,

$$\tilde{E}_z^n(i, j, k) \leftarrow \sin(2\pi f n \delta t) + \tilde{E}_z^n(i, j_s, k)$$

where $j_s = 3$ or any plane near $y = 0$.

- (v) Time step until steady state is reached.

4. Obtain the maximum absolute values (envelopes) of field components in the last half-wave and output the results.

Figure 3.32 illustrates the results of the program. The values of $|E_y|$ and $|E_z|$ near the sphere axis are plotted against j for observation period $460 \leq n \leq 500$. The computed results are compared with Mie's exact solution [82] covered in Section 2.8. The code for calculating the exact solution is also found in Bommel's work [80]. ■

3.9 Absorbing Boundary Conditions for FDTD

The finite difference time domain (FDTD) method is a robust, flexible (adaptable to complex geometries), efficient, versatile, easy-to-understand, easy-to-implement, and user-friendly technique to solve Maxwell's equations in the time domain. Although the method did not receive much attention it deserved when it was suggested, it is now becoming the most popular method of choice in computational EM. It is finding

```

0001 C*****
0002 C APPLICATION OF THE FINITE DIFFERENCE METHOD
0003 C This program involves the penetration of a
0004 C lossless dielectric SPHERE by a plane wave.
0005 C The program provides in the maximum absolute value of
0006 C Ey and Ez during the final half-wave of time-stepping
0007 C Assumption:
0008 C +y-directed incident wave with components Ez and Hx.
0009 C I,J,K,NN correspond to X,Y,Z, and Time.
0010 C IMAX,JMAX,KMAX are the maximum values of x,y,z
0011 C NNMAX is the total number of timesteps.
0012 C NNW represents one half-wave cycle.
0013 C MED is the number of different uniform media
      sections.
0014 C JS is the j-position of the plane wave front.
0015 C
0016 C THIS PROGRAM WAS DEVELOPED BY V. BEMMEL [80]
0017 C AND LATER IMPROVED BY D. TERRY
0018 C*****
0019
0020 PARAMETER( IMAX=19, JMAX=39, KMAX=19)
0021 PARAMETER( NNMAX=500, NNW=40, MED=2, JS=3 )
0022 PARAMETER( DELTA=3E-3, CL=3.0E8, F=2.5E9 )
0023 PARAMETER( PIE=3.141592654)
0024
0025 C Define scatterer dimensions
0026 PARAMETER( OI=19.5, OJ=20.0, OK=19.0, RADIUS=15.0)
0027
0028 DIMENSION EX(0:IMAX+1, 0:JMAX+1, 0:KMAX+1, 0:NNMAX),
0029 & EY(0:IMAX+1, 0:JMAX+1, 0:KMAX+1, 0:NNMAX),
0030 & EZ(0:IMAX+1, 0:JMAX+1, 0:KMAX+1, 0:NNMAX),
0031 & HX(0:IMAX+1, 0:JMAX+1, 0:KMAX+1, 0:NNMAX),
0032 & HY(0:IMAX+1, 0:JMAX+1, 0:KMAX+1, 0:NNMAX),
0033 & HZ(0:IMAX+1, 0:JMAX+1, 0:KMAX+1, 0:NNMAX),
0034 & EY1(0:JMAX+1), EZ1(0:JMAX+1),
0035 & ER(MED), SIG(MED), CA(MED), CB(MED)
0036
0037 DIMENSION IXMED(0:IMAX+1, 0:JMAX+1, 0:KMAX+1)
0038 DIMENSION IYMED(0:IMAX+1, 0:JMAX+1, 0:KMAX+1)
0039 DIMENSION IZMED(0:IMAX+1, 0:JMAX+1, 0:KMAX+1)
0040
0041 DIMENSION CBMRB( 2 ) ! STORE CB(M)/RB HERE
0042 DATA ER/1.0,4.0/ ! CONSTITUTIVE PARAMETERS
0043 DATA SIG/0.1,0.0/
0044 C
0045 C Statement function to compute position w.r.t. center
      of sphere
0046 C
0047 position(RI,RJ,RK)=SQRT((RI-OI)**2+(RJ-OJ)
      **2+(RK-OK)**2)
0048
0049 EO=(1E-9)/(36*PIE)
0050 UO=(1E-7)*4*PIE
0051 DT=DELTA/(2*CL)
0052 RA=(DT**2)/(UO*EO*(DELTA**2))
0053 RB=DT/(UO*DELTA)
0054 TPIFDT = 2.0*PIE*F*DT

```

Figure 3.31
Computer program for FDTD three-dimensional scattering problem (*Continued*).

```

0055 C*****
0056 C STEP # 1 - COMPUTE MEDIA PARAMETERS
0057 C*****
0058     DO 1 M=1,MED
0059         CA(M)=1.0-R*SIG(M)/ER(M)
0060         CB(M)=RA/ER(M)
0061         CBMRB(M) = CB(M)/RB
0062     1   CONTINUE
0063 C
0064 C (i) CALCULATE THE REAL/ACTUAL GRID POINTS
0065 C
0066 C Initialize the media arrays.Index (M) determines which
0067 C medium each point is actually located in and is used to
0068 C index into arrays which determine the constitutive
0069 C parameters of the medium.There are separate M
    determining
0070 C arrays for EX, EY, and EZ. These arrays correlate the
0071 C integer values of I,J,K to the actual position within
0072 C the lattice.Computing these values now and storing them
    in these
0073 C arrays as opposed to computing them each time they are
0074 C needed saves a large amount of computation time.
0075 C
0076     DO 3 I=0, IMAX+1
0077     DO 3 J=0, JMAX+1
0078     DO 3 K=0, KMAX+1
0079     IF(position(float(I)+0.5,float(J),float(K))
    .LE.RADIUS) then
0080         IXMED( I, J, K ) = 2
0081     else
0082         IXMED( I, J, K ) = 1
0083     endif
0084     IF(position(float(I),float(J)+0.5,float(K))
    .LE.RADIUS) then
0085         IYMED( I, J, K ) = 2
0086     else
0087         IYMED( I, J, K ) = 1
0088     endif
0089     IF(position(float(I),float(J),float(K)+0.5)
    .LE.RADIUS) then
0090         IZMED( I, J, K ) = 2
0091     else
0092         IZMED( I, J, K ) = 1
0093     endif
0094     3   CONTINUE

0095 C*****
0096 C STEP # 2 - INITIALIZE FIELD COMPONENTS
0097 C*****
0098 C components for output
0099     DO 4 J=0,JMAX+1
0100         EY1(J)=0.
0101         EZ1(J)=0.
0102     4   CONTINUE
0103
0104     DO 5 I=0,IMAX+1
0105     DO 5 J=0,JMAX+1
0106     DO 5 K=0,KMAX+1
0107     DO 5 N = 0, NMAX
0108         EX(I,J,K,N)=0.
0109         EY(I,J,K,N)=0.

```

Figure 3.31

(Cont.) Computer program for FDTD three-dimensional scattering problem
(Continued).

```

0110         EZ(I,J,K,N)=0.
0111         HX(I,J,K,N)=0.
0112         HY(I,J,K,N)=0.
0113         HZ(I,J,K,N)=0.
0114     5     CONTINUE
0115         print *, 'initialization complete'

0116     C*****
0117     C STEP # 3 - USE FD/TD ALGORITHM TO GENERATE
0118     C FIELD COMPONENTS
0119     C*****
0120     C SINCE ONLY FIELD COMPONENTS AT CURRENT TIME (t) AND
0121     C TWO TIME STEPS ( t-1 AND t-2) ARE REQUIRED FOR
0122     C COMPUTATION,
0123     C WE SAVE MEMORY SPACE BY USING THE FOLLOWING INDICES
0124     C   NCUR is index in for time t
0125     C   NPR1 is index in for t-1
0126     C   NPR2 is index in for t-2
0127     C
0128     C   NCUR = 2
0129     C   NPR1 = 1
0130     C   NPR2 = 0
0131     C   DO 15 NN = 1, NNMAX ! TIME LOOP
0132     C   IF (MOD( NN,10).EQ.0) THEN
0133     C   print *, 'NN=', NN ! DISPLAY PROGRESS
0134     C   ENDDIF
0135     C   Next time step - move indices up a notch.
0136     C   NPR2 = NPR1
0137     C   NPR1 = NCUR
0138     C   NCUR = MOD( NCUR+1, 3)
0139     C   DO 20 K=0, KMAX ! Z LOOP
0140     C   DO 25 J=0, JMAX ! Y LOOP
0141     C   DO 30 I=0, IMAX ! X LOOP
0142     C
0143     C (ii)-APPLY SOFT LATTICE TRUNCATION CONDITIONS
0144     C
0145     C---x=delta/2
0146     C   IF(I.EQ.0) THEN
0147     C   IF ((K.NE.KMAX).AND.(K.NE.0)) THEN
0148     C   HY(0,J,K,NCUR) = (HY(1,J,K-1,NPR2)
0149     C   + HY(1,J,K,NPR2)+HY(1,J,K+1,NPR2))/3.
0150     C   HZ(0,J,K,NCUR)=(HZ(1,J,K-1,NPR2)
0151     C   + HZ(1,J,K,NPR2)+HZ(1,J,K+1,NPR2))/3.
0152     C   else
0153     C   IF (K.EQ.KMAX) THEN
0154     C   HY(0,J,KMAX,NCUR) = (HY(1,J,KMAX-1,NPR2)
0155     C   + HY(1,J,KMAX,NPR2))/2.
0156     C   HZ(0,J,K,NCUR)=( HZ(1,J,K-1,NPR2)
0157     C   + HZ(1,J,K,NPR2) )/2.
0158     C   ELSE
0159     C   HY(0,J,K,NCUR) = ( HY(1,J,K,NPR2)
0160     C   + HY(1,J,K+1,NPR2))/2.
0161     C   HZ(0,J,0,NPR2)=(HZ(1,J,0,NPR2)
0162     C   + HZ(1,J,1,NPR2))/2.
0163     C   ENDDIF
0164     C   ENDDIF
0165     C---y=0
0166     C   IF(J.EQ.0) THEN
0167     C   EX(I,0,K,NCUR)=EX(I,1,K,NPR2)
0168     C   EZ(I,0,K,NCUR)=EZ(I,1,K,NPR2)

```

Figure 3.31

(Cont.) Computer program for FDTD three-dimensional scattering problem
(Continued).

```

0169             ELSE
0170 C---y=ymax
0171     IF(J.EQ.JMAX) THEN
0172     EX(I,JMAX,K,NCUR)=EX(I,JMAX-1,K,NPR2)
0173     EZ(I,JMAX,K,NCUR)=EZ(I,JMAX-1,K,NPR2)
0174     ENDIF
0175     ENDIF
0176 C---z=0
0177     IF(K.EQ.0) THEN
0178     IF ((I.NE.0).AND.(I.NE.IMAX)) THEN
0179     EX(I,J,O,NCUR) = (EX(I-1,J,1,NPR2)
0180     & + EX(I,J,1,NPR2)+EX(I+1,J,1,NPR2))/3.
0181     EY(I,J,O,NCUR) = (EY(I-1,J,1,NPR2)
0182     & + EY(I,J,1,NPR2)+EY(I+1,J,1,NPR2))/3.
0183     ELSE
0184     IF(I.EQ.0) THEN
0185     EX(0,J,O,NCUR)=(EX(0,J,1,NPR2)+EX(1,J,1,NPR2))/2.
0186     EY(I,J,O,NCUR)=(EY(I,J,1,NPR2)+EY(I+1,J,1,NPR2))/2.
0187     ELSE
0188     EX(I,J,O,NCUR)=(EX(I-1,J,1,NPR2)+EX(I,J,1,NPR2))/2.
0189     EY(I,J,O,NCUR)=(EY(I-1,J,1,NPR2)+EY(I,J,1,NPR2))/2.
0190     ENDIF
0191     ENDIF
0192     ENDIF
0193 C
0194 C (iii) APPLY FD/TD ALGORITHM
0195 C
0196 C-----a. HX generation:
0197     HX(I,J,K,NCUR)=HX(I,J,K,NPR1)+RB*(EY(I,J,K+1,NPR1)
0198     & - EY(I,J,K,NPR1)+EZ(I,J,K,NPR1)-EZ(I,J+1,K,NPR1))
0199 C-----b. HY generation:
0200     HY(I,J,K,NCUR)=HY(I,J,K,NPR1)+RB*(EZ(I+1,J,K,NPR1)
0201     & - EZ(I,J,K,NPR1)+EX(I,J,K,NPR1)-EX(I,J,K+1,NPR1))
0202 C-----c. HZ generation:
0203     HZ(I,J,K,NCUR)=HZ(I,J,K,NPR1)+RB*(EX(I,J+1,K,NPR1)
0204     & - EX(I,J,K,NPR1)+EY(I,J,K,NPR1)-EY(I+1,J,K,NPR1))
0205 C---k=kmax ! SYMMETRY
0206     IF(K.EQ.KMAX) THEN
0207     HX(I,J,KMAX,NCUR)=HX(I,J,KMAX-1,NCUR)
0208     HY(I,J,KMAX,NCUR)=HY(I,J,KMAX-1,NCUR)
0209     ENDIF
0210 C-----d. EX generation:
0211     IF((J.NE.0).AND.(J.NE.JMAX).AND.(K.NE.0)) THEN
0212     M = IYMED( I, J, K )
0213     EX(I,J,K,NCUR) = CA(M)*EX(I,J,K,NPR1) + CBMRB(M)*
0214     & (HZ(I,J,K,NCUR)-HZ(I,J-1,K,NCUR)+HY(I,J,K-1,NCUR)
0215     & -HY(I,J,K,NCUR))
0216     ENDIF
0217 C-----e. EY generation:
0218     IF(K.NE.0) THEN
0219     M = IYMED( I, J, K )
0220     EY(I,J,K,NCUR)=CA(M)*EY(I,J,K,NPR1) + CBMRB(M)*
0221     & HX(I,J,K,NCUR)-HX(I,J,K-1,NCUR)+HZ(I-1,J,K,NCUR)
0222     & -HZ(I,J,K,NCUR))
0223     ENDIF
0224 C-----f. EZ generation:
0225     IF ((J.NE.0).AND.(J.NE.JMAX)) THEN
0226     M = IZMED( I, J, K )
0227 C sig(ext)=0 for Ez only from Taflove[14]
0228     IF(M.EQ.1) THEN
0229     CAM=1.0
0230     ELSE

```

Figure 3.31

(Cont.) Computer program for FDTD three-dimensional scattering problem
(Continued).

```

0231         CAM=CA(M)
0232         ENDIF
0233         EZ(I,J,K,NCUR)=CAM*EZ(I,J,K,NCUR)+CBMRB(M)*
0234         * (HY(I,J,K,NCUR)-HY(I-1,J,K,NCUR)+HX(I,J-1,K,NCUR)
0235         * -HX(I,J,K,NCUR))
0236     C
0237     C (iv) APPLY THE PLANE-WAVE SOURCE
0238     C
0239         IF(J.EQ.JS) THEN
0240             EZ(I,JS,K,NCUR) = EZ(I,JS,K,NCUR)+SIN( TPIFDT*NN )
0241         ENDIF
0242         ENDIF
0243     C---i=imax+1/2 ! SYMMETRY
0244         IF(I.EQ.IMAX) THEN
0245             EY(IMAX+1,J,K,NCUR)=EY(IMAX,J,K,NCUR)
0246             EZ(IMAX+1,J,K,NCUR)=EZ(IMAX,J,K,NCUR)
0247         ENDIF
0248     C---k=kmax
0249         IF(K.EQ.KMAX) THEN
0250             EX(I,J,KMAX+1,NCUR)=EX(I,J,KMAX-1,NCUR)
0251             EY(I,J,KMAX+1,NCUR)=EY(I,J,KMAX-1,NCUR)
0252         ENDIF
0253     30 CONTINUE ! I LOOP

0254     C*****
0255     C STEP # 4 - RETAIN THE MAXIMUM ABSOLUTE VALUES DURING
0256     C THE LAST HALF-WAVE
0257     C*****
0258         IF ( (K.EQ.KMAX).AND.(NN.GT.(NNMAX-NHW)) ) THEN
0259             TEMP = ABS( EY(IMAX,J,KMAX-1,NCUR) )
0260             IF (TEMP .GT. EY1(J) ) THEN
0261                 EY1(J) = TEMP
0262             ENDIF
0263             TEMP = ABS( EZ(IMAX,J,KMAX,NCUR) )
0264             IF (TEMP .GT. EZ1(J) ) THEN
0265                 EZ1(J) = TEMP
0266             ENDIF
0267         ENDIF
0268     25 CONTINUE ! J LOOP
0269     20 CONTINUE ! K LOOP
0270     15 CONTINUE ! NN (time) LOOP
0271     C*****
0272     C----Output E as a function of j
0273         DO 130 J = 0, JMAX-1
0274             WRITE(6,135) J+1, float(J), EY1(J)
0275     130 CONTINUE
0276         DO 140 J = 0, JMAX-1
0277             WRITE(6,135) J+1, float(J), EZ1(J)
0278     140 CONTINUE
0279     135 FORMAT(I5,2F15.8)
0280     STOP
0281     END

```

Figure 3.31

(Cont.) Computer program for FDTD three-dimensional scattering problem.

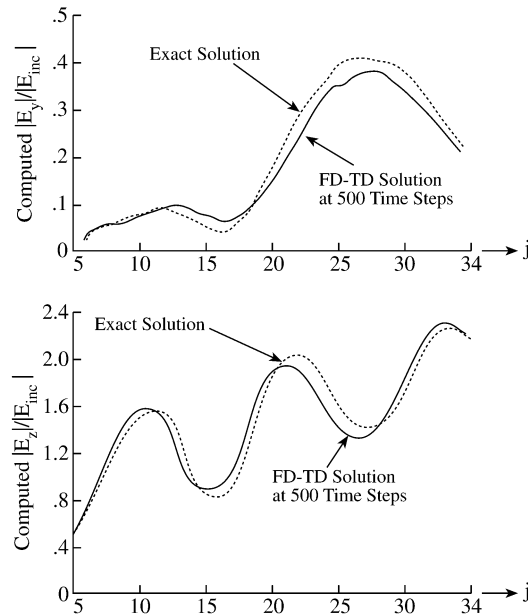


Figure 3.32

Computed $E_y(19.5, j, 18)$ and $E_z(19, j, 18.5)$ within the lossless dielectric sphere.

widespread use for solving open-region scattering, radiation, penetration/absorption, electromagnetic interference (EMI), electromagnetic compatibility (EMC), diffusion, transient, bioelectromagnetics, and microwave circuit modeling problems. However, the method exhibits some problems such as slow convergence for solving resonant structures, requirement of large memory for inhomogeneous waveguide structures due to the necessity of a full-wave analysis, inability to properly handle curved boundaries due to its orthogonal nature, low stability, and low accuracy unless fine mesh is used, to mention a few. These problems prohibit the application of the standard FDTD technique and have led to various forms of its modifications [83]–[93] and hybrid FDTD methods [94]–[96]. Although these new FDTD methods have enhanced the standard FDTD (increase accuracy and stability, etc.), some researchers still prefer the standard FDTD.

One of the major problems inherent in the standard FDTD, however, is that the requirement for artificial mesh truncation (boundary) condition. The artificial termination truncates the solution region electrically close to the radiating/scattering object but effectively simulates the solution to infinity. These artificial termination conditions are known as *absorbing boundary conditions* (ABCs) as they theoretically absorb incident and scattered fields. The accuracy of the ABC dictates the accuracy of the FDTD method. The need for accurate ABCs has resulted in various types of ABCs [97]–[107], which are fully discussed in [104]. Due to space limitation, we will

only consider Berenger's *perfectly matched layer* (PML) type of ABC [100]–[104] since PML has been the most widely accepted and is set to revolutionize the FDTD method.

In the perfectly matched layer (PML) truncation technique, an artificial layer of absorbing material is placed around the outer boundary of the computational domain. The goal is to ensure that a plane wave that is incident from FDTD free space to the PML region at an arbitrary angle is completely absorbed there without reflection. This is the same as saying that there is complete transmission of the incident plane wave at the interface between free space and the PML region (see Fig. 3.33). Thus the FDTD and the PML region are said to be *perfectly matched*.

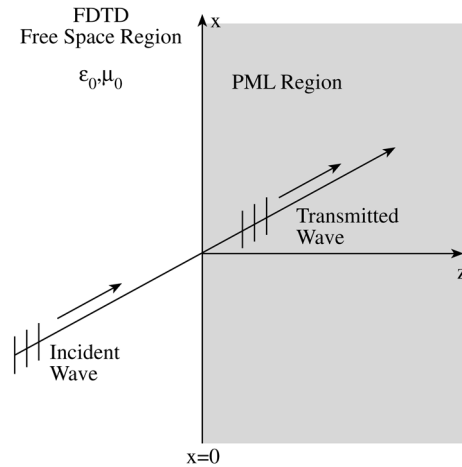


Figure 3.33
Reflectionless transmission of a plane wave at a PML/free-space interface.

To illustrate the PML technique, consider Maxwell's equation in two dimensions for transverse electric (TE) case with field components E_x , E_y and H_z and no variation with z . Expanding Eqs. (1.22c) and (1.22d) in Cartesian coordinates and setting $E_z = 0 = \frac{\partial}{\partial z}$, we obtain

$$\epsilon_o \frac{\partial E_x}{\partial t} + \sigma E_x = \frac{\partial H_z}{\partial y} \quad (3.107a)$$

$$\epsilon_o \frac{\partial E_y}{\partial t} + \sigma E_y = -\frac{\partial H_z}{\partial x} \quad (3.107b)$$

$$\mu_o \frac{\partial H_z}{\partial t} + \sigma^* H_z = \frac{\partial E_x}{\partial y} - \frac{\partial E_y}{\partial x} \quad (3.107c)$$

where the PML, as a lossy medium, is characterized by an electrical conductivity σ

and a magnetic conductivity σ^* . The conductivities are related as

$$\frac{\sigma}{\epsilon_0} = \frac{\sigma^*}{\mu_0} \quad (3.108)$$

This relationship ensures a required level of attenuation and forces the wave impedance of the PML to be equal to that of free space. Thus a reflectionless transmission of a plane wave propagation across the interface is permitted. For oblique incident angles, the conductivity of the PML must have a certain anisotropy characteristic to ensure reflectionless transmission. To achieve this, the H_z component must be split into two subcomponents, H_{zx} and H_{zy} , with the possibility of assigning losses to the individual split field components. This is the cornerstone of the PML technique. It leads to four components E_x , E_y , H_{zx} , and H_{zy} and four (rather than the usual three) coupled field equations.

$$\epsilon_0 \frac{\partial E_x}{\partial t} + \sigma_y E_x = \frac{\partial(H_{zx} + H_{zy})}{\partial y} \quad (3.109a)$$

$$\epsilon_0 \frac{\partial E_y}{\partial t} + \sigma_x E_y = -\frac{\partial(H_{zx} + H_{zy})}{\partial x} \quad (3.109b)$$

$$\mu_0 \frac{\partial H_{zx}}{\partial t} + \sigma_x^* H_{zx} = -\frac{\partial E_y}{\partial x} \quad (3.109c)$$

$$\mu_0 \frac{\partial H_{zy}}{\partial t} + \sigma_y^* H_{zy} = \frac{\partial E_x}{\partial y} \quad (3.109d)$$

These equations can be discretized to provide the FDTD time-stepping equations for the PML region. The standard Yee time-stepping cannot be used because of the rapid attenuation to outgoing waves afforded by a PML medium. We use the exponentially differenced equations to preclude any possibility of diffusion instability. In the usual FDTD notations, the resulting four time-stepping equations for the PML region are [101]:

$$\begin{aligned} E_x^{n+1}(i + 1/2, j) &= e^{-\sigma_y(j)\delta t/\epsilon_0} E_x^n(i + 1/2, j) \\ &+ \frac{(1 - e^{-\sigma_y(j)\delta t/\epsilon_0})}{\sigma_y(j)\delta} \left[H_{zx}^{n+1/2}(i + 1/2, j + 1/2) + H_{zy}^{n+1/2}(i + 1/2, j + 1/2) \right. \\ &\left. - H_{zx}^{n+1/2}(i + 1/2, j - 1/2) - H_{zy}^{n+1/2}(i + 1/2, j - 1/2) \right] \end{aligned} \quad (3.110a)$$

$$\begin{aligned} E_y^{n+1}(i, j + 1/2) &= e^{-\sigma_x(i)\delta t/\epsilon_0} E_y^n(i, j + 1/2, k) \\ &+ \frac{(1 - e^{-\sigma_x(i)\delta t/\epsilon_0})}{\sigma_x(i)\delta} \left[H_{zx}^{n+1/2}(i - 1/2, j + 1/2) + H_{zy}^{n+1/2}(i - 1/2, j + 1/2) \right. \\ &\left. - H_{zx}^{n+1/2}(i + 1/2, j + 1/2) - H_{zy}^{n+1/2}(i + 1/2, j + 1/2) \right] \end{aligned} \quad (3.110b)$$

$$H_{zx}^{n+1/2}(i+1/2, j+1/2) = e^{-\sigma_x^*(i+1/2)\delta t/\mu_0} H_{zx}^{n-1/2}(i+1/2, j+1/2) + \frac{(1 - e^{-\sigma_x^*(i+1/2)\delta t/\mu_0})}{\sigma_x^*(i+1/2)\delta} [E_y^n(i, j+1/2) - E_y^n(i+1, j+1/2)] \quad (3.110c)$$

$$H_{zy}^{n+1/2}(i+1/2, j+1/2) = e^{-\sigma_y^*(i+1/2)\delta t/\mu_0} H_{zy}^{n-1/2}(i+1/2, j+1/2) + \frac{(1 - e^{-\sigma_y^*(i+1/2)\delta t/\mu_0})}{\sigma_y^*(i+1/2)\delta} [E_x^n(i+1/2, j+1) - E_x^n(i+1/2, j)] \quad (3.110d)$$

These equations can be directly implemented in an FDTD simulation to model PML medium. All that is required to select the depth of the PML and its conductivity. In theory, the PML could δ deep and have near-infinite conductivity. It has been shown, however, that increasing the conductivity gradually with depth minimizes reflections; hence the “layering” of the medium and the dependence of σ on i and j .

The TM case can be obtained by duality, with E_z split so that $E_z = E_{zx} + E_{zy}$. In three dimensions, all six Cartesian field components are split so that the resulting PML modification of Maxwell’s equations yields 12 equations [104].

3.10 Finite Differencing for Nonrectangular Systems

So far in this chapter, we have considered only rectangular solution regions within which a rectangular grid can be readily placed. Although we can always replace a nonrectangular solution region by an approximate rectangular one, our discussion in this chapter would be incomplete if we failed to apply the method to nonrectangular coordinates since it is sometimes preferable to use these coordinates. We will demonstrate the finite differencing technique in cylindrical coordinates (ρ, ϕ, z) and spherical coordinates (r, θ, ϕ) by solving Laplace’s equation $\nabla^2 V = 0$. The idea is readily extended to other PDEs.

3.10.1 Cylindrical Coordinates

Laplace’s equation in cylindrical coordinates can be written as

$$\nabla^2 V = \frac{\partial^2 V}{\partial \rho^2} + \frac{1}{\rho} \frac{\partial V}{\partial \rho} + \frac{1}{\rho^2} \frac{\partial^2 V}{\partial \phi^2} + \frac{\partial^2 V}{\partial z^2}. \quad (3.111)$$

Refer to the cylindrical system and finite difference molecule shown in Fig. 3.34. At point $O(\rho_o, \phi_o, z_o)$, the equivalent finite difference approximation is

$$\frac{V_1 - 2V_o + V_2}{(\Delta\rho)^2} + \frac{1}{\rho_o} \frac{V_1 - V_2}{2\Delta\rho} + \frac{V_3 - 2V_o + V_4}{(\rho_o\Delta\phi)^2} + \frac{V_5 - 2V_o + V_6}{(\Delta z)^2} = 0 \quad (3.112)$$

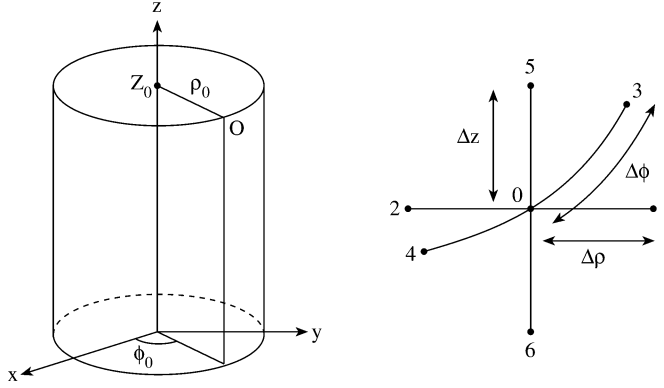


Figure 3.34
Typical node in cylindrical coordinate.

where $\Delta\rho$, $\Delta\phi$ and Δz are the step sizes along ρ , ϕ , and z , respectively, and

$$\begin{aligned} V_o &= V(\rho_o, \phi_o, z_o), \quad V_1 = V(\rho_o + \Delta\rho, \phi_o, z_o), \quad V_2 = V(\rho_o - \Delta\rho, \phi_o, z_o), \\ V_3 &= V(\rho_o, \phi_o + \rho_o \Delta\phi, z_o), \quad V_4 = V(\rho_o, \phi_o - \rho_o \Delta\phi, z_o), \\ V_5 &= V(\rho_o, \phi_o, z_o + \Delta z), \quad V_6 = V(\rho_o, \phi_o, z_o - \Delta z) \end{aligned} \quad (3.113)$$

We now consider a special case of Eq. (3.112) for an axisymmetric system [108]. In this case, there is no dependence on ϕ so that $V = V(\rho, z)$. If we assume square nets so that $\Delta\rho = \Delta z = h$, the solution region is discretized as in Fig. 3.35 and Eq. (3.112) becomes

$$\left(1 + \frac{h}{2\rho_o}\right) V_1 + \left(1 - \frac{h}{2\rho_o}\right) V_2 + V_5 + V_6 - 4V_o = 0 \quad (3.114)$$

If point O is at $(\rho_o, z_o) = (ih, jh)$, then

$$1 + \frac{h}{2\rho_o} = \frac{2i+1}{2i}, \quad 1 - \frac{h}{2\rho_o} = \frac{2i-1}{2i}$$

so that Eq. (3.114) becomes

$$\boxed{V(i, j) = \frac{1}{4} \left[V(i, j-1) + V(i, j+1) + \left(\frac{2i-1}{2i}\right) V(i-1, j) + \left(\frac{2i+1}{2i}\right) V(i+1, j) \right]} \quad (3.115)$$

Notice that in Eq. (3.114), it appears we have a singularity for $\rho_o = 0$. However, by symmetry, all odd order derivatives must be zero. Hence

$$\left. \frac{\partial V}{\partial \rho} \right|_{\rho=0} = 0 \quad (3.116)$$

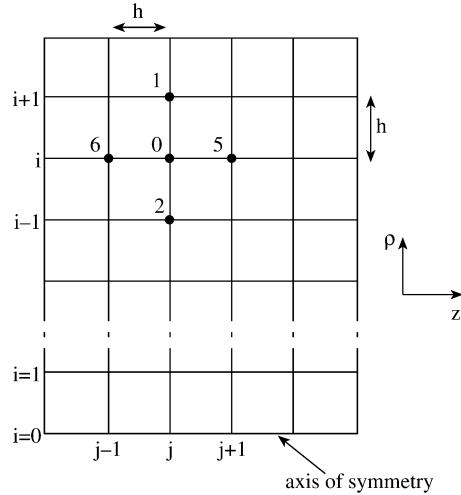


Figure 3.35
Finite difference grid for an axisymmetric system.

since

$$V(\Delta\rho, z_o) = V(-\Delta\rho, z_o) \quad (3.117)$$

Therefore by L'Hopital's rule,

$$\lim_{\rho_o \rightarrow 0} \frac{1}{\rho_o} \frac{\partial V}{\partial \rho} \Big|_{\rho_o} = \frac{\partial^2 V}{\partial \rho^2} \Big|_{\rho_o} \quad (3.118)$$

Thus, at $\rho = 0$, Laplace's equation becomes

$$2 \frac{\partial^2 V}{\partial \rho^2} + \frac{\partial^2 V}{\partial z^2} = 0 \quad (3.119)$$

The finite difference equivalent to Eq. (3.119) is

$$V_o = \frac{1}{6}(4V_1 + V_5 + V_6)$$

or

$$V(0, j) = \frac{1}{6} [V(0, j-1) + V(0, j+1) + 4V(1, j)] \quad (3.120)$$

which is used at $\rho = 0$.

To solve Poisson's equation $\nabla^2 V = -\rho_v/\epsilon$ in cylindrical coordinates, we obtain the finite difference form by replacing zero on the right-hand side of Eq. (3.112) with $g = -\rho_v/\epsilon$. We obtain

$$V(i, j) = \frac{1}{4} \left[V(i, j+1) + V(i, j-1) + \frac{2i-1}{2i} V(i-1, j) + \frac{2i+1}{2i} V(i+1, j) + gh^2 \right] \quad (3.121)$$

where h is the step size.

As in Section 3.7.1, the boundary condition $D_{1n} = D_{2n}$ must be imposed at the interface between two media. As an alternative to applying Gauss's law as in Section 3.7.1, we will apply Taylor series expansion [109]. Applying the series

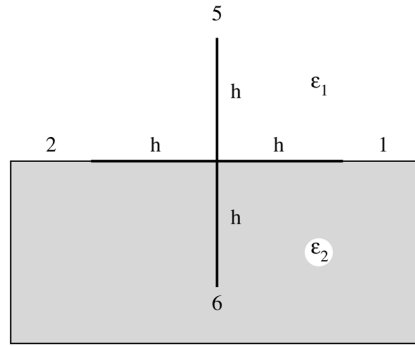


Figure 3.36
Interface between two dielectric media.

expansion to point 1, 2, 5 in medium 1 in Fig. 3.36, we obtain

$$\begin{aligned} V_1 &= V_o + \frac{\partial V_o^{(1)}}{\partial \rho} h + \frac{\partial^2 V_o^{(1)}}{\partial \rho^2} \frac{h^2}{2} + \dots \\ V_2 &= V_o - \frac{\partial V_o^{(1)}}{\partial \rho} h + \frac{\partial^2 V_o^{(1)}}{\partial \rho^2} \frac{h^2}{2} - \dots \\ V_5 &= V_o + \frac{\partial V_o^{(1)}}{\partial z} h + \frac{\partial^2 V_o^{(1)}}{\partial z^2} \frac{h^2}{2} + \dots \end{aligned} \quad (3.122)$$

where superscript (1) denotes medium 1. Combining Eqs. (3.111) and (3.122) results in

$$h^2 \nabla^2 V = V_1 + V_2 + 2V_5 - 4V_o - 2h \frac{\partial V_o^{(1)}}{\partial z} + \frac{h(V_1 - V_2)}{2\rho_o} = 0$$

or

$$\frac{\partial V_o^{(1)}}{\partial z} = \frac{V_1 + V_2 + 2V_5 - 4V_o + \frac{h(V_1 - V_2)}{2\rho_o}}{2h} \quad (3.123)$$

Similarly, applying Taylor series to points 1, 2, and 6 in medium 2, we get

$$\begin{aligned} V_1 &= V_o + \frac{\partial V_o^{(1)}}{\partial \rho} h + \frac{\partial^2 V_o^{(1)}}{\partial \rho^2} \frac{h^2}{2} + \dots \\ V_2 &= V_o - \frac{\partial V_o^{(1)}}{\partial \rho} h + \frac{\partial^2 V_o^{(1)}}{\partial \rho^2} \frac{h^2}{2} - \dots \\ V_6 &= V_o - \frac{\partial V_o^{(1)}}{\partial z} h + \frac{\partial^2 V_o^{(1)}}{\partial z^2} \frac{h^2}{2} - \dots \end{aligned} \quad (3.124)$$

Combining Eqs. (3.111) and (3.124) leads to

$$h^2 \nabla^2 V = V_1 + V_2 + 2V_6 - 4V_o - 2h \frac{\partial V_o^{(2)}}{\partial z} + \frac{h(V_1 - V_2)}{2\rho_o} = 0$$

or

$$-\frac{\partial V_o^{(2)}}{\partial z} = \frac{V_1 + V_2 + 2V_6 - 4V_o + \frac{h(V_1 - V_2)}{2\rho_o}}{2h} \quad (3.125)$$

But $D_{1n} = D_{2n}$ or

$$\epsilon_1 \frac{\partial V_o^{(1)}}{\partial z} = \epsilon_2 \frac{\partial V_o^{(2)}}{\partial z} \quad (3.126)$$

Substituting Eqs. (3.123) and (3.125) into Eq. (3.126) and solving for V_o yields

$$V_o = \frac{1}{4} \left(1 + \frac{h}{2\rho_o}\right) V_1 + \frac{1}{4} \left(1 - \frac{h}{2\rho_o}\right) V_2 + \frac{\epsilon_1}{2(\epsilon_1 + \epsilon_2)} V_5 + \frac{\epsilon_2}{2(\epsilon_1 + \epsilon_2)} V_6 \quad (3.127)$$

Equation (3.127) is only applicable to interface points. Notice that Eq. (3.127) becomes Eq. (3.114) if $\epsilon_1 = \epsilon_2$.

Typical examples of finite difference approximations for boundary points, written for square nets in rectangular and cylindrical systems, are tabulated in [Table 3.9](#). For more examples, see [12, 110]. The FDTD has also been applied in solving time-varying axisymmetric problems [93, 111].

3.10.2 Spherical Coordinates

In spherical coordinates, Laplace's equation can be written as

$$\nabla^2 V = \frac{\partial^2 V}{\partial r^2} + \frac{2}{r} \frac{\partial V}{\partial r} + \frac{1}{r^2} \frac{\partial^2 V}{\partial \theta^2} + \frac{\cot \theta}{r^2} \frac{\partial V}{\partial \theta} + \frac{1}{r^2 \sin^2 \theta} \frac{\partial^2 V}{\partial \phi^2} = 0 \quad (3.128)$$

At a grid point $O(r_o, \theta_o, \phi_o)$ shown in [Fig. 3.37](#), the finite difference approximation to Eq. (3.128) is

$$\begin{aligned} & \frac{V_1 - 2V_o + V_2}{(\Delta r)^2} + \frac{2}{r_o} \left(\frac{V_1 - V_2}{2\Delta r} \right) + \frac{V_6 - 2V_o + V_5}{(r_o \Delta \theta)^2} \\ & + \frac{\cot \theta_o}{r_o^2} \left(\frac{V_5 - V_6}{2\Delta \theta} \right) + \frac{V_3 - 2V_o + V_4}{(r_o \Delta \phi \sin \theta_o)^2} = 0 \end{aligned} \quad (3.129)$$

Note that θ increases from node 6 to 5 and hence we have $V_5 - V_6$ and not $V_6 - V_5$ in Eq. (3.129).

Example 3.9

Consider an earthed metal cylindrical tank partly filled with a charge liquid, such as hydrocarbons, as illustrated in [Fig. 3.38 \(a\)](#). Using the finite difference method,

Table 3.9 Finite Difference Approximations at Boundary Points.

Description	Figure	Cartesian Equation	Cylindrical Equation
1. Bottom edge		$4V_0 = V_1 + V_2 + 2V_3$	$4V_0 = V_1 + V_2 + 4V_3$
2. Top edge		$4V_0 = V_1 + V_2 + 2V_4$	$4V_0 = V_1 + V_2 + 2V_3$
3. Left edge		$4V_0 = 2V_1 + V_3 + V_4$	$8V_0 = 4V_1 + \left(\frac{2i+1}{i}\right)V_3 + \left(\frac{2i-1}{i}\right)V_4$
4. Right edge		$4V_0 = 2V_1 + V_3 + V_4$	$8V_0 = 4V_2 + \left(\frac{2i+1}{i}\right)V_3 + \left(\frac{2i-1}{i}\right)V_4$
5. Bottom left corner point		$2V_0 = V_1 + V_3$	$3V_0 = V_1 + 2V_3$
6. Bottom right corner point		$2V_0 = V_2 + V_3$	$3V_0 = V_2 + 2V_3$
7. Top left corner point		$2V_0 = V_1 + V_4$	$3V_0 = V_1 + 2V_4$
8. Top right corner point		$2V_0 = V_2 + V_4$	$3V_0 = V_2 + 2V_4$

determine the potential distribution in the entire domain. Plot the potential along $\rho = 0.5$, $0 < z < 2$ m and on the surface of the liquid. Take

$$\begin{aligned}
 a &= b = c = 1.0 \text{ m} , \\
 \epsilon_r &= 2.0 \text{ (hydrocarbons)} , \\
 \rho_v &= 10^{-5} \text{ C/m}^3 \quad \square
 \end{aligned}$$

Solution The exact analytic solution to this problem was given in Section 2.7.2.

It is apparent from Fig. 3.38 (a) and from the fact that ρ_v is uniform that $V = V(\rho, z)$ (i.e., the problem is two-dimensional) and the domain of the problem is symmetrical about the z -axis. Therefore, it is only necessary to investigate the solution region in Fig. 3.38 (b) and impose the condition that the z -axis is a flux line, i.e., $\partial V / \partial n = \partial V / \partial \rho = 0$.

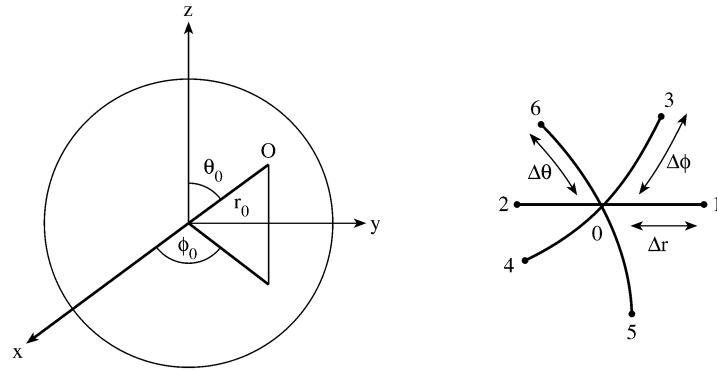


Figure 3.37
Typical node in spherical coordinates.

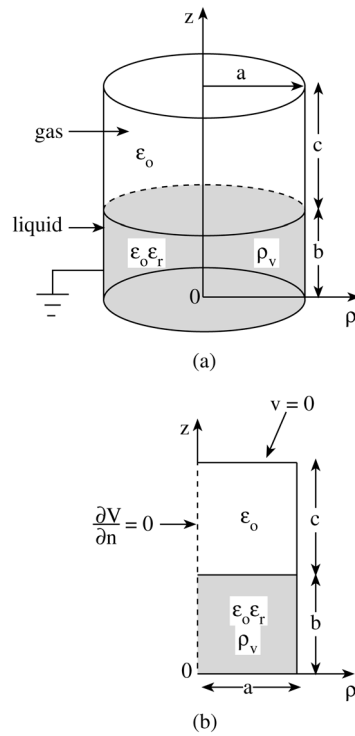


Figure 3.38
For Example 3.9: (a) earth cylindrical tank, (b) solution region.

The finite difference grid of Fig. 3.35 is used with $0 \leq i \leq I_{\max}$ and $0 \leq j \leq J_{\max}$. Choosing $\Delta\rho = \Delta z = h = 0.05$ m makes $I_{\max} = 20$ and $J_{\max} = 40$. Equation (3.115) is applied for gas space, and Eq. (3.123) for liquid space. Along the z -axis, i.e., $i = 0$, we impose the Neumann condition in Eq. (3.120). To account for the fact that the gas has dielectric constant ϵ_{r1} while the liquid has ϵ_{r2} , we impose the boundary condition in Eq. (3.127) on the liquid-gas interface.

Based on these ideas, the computer program shown in Fig. 3.39 was developed to determine the potential distribution in the entire domain. The values of the potential along $\rho = 0.5$, $0 < z < 2$ and along the gas-liquid interface are plotted in Fig. 3.40. It is evident from the figure that the finite difference solution compares well with the exact solution in Section 2.7.2. It is the simplicity in concept and ease of programming finite difference schemes that make them very attractive for solving problems such as this.

3.11 Numerical Integration

Numerical integration (also called *numerical quadrature*) is used in science and engineering whenever a function cannot easily be integrated in closed form or when the function is described in the form of discrete data. Integration is a more stable and reliable process than differentiation. The term quadrature or integration rule will be used to indicate any formula that yields an integral approximation. Several integration rules have been developed over the years. The common ones include:

- Euler's rule,
- Trapezoidal rule,
- Simpson's rule,
- Newton-Cotes rules, and
- Gaussian (quadrature) rules.

The first three are simple and will be considered first to help build up background for other rules which are more general and accurate. A discussion on the subject of numerical integration with diverse FORTRAN codes can be found in Davis and Rabinowitz [112]. A program package called QUADPACK for automatic integration covering a wide variety of problems and various degrees of difficulty is presented in Piessens et al. [113]. Our discussion will be brief but sufficient for the purpose of this text.

```

0001 C *****
0002 C FORTRAN CODE FOR EXAMPLE 3.9
0003 C AN AXISYMMETRIC PROBLEM OF AN EARTHED CYLINDER
0004 C PARTIALLY FILLED WITH A CHARGED LIQUID
0005 C SOLVED USING FINITE DIFFERENCE SCHEME
0006 C *****
0007
0008     DIMENSION V(0:50,0:50)
0009     DATA A,B,C/1.0,1.0,1.0/
0010     DATA ER1,ER2,E0/1.0,2.0,8.854E-12/
0011
0012     H = 0.05
0013     NA = A/H ! same as Imax
0014     NB = B/H
0015     NC = C/H
0016     NBC = NB + NC ! same as Jmax
0017     NMAX = 500 ! NO. OF ITERATIONS
0018     RHOV = 1.E-5
0019     G = -RHOV/(ER2*E0)
0020     GH2 = G*H*H
0021 C
0022 C INITIALIZE - THIS ALSO TAKES CARE OF DIRICHLET
      CONDITIONS
0023 C
0024     DO 10 I = 0,NA
0025     DO 10 J = 0,NBC
0026     V(I,J) = 0.0
0027 10 CONTINUE
0028 C
0029 C NOW, APPLY FINITE DIFFERENCE SCHEME
0030 C
0031     DO 60 N = 1,NMAX
0032     DO 40 I=1,NA-1
0033     FM = FLOAT(2*I - 1)/FLOAT(2*I)
0034     FP = FLOAT(2*I + 1)/FLOAT(2*I)
0035 C IN LIQUID
0036     DO 20 J = 1,NB-1
0037     V(I,J) = 0.25*( V(I,J-1) + V(I,J+1) + FM*V(I-1,J)
0038     & + FP*V(I+1,J) - GH2 )
0039 20 CONTINUE
0040 C IN GAS
0041     DO 30 J = NB+1,NBC-1
0042     V(I,J) = 0.25*( V(I,J-1) + V(I,J+1) + FM*V(I-1,J)
0043     & + FP*V(I+1,J) )
0044 30 CONTINUE
0045 C ALONG THE GAS-LIQUID INTERFACE
0046     V(I,NB)=V(I,NB+1)*ER1/(ER1+ER2)
      +V(I,NB-1)*ER2/(ER1+ER2)+FM*V(I-1,NB)+FP*V(I+1,NB)
0047 40 CONTINUE
0048 C IMPOSE NEUMANN CONDITION ALONG THE Z-AXIS
0049     DO 50 J = 1,NBC-1
0050     V(0,J) = ( 4.0*V(1,J) + V(0,J-1) + V(0,J+1) )
0051 50 CONTINUE
0052 60 CONTINUE
0053 C
0054 C OUTPUT THE POTENTIAL ALONG RHO = 0.5, 0 < Z < 1.0
0055 C
0056     NR5=0.5/H
0057     DO 80 J = 0,NBC
0058     WRITE(6,90) J, V(NR5,J)/1000.0 ! IN kV

```

Figure 3.39
FORTRAN code for Example 3.9 (Continued).

```

0059      80      CONTINUE
0060      90      FORMAT(2X,'J=',I3,3X,'V(0.5,J)=',E12.5,/)
0061      C
0062      C OUTPUT THE POTENTIAL ON THE INTERFACE BETWEEN
          GAS-LIQUID
0063      C
0064      DO 100 I = 0,NA
0065      WRITE(6,110) I, V(I,NB)/1000.0 ! IN kV
0066      100     CONTINUE
0067      110     FORMAT(2X,'I=',I3,3X,'V(I,NB)=',E12.5,/)
0068      STOP
0069      END

```

Figure 3.39
(Cont.) FORTRAN code for Example 3.9.

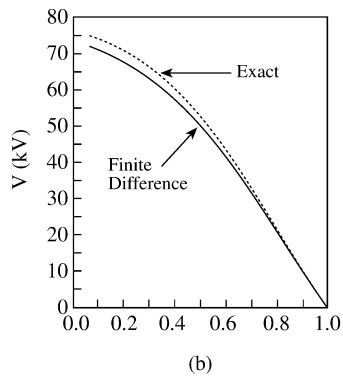
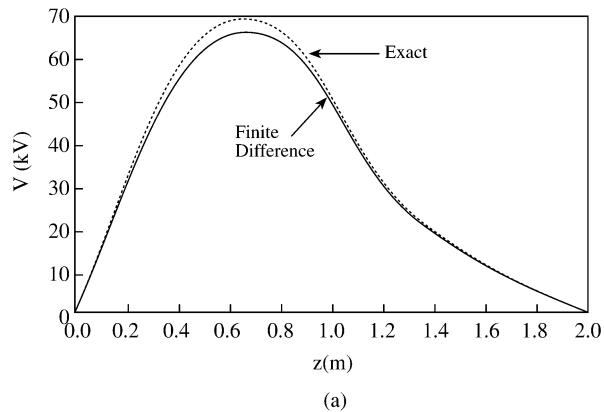


Figure 3.40
Potential distribution in the tank of Fig. 3.38: (a) along $\rho = 0.5$ m, $0 \leq z \leq 2$ m;
(b) along the gas-liquid interface.

3.11.1 Euler's Rule

To apply the Euler or rectangular rule in evaluating the integral

$$I = \int_a^b f(x) dx, \quad (3.130)$$

where $f(x)$ is shown in Fig. 3.41, we seek an approximation for the area under the curve. We divide the curve into n equal intervals as shown. The subarea under the

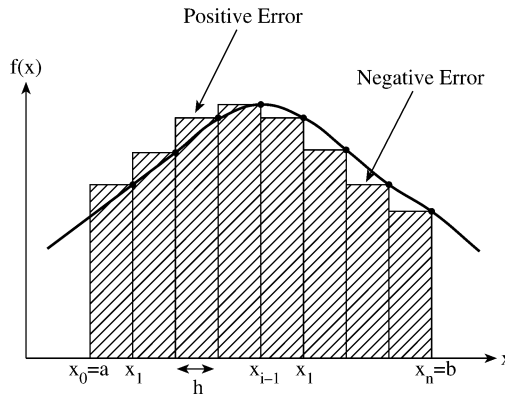


Figure 3.41
Integration using Euler's rule.

curve within $x_{i-1} < x < x_i$ is

$$A_i = \int_{x_{i-1}}^{x_i} f(x) dx \simeq hf_i \quad (3.131)$$

where $f_i = f(x_i)$. The total area under the curve is

$$\begin{aligned} I &= \int_a^b f(x) dx \simeq \sum_{i=1}^n A_i \\ &= h[f_1 + f_2 + \cdots + f_n] \end{aligned}$$

or

$$I = h \sum_{i=1}^n f_i \quad (3.132)$$

It is clear from Fig. 3.41 that this quadrature method gives an inaccurate result since each A_i is less or greater than the true area introducing negative or positive error, respectively.

3.11.2 Trapezoidal Rule

To evaluate the same integral in Eq. (3.130) using the trapezoidal rule, the subareas are chosen as shown in Fig. 3.42. For the interval $x_{i-1} < x < x_i$,

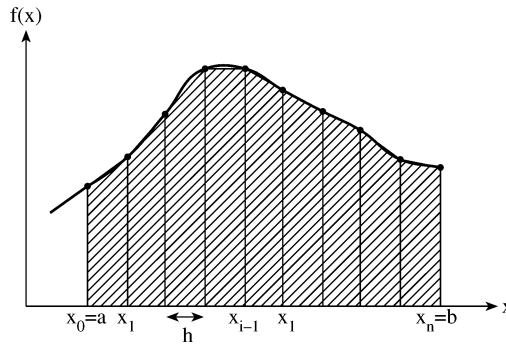


Figure 3.42
Integration using the trapezoidal rule.

$$A_i = \int_{x_{i-1}}^{x_i} f(x) dx \simeq \left(\frac{f_{i-1} + f_i}{2} \right) h \quad (3.133)$$

Hence

$$\begin{aligned} I &= \int_a^b f(x) dx \simeq \sum_{i=1}^n A_i \\ &= h \left[\frac{f_0 + f_1}{2} + \frac{f_1 + f_2}{2} + \dots + \frac{f_{n-2} + f_{n-1}}{2} + \frac{f_{n-1} + f_n}{2} \right] \\ &= \frac{h}{2} [f_0 + 2f_1 + 2f_2 + \dots + 2f_{n-1} + f_n] \end{aligned}$$

or

$$I = h \sum_{i=1}^{n-1} f_i + \frac{h}{2} (f_0 + f_n) \quad (3.134)$$

3.11.3 Simpson's Rule

Simpson's rule gives a still more accurate result than the trapezoidal rule. While the trapezoidal rule approximates the curve by connecting successive points on the curve by straight lines, Simpson's rule connects successive groups of three points on the curve by a second-degree polynomial (i.e., a parabola). Thus

$$A_i = \int_{x_{i-1}}^{x_i} f(x) dx \simeq \frac{h}{3} (f_{i-1} + f_i + f_{i+1}) \quad (3.135)$$

Therefore

$$I = \int_a^b f(x) dx \simeq \sum_{i=1}^n A_i$$

$$I = \frac{h}{3} [f_0 + 4f_1 + 2f_2 + 4f_3 + \dots + 2f_{n-2} + 4f_{n-1} + f_n] \quad (3.136)$$

where n is even.

The computational molecules for Euler's, trapezoidal, and Simpson's rules are shown in Fig. 3.43. Now that we have considered simple quadrature rules to help build up background, we now consider more general, accurate methods.

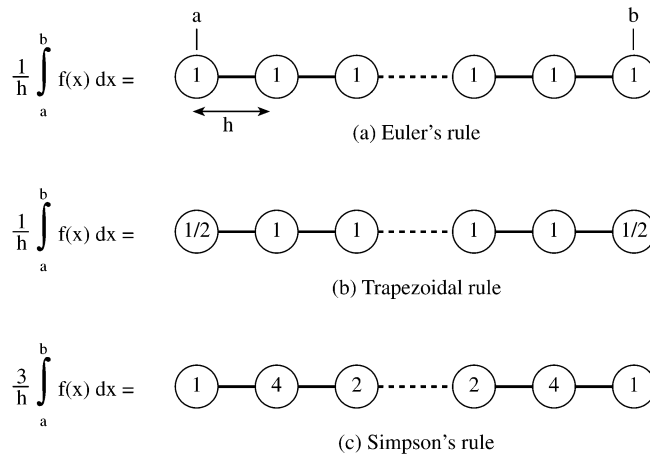


Figure 3.43
Computational molecules for integration.

3.11.4 Newton-Cotes Rules

To apply a Newton-Cotes rule to evaluate the integral in Eq. (3.130), we divide the interval $a < x < b$ into m equal intervals so that

$$h = \frac{b - a}{m} \quad (3.137)$$

where m is a multiple of n , and n is the number of intervals covered at a time or the order of the approximating polynomial. The subarea in the interval $x_{n(i-1)} < x < x_{ni}$ is

$$A_i = \int_{x_{n(i-1)}}^{x_{ni}} f(x) dx \simeq \frac{nh}{N} \sum_{k=0}^n C_k^n f(x_{n(i-1)+k}) \quad (3.138)$$

The coefficients C_k^n , $0 \leq k \leq n$, are called Newton-Cotes numbers and tabulated in Table 3.10. The numbers are obtained from

$$C_k^n = \frac{1}{n} \int_0^N L_k(s) ds \quad (3.139)$$

where

$$L_k(s) = \prod_{j=0, j \neq k}^n \frac{s-j}{k-j} \quad (3.140)$$

It is easily shown that the coefficients are symmetric, i.e.,

$$C_k^n = C_{n-k}^n \quad (3.141a)$$

and they sum up to unity, i.e.,

$$\sum_{k=0}^n C_k^n = 1 \quad (3.141b)$$

Table 3.10 Newton-Cotes Numbers.

n	N	NC_0^n	NC_1^n	NC_2^n	NC_3^n	NC_4^n	NC_5^n	NC_6^n	NC_7^n	NC_8^n
1	2	1	1							
2	6	1	4	1						
3	8	1	3	3	1					
4	90	7	32	12	32	7				
5	288	19	75	50	50	75	19			
6	840	41	216	27	272	27	216	41		
7	17280	751	3577	1323	2989	2989	1323	3577	751	
8	24350	989	5888	-928	10946	-4540	10946	-928	5888	989

For example, for $n = 2$,

$$C_0^2 = \frac{1}{2} \int_0^6 \frac{(s-1)(s-2)}{(-1)(-2)} ds = \frac{1}{6},$$

$$C_1^2 = \frac{1}{2} \int_0^6 \frac{s(s-2)}{1(-1)} ds = \frac{4}{6},$$

$$C_2^2 = \frac{1}{2} \int_0^6 \frac{s(s-1)}{2(1)} ds = \frac{1}{6}$$

Once the subareas are found using Eq. (3.138), then

$$I = \int_a^b f(x) dx \simeq \sum_{i=1}^{m/n} A_i \quad (3.142)$$

The most widely known Newton-Cotes formulas are:

$n = 1$ (2-point; trapezoidal rule)

$$A_i \simeq \frac{h}{2} (f_{i+1} + f_i) , \quad (3.143)$$

$n = 2$ (3-point; Simpson's 1/3 rule)

$$A_i \simeq \frac{h}{3} (f_{i-1} + 4f_i + f_{i+1}) , \quad (3.144)$$

$n = 3$ (4-point; Newton's rule)

$$A_i \simeq \frac{3h}{8} (f_i + 3f_{i+1} + 3f_{i+2} + f_{i+3}) \quad (3.145)$$

3.11.5 Gaussian Rules

The integration rules considered so far involve the use of equally spaced abscissa points. The idea of integration rules using unequally spaced abscissa points stems from Gauss. The Gaussian rules are more complicated but more accurate than the Newton-Cotes rules. A Gaussian rule has the general form

$$\int_a^b f(x) dx \simeq \sum_{i=1}^n w_i f(x_i) \quad (3.146)$$

where (a, b) is the interval for which a sequence of orthogonal polynomials $\{w_i(x)\}$ exists, x_i are the zeros of $w_i(x)$, and the weights w_i are such that Eq. (3.146) is of degree of precision $2n - 1$. Any of the orthogonal polynomials discussed in Chapter 2 can be used to give a particular Gaussian rule. Commonly used rules are Gauss-Legendre, Gauss-Chebyshev, etc., since the sample point x_i are the roots of the Legendre, Chebyshev, etc., of degree n . For the Legendre ($n = 1$ to 16) and Laguerre ($n = 1$ to 16) polynomials, the zeros x_i and weights w_i have been tabulated in [114].

Using Gauss-Legendre rule,

$$\int_a^b f(x) dx \simeq \frac{b-a}{2} \sum_{i=1}^n w_i f(u_i) \quad (3.147)$$

where $u_i = \frac{b-a}{2}x_i + \frac{b+a}{2}$ are the transformation of the roots x_i of Legendre polynomials from limits $(-1, 1)$ to finite limits (a, b) . The values of the abscissas x_i and weights w_i for n up to 7 are presented in Table 3.11; for higher values of n , the interested reader is referred to [114, 115]. Note that $-1 < x_i < 1$ and $\sum_{i=1}^n w_i = 2$.

The Gauss-Chebyshev rule is similar to Gauss-Legendre rule. We use Eq. (3.147) except that the sample points x_i , the roots of Chebyshev polynomial $T_n(x)$, are

$$x_i = \cos \frac{(2i-1)\pi}{2n}, \quad i = 1, 2, \dots, n \quad (3.148)$$

Table 3.11 Abscissas (Roots of Legendre Polynomials) and Weights for Gauss-Legendre Integration

$\pm x_i$	w_i
$n = 2$	
0.57735 02691 89626	1.00000 00000 00000
$n = 3$	
0.00000 00000 00000	0.88888 88888 88889
0.77459 66692 41483	0.55555 55555 55556
$n = 4$	
0.33998 10435 84856	0.65214 51548 62546
0.86113 63115 94053	0.34785 48451 37454
$n = 5$	
0.00000 00000 00000	0.56888 88888 88889
0.53846 93101 05683	0.47862 86704 99366
0.90617 98459 38664	0.23692 68850 56189
$n = 6$	
0.23861 91860 83197	0.46791 39345 72691
0.66120 93864 66265	0.36076 15730 48139
0.93246 95142 03152	0.17132 44923 79170
$n = 7$	
0.00000 00000 00000	0.41795 91836 73469
0.40584 51513 77397	0.38183 00505 05119
0.74153 11855 99394	0.27970 53914 89277
0.94910 79123 42759	0.12948 49661 68870

and the weights are all equal [116], i.e.,

$$w_i = \frac{\pi}{n} \quad (3.149)$$

When either of the limits of integration a or b or both are $\pm\infty$, we use Gauss-Laguerre or Gauss-Hermite rule. For the Gauss-Laguerre rule,

$$\int_0^\infty f(x) dx \simeq \sum_{i=1}^n w_i f(x_i) \quad (3.150)$$

where the appropriate abscissas x_i , the roots of Laguerre polynomials, and weights w_i are listed for n up to 7 in Table 3.12. For the Gauss-Hermite rule,

$$\int_{-\infty}^\infty f(x) dx \simeq \sum_{i=1}^n w_i f(x_i) \quad (3.151)$$

where the abscissas x_i , the roots of the Hermite polynomials, and weights w_i are listed for n up to 7 in Table 3.13. An integral over (a, ∞) is taken care of by a change

of variable so that

$$\int_a^\infty f(x) dx = \int_0^\infty f(y+a) dy \quad (3.152)$$

Table 3.12 Abscissas (Roots of Laguerre Polynomials) and Weights for Gauss-Laguerre Integration.

$\pm x_i$	w_i
$n = 2$	
0.58578 64376 27	1.53332 603312
3.41421 35623 73	4.45095 733505
$n = 3$	
0.41577 45567 83	1.07769 285927
2.29428 03602 79	2.76214 296190
6.28994 50829 37	5.60109 462543
$n = 4$	
0.32254 76896 19	0.83273 912383
1.74576 11011 58	2.04810 243845
4.53662 02969 21	3.63114 630582
9.39507 09123 01	6.48714 508441
$n = 5$	
0.26356 03197 18	0.67909 404220
1.41340 30591 07	1.63848 787360
3.59642 57710 41	2.76944 324237
12.64080 08442 76	7.21918 635435
$n = 6$	
0.22284 66041 79	0.57353 550742
1.18893 21016 73	1.36925 259071
2.99273 63260 59	2.26068 459338
5.77514 35691 05	3.35052 458236
9.83746 74183 83	4.88682 680021
15.98287 39806 02	7.84901 594560
$n = 7$	
0.19304 36765 60	0.49647 759754
1.02666 48953 39	1.17764 306086
2.56787 67449 51	1.91824 978166
4.90035 30845 26	2.77184 863623
8.18215 34445 63	3.84124 912249
12.73418 02917 98	5.38067 820792
19.39572 78622 63	8.40543 248683

We apply Eq. (3.146) with $f(x)$ evaluated at points $x_i + a$, $i = 1, 2, \dots, n$ and x_i s are tabulated in [Table 3.12](#).

Table 3.13 Abscissas (Roots of Hermite Polynomials) and Weights for Gauss-Hermite Integration.

$\pm x_i$	w_i
$n = 2$	
0.70710 67811 86548	1.46114 11826 611
$n = 3$	
0.00000 00000 00000	1.18163 59006 037
1.22474 48713 91589	1.32393 11752 136
$n = 4$	
0.52464 76232 75290	1.05996 44828 950
1.65068 01238 85785	1.24022 58176 958
$n = 5$	
0.00000 00000 00000	0.94530 87204 829
0.95857 24646 13819	0.98658 09967 514
2.02018 28704 56086	1.18148 86255 360
$n = 6$	
0.43607 74119 27617	0.87640 13344 362
1.33584 90740 13697	0.93558 05576 312
2.35060 49736 74492	1.13690 83326 745
$n = 7$	
0.00000 00000 00000	0.81026 46175 568
0.81628 78828 58965	0.82868 73032 836
1.67355 16287 67471	0.89718 46002 252
2.65196 13568 35233	1.10133 07296 103

A major drawback with Gaussian rules is that if one wishes to improve the accuracy, one must increase n which means that the values of w_i and x_i must be included in the program for each value of n . Another disadvantage is that the function $f(x)$ must be explicit since the sample points x_i are unassigned.

3.11.6 Multiple Integration

This is an extension of one-dimensional (1D) integration discussed so far. A double integral is evaluated by means of two successive applications of the rules presented above for single integral [117]. To evaluate the integral using the Newton-Cotes or Simpson's 1/3 rule ($n = 2$), for example,

$$I = \int_a^b \int_c^d f(x, y) dx dy \quad (3.153)$$

over a rectangular region $a < x < b$, $c < y < d$, we divide the region into $m \cdot l$ smaller rectangles with sides

$$h_x = \frac{b-a}{m} \quad (3.154a)$$

$$h_y = \frac{d-c}{l} \quad (3.154b)$$

where m and l are multiples of $n = 2$. The subarea

$$A_{ij} = \int_{y_n(j-1)}^{y_n(j+1)} dy \int_{x_n(i-1)}^{x_n(i+1)} f(x, y) dx \quad (3.155)$$

is evaluated by integrating along x and then along y according to Eq. (3.140):

$$A_{ij} \simeq \frac{h_x}{3} (g_{j-1} + 4g_j + g_{j+1}) \quad (3.156)$$

where

$$g_j \simeq \frac{h_y}{3} (f_{i-1,j} + 4f_{i,j} + f_{i+1,j}) \quad (3.157)$$

Substitution of Eq. (3.157) into Eq. (3.156) yields

$$A_{ij} = \frac{h_x h_y}{9} [(f_{i+1,j+1} + f_{i+1,j-1} + f_{i-1,j+1} + f_{i-1,j-1}) + 4(f_{i,j+1} + f_{i,j-1} + f_{i+1,j} + f_{i-1,j}) + 16f_{i,j}] \quad (3.158)$$

The corresponding schematic or integration molecule is shown in Fig. 3.44. Summing the value of A_{ij} for all subareas yields

$$I = \sum_{i=1}^{m/n} \sum_{j=1}^{l/n} A_{ij} \quad (3.159)$$

The procedure applied in the 2D integral can be extended to a 3D integral. To evaluate

$$I = \int_a^b \int_c^d \int_e^f f(x, y, z) dx dy dz \quad (3.160)$$

using the $n = 2$ rule, the cuboid $a < x < b$, $c < y < d$, $e < z < f$ is divided into $m \cdot l \cdot p$ smaller cuboids of sides

$$\begin{aligned} h_x &= \frac{b-a}{m} \\ h_y &= \frac{d-c}{l} \\ h_z &= \frac{f-e}{p} \end{aligned} \quad (3.161)$$

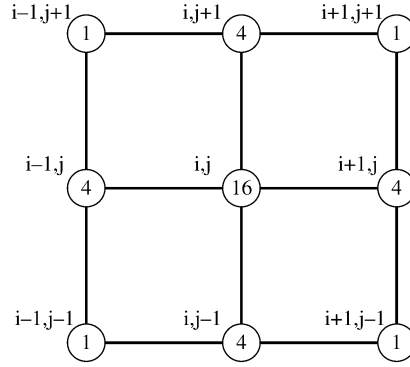


Figure 3.44
Double integration molecule for Simpson's 1/3 rule.

where m , l , and p are multiples of $n = 2$. The subvolume A_{ijk} is evaluated by integrating along x according to Eq. (3.144) to obtain

$$g_{j,k} = \frac{h_x}{3} (f_{i+1,j,k} + 4f_{i,j,k} + f_{i-1,j,k}) , \quad (3.162)$$

then along y

$$g_k = \frac{h_y}{3} (g_{j+1,k} + 4g_{j,k} + g_{j-1,k}) , \quad (3.163)$$

and finally along z to obtain

$$A_{ijk} = \frac{h_z}{3} (g_{k+1} + 4g_k + g_{k-1}) \quad (3.164)$$

Substituting Eqs. (3.162) and (3.163) into Eq. (3.164) results in [117]

$$\begin{aligned} A_{ijk} = \frac{h_x h_y h_z}{27} [& (f_{i-1,j-1,k+1} + 4f_{i-1,j,k+1} + f_{i-1,j+1,k+1}) \\ & + (4f_{i,j-1,k+1} + 16f_{i,j,k+1} + 4f_{i,j+1,k+1}) \\ & + (f_{i+1,j-1,k+1} + 4f_{i+1,j,k+1} + f_{i+1,j+1,k+1}) \\ & + (4f_{i-1,j-1,k} + 16f_{i-1,j,k} + 4f_{i-1,j+1,k}) \\ & + (16f_{i,j-1,k} + 64f_{i,j,k} + 16f_{i,j+1,k}) \\ & + (4f_{i+1,j-1,k} + 16f_{i+1,j,k} + 4f_{i+1,j+1,k}) \\ & + (f_{i-1,j-1,k-1} + 4f_{i-1,j,k-1} + f_{i-1,j+1,k-1}) \\ & + (4f_{i,j-1,k-1} + 16f_{i,j,k-1} + 4f_{i,j+1,k-1}) \\ & + (f_{i+1,j-1,k-1} + 4f_{i+1,j,k-1} + f_{i+1,j+1,k-1})] \quad (3.165) \end{aligned}$$

The integration molecule is portrayed in Fig. 3.45. Observe that the molecule is symmetric with respect to all planes that cut the molecule in half.

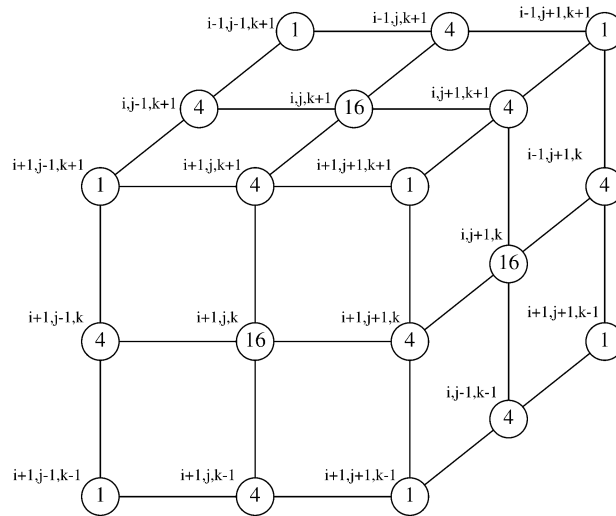


Figure 3.45
Triple integration molecule for Simpson's 1/3 rule.

Example 3.10

Write a program that uses the Newton-Cotes rule ($n = 6$) to evaluate Bessel function of order m , i.e.,

$$J_m(x) = \frac{1}{\pi} \int_0^\pi \cos(x \sin \theta - m\theta) d\theta$$

Run the program for $m = 0$ and $x = 0.1, 0.2, \dots, 2.0$. □

Solution The computer program is shown in Fig. 3.46. The program is based on Eqs. (3.138) and (3.142). It evaluates the integral within a subinterval $\theta_{n(i-1)} < \theta < \theta_{ni}$. The summation over all the subintervals gives the required integral. The result for $m = 0$ and $0.1 < x < 2.0$ is shown in Table 3.14; the values agree up to six significant figures with those in standard tables [115, p. 390]. The program is intentionally made general so that n , the corresponding Newton-Cotes numbers, and the integrand can be changed easily. Although the integrand in Fig. 3.46 is real, the program can be modified for complex integrand by simply declaring complex the affected variables. ■

```

0001
0002 C *****
0003 C INTEGRATION BY NEWTON-COTES RULE (N=6)
0004 C
0005 C A, B = ARE THE INTEGRATION LIMITS
0006 C SUM = THE RESULT OF THE INTEGRATION
0007 C THE FUNCTION TO BE INTEGRATED MUST BE DEFINED IN
0008 C A SUBPROGRAM FUNCTION FUN(ARGUMENTS)
0009 C
0010 C SPECIFICALLY, THIS PROGRAM EVALUATES BESSEL FUNCTION
0011 C JN(X), OF ORDER N AND ARGUMENT X
0012 C *****
0013
0014 DATA PIE/3.1415927/
0015
0016 A=0.0
0017 B=PIE
0018 N=4
0019 DO 20 I=1,20
0020 X=0.1*FLOAT(I)
0021 CALL INTEGRATION(A,B,N,X,SUM)
0022 WRITE(6,10) X,SUM
0023 PRINT *,X,SUM
0024 10 FORMAT(2X,'X = ',F6.3,2X,'JO = ',E20.12,/)
0025 20 CONTINUE
0026 STOP
0027 END

0001 C *****
0002 C SUBROUTINE FOR INTEGRATION USING NEWTON-COTES RULE (N=6)
0003 C A IS THE LOWER LIMIT OF INTEGRATION
0004 C B IS THE UPPER LIMIT OF INTEGRATION
0005 C H IS THE INTERVAL SIZE
0006 C *****
0007 C SUBROUTINE INTEGRATION(AA,BB,NO,X,SUM)
0008 C IMPLICIT REAL(A-H,O-Z)
0009 C DIMENSION C(0:6)
0010 C DATA NC /840/
0011 C DATA ( C(I),I=0,6 )/41.,216.,27.,272.,27.,216.,41./
0012
0013 C START COMPUTATION
0014
0015 N=6
0016 M=240 ! M MUST BE A MULTIPLE OF N
0017 H=(BB-AA)/FLOAT(M)
0018 SUM=0.0
0019 NN=M/N
0020 T=AA
0021 DO 20 I=1,NN
0022 DO 10 J=0,N
0023 A=C(J)*FUN(T,NO,X)
0024 SUM=SUM + A
0025 T=T + H
0026 10 CONTINUE
0027 20 T=T - H
0028 CONTINUE
0029 SUM=SUM*H*FLOAT(N)/FLOAT(NC)
0030 RETURN
0031 END

```

Figure 3.46
Computer program for Example 3.10 (Continued).

```

0001 C *****
0002 C THE FUNCTION TO BE INTEGRATED
0003 C *****
0004 C FUNCTION FUN(THETA,N,X)
0005 DATA PIE/3.1415927/
0006
0007 FUN = COS( X*SIN(THETA) - FLOAT(N)*THETA )/PIE
0008 RETURN
0009 END

```

Figure 3.46
(Cont.) Computer program for Example 3.10.

Table 3.14 Result of
the Program in
Fig. 3.45 for $m = 0$.

x	$J_0(x)$
0.1	0.9975015
0.2	0.9900251
0.3	0.9776263
0.4	0.9603984
0.5	0.9384694
⋮	⋮
1.5	0.5118274
1.6	0.4554018
1.7	0.3979859
1.8	0.3399859
1.9	0.2818182
2.0	0.2238902

3.12 Concluding Remarks

Only a brief treatment of the finite difference analysis of PDEs is given here. There are many valuable references on the subject which answer many of the questions left unanswered here [3]–[8], [10, 104, 105]. The book by Smith [5] gives an excellent exposition with numerous examples. The problems of stability and convergence of finite difference solutions are further discussed in [118, 119], while the error estimates in [120].

As noted in Section 3.8, the finite difference method has some inherent advantages and disadvantages. It is conceptually simple and easy to program. The finite difference approximation to a given PDE is by no means unique; more accurate expressions can be obtained by employing more elaborate and complicated formulas. However, the relatively simple approximations may be employed to yield solutions

of any specified accuracy simply by reducing the mesh size provided that the criteria for stability and convergence are met.

A very important difficulty in finite differencing of PDEs, especially parabolic and hyperbolic types, is that if one value of Φ is not calculated and therefore set equal to zero by mistake, the solution may become unstable. For example, in finding the difference between $\Phi_i = 1000$ and $\Phi_{i+1} = 1002$, if Φ_{i+1} is set equal to zero by mistake, the difference of 1000 instead of 2 may cause instability. To guard against such error, care must be taken to ensure that Φ is calculated at every point, particularly at boundary points.

A serious limitation of the finite difference method is that interpolation of some kind must be used to determine solutions at points not on the grid. Suppose we want to find Φ at a point P which is not on the grid, as in Fig. 3.47. Assuming Φ is known at the four grid points surrounding P , at a distance x_o along the bottom edge of the rectangle in Fig. 3.47,

$$\Phi_b = \frac{x_o}{\Delta x} [\Phi(i+1, j) - \Phi(i, j)] + \Phi(i, j) \quad (3.166)$$

At a distance x_o along the top edge,

$$\Phi_t = \frac{x_o}{\Delta x} [\Phi(i+1, j+1) - \Phi(i, j+1)] + \Phi(i, j+1) \quad (3.167)$$

The value of Φ at P is estimated by combining Eqs. (3.166) and (3.167), i.e.,

$$\Phi_P = \frac{y_o}{\Delta y} (\Phi_t - \Phi_b) + \Phi_b \quad (3.168)$$

One obvious way to avoid interpolation is to use a finer grid if possible.

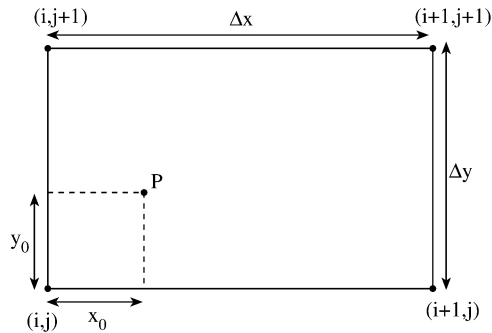


Figure 3.47
Evaluating Φ at a point P not on the grid.

References

- [1] L.D. Kovach, *Boundary-value Problems*. Reading, MA: Addison-Wesley, 1984, pp. 355–379.
- [2] A. Thom and C.J. Apelt, *Field Computations in Engineering and Physics*. London: D. Van Nostrand, 1961, p. v.
- [3] R.D. Richtmyer and K.W. Morton, *Difference Methods for Initial-value Problems*, 2nd ed. New York: Interscience Publ., 1976, pp. 185–193.
- [4] D. Potter, *Computational Physics*. London: John Wiley, 1973, pp. 40–79.
- [5] G.D. Smith, *Numerical Solution of Partial Differential Equations: Finite Difference Methods*, 3rd ed., Oxford Univ. Press, New York, 1985.
- [6] J.H. Ferziger, *Numerical Methods for Engineering Application*. New York: John Wiley, 1981.
- [7] L. Lapidus and G.F. Pinder, *Numerical Solution of Partial Differential Equations in Science and Engineering*. New York: John Wiley, 1982, pp. 166–185.
- [8] V. Vemuri and W.J. Karplus, *Digital Computer Treatment of Partial Differential Equations*. Englewood Cliffs, NJ: Prentice-Hall, 1981, pp. 88–92.
- [9] A. Wexler, “Computation of electromagnetic fields,” *IEEE Trans. Micro. Theo. Tech.*, vol. MTT-17, no. 8, Aug. 1969, pp. 416–439.
- [10] G. de Vahl Davis, *Numerical Methods in Engineering and Science*. London: Allen & Unwin, 1986.
- [11] Special issue of IEEE Transactions on Microwave Theory and Techniques, vol. MTT-17, no. 8, Aug. 1969 on “Computer-oriented microwave practices” covers various applications of finite difference methods to EM problems.
- [12] H.E. Green, “The numerical solution of some important transmission-line problems,” *IEEE Trans. Micro. Theo. Tech.*, vol. MTT-13, no. 5, Sept. 1965, pp. 676–692.
- [13] M.N.O. Sadiku, “Finite difference solution of electrodynamic problems,” *Int. Jour. Elect. Engr. Educ.*, vol. 28, April 1991, pp. 107–122.
- [14] M.F. Iskander, “A new course on computational methods in electromagnetics,” *IEEE Trans. Educ.*, vol. 31, no. 2, May 1988, pp. 101–115.
- [15] W.S. Metcalf, “Characteristic impedance of rectangular transmission lines,” *Proc. IEE*, vol. 112, no. 11, Nov. 1965, pp. 2033–2039.

- [16] M.V. Schneider, "Computation of impedance and attenuation of TEM-lines by finite difference methods," *IEEE Micro. Theo. Tech.*, vol. MTT-13, no. 6, Nov. 1965, pp. 793–800.
- [17] M. Sendaula, M. Sadiku, and R. Heiman, "Crosstalk computation in coupled transmission lines," *Proc. IEEE Southeastcon*, April 1991, pp. 790–795.
- [18] A.R. Djordjevic, et al., "Time-domain response of multiconductor transmission lines," *Proc. IEEE*, vol. 75, no. 6, June 1987, pp. 743–764.
- [19] R.R. Gupta, "Accurate impedance determination of coupled TEM conductors," *IEEE Trans. Micro. Theo. Tech.*, vol. MTT-17, no. 12, Aug. 1969, pp. 479–489.
- [20] E. Yamashita, et al., "Characterization method and simple design formulas of MDS lines proposed for MMIC's," *IEEE Trans. Micro. Theo. Tech.*, vol. MTT-35, no. 12, Dec. 1987, pp. 1355–1362.
- [21] J.R. Molberg and D.K. Reynolds, "Iterative solutions of the scalar Helmholtz equations in lossy regions," *IEEE Trans. Micro. Theo. Tech.*, vol. MTT-17, no. 8, Aug. 1969, pp. 460–477.
- [22] J.B. Davies and C.A. Muilwyk, "Numerical solution of uniform hollow waveguides with boundaries of arbitrary shape," *Proc. IEEE*, vol. 113, no. 2, Feb. 1966, pp. 277–284.
- [23] J.S. Hornsby and A. Gopinath, "Numerical analysis of a dielectric-loaded waveguide with a microstrip line—finite-difference methods," *IEEE Trans. Micro. Theo. Tech.*, vol. MTT-17, no. 9, Sept. 1969, pp. 684–690.
- [24] M.J. Beubien and A. Wexler, "An accurate finite-difference method for higher-order waveguide modes," *IEEE Trans. Micro. Theo. Tech.*, vol. MTT-16, no. 12, Dec. 1968, pp. 1007–1017.
- [25] C.A. Muilwyk and J.B. Davies, "The numerical solution of rectangular waveguide junctions and discontinuities of arbitrary cross section," *IEEE Trans. Micro. Theo. Tech.*, vol. MTT-15, no. 8, Aug. 1967, pp. 450–455.
- [26] J.H. Collins and P. Daly, "Calculations for guided electromagnetic waves using finite-difference methods," *J. Electronics & Control*, vol. 14, 1963, pp. 361–380.
- [27] T. Itoh (ed.), *Numerical Techniques for Microwaves and Millimeterwave Passive Structures*. New York: John Wiley, 1989.
- [28] D.H. Sinnott, et al., "The finite difference solution of microwave circuit problems," *IEEE Trans. Micro. Theo. Tech.*, vol. MTT-17, no. 8, Aug. 1969, pp. 464–478.
- [29] W.K. Gwarek, "Analysis of an arbitrarily-shaped planar circuit—a time-domain approach," *IEEE Trans. Micro. Theo. Tech.*, vol. MTT-33, no. 10, Oct. 1985, pp. 1067–1072.

- [30] M. De Pourceq, "Field and power-density calculations in closed microwave systems by three-dimensional finite differences," *IEEE Proc.*, vol. 132, Pt. H, no. 6, Oct. 1985, pp. 360–368.
- [31] A. Taflove and K.R. Umashankar, "Solution of complex electromagnetic penetration and scattering problems in unbounded regions," in A.J. Kalinowski (ed.), *Computational Methods for Infinite Domain Media-structure Interaction*. Washington, DC: ASME, vol. 46, 1981, pp. 83–113.
- [32] A. Taflove, "Application of the finite-difference time-domain method to sinusoidal steady-state electromagnetic-penetration problems," *IEEE Trans. EM Comp.*, vol. EMC-22, no. 3, Aug. 1980, pp. 191–202.
- [33] K.S. Kunz and K.M. Lee, "A three-dimensional finite-difference solution of the external response of an aircraft to a complex transient EM environment" (2 parts), *IEEE Trans. EM Comp.*, vol. EMC-20, no. 2, May 1978, pp. 328–341.
- [34] M.L. Oristaglio and G.W. Hohman, "Diffusion of electromagnetic fields into a two-dimensional earth: a finite-difference approach," *Geophysics*, vol. 49, no. 7, July 1984, pp. 870–894.
- [35] K. Umashankar and A. Taflove, "A novel method to analyze electromagnetic scattering of complex objects," *IEEE Trans. EM Comp.*, vol. EMC-24, no. 4, Nov. 1982, pp. 397–405.
- [36] R.W.M. Lau and R.J. Sheppard, "The modelling of biological systems in three dimensions using the time domain finite-difference method" (2 parts), *Phys. Med. Biol.*, vol. 31, no. 11, 1986, pp. 1247–1266.
- [37] F. Sandy and J. Sage, "Use of finite difference approximations to partial differential equations for problems having boundaries at infinity," *IEEE Trans. Micro. Theo. Tech.*, May 1971, pp. 484–486.
- [38] K.B. Whiting, "A treatment for boundary singularities in finite difference solutions of Laplace's equation," *IEEE Trans. Micro. Theo. Tech.*, vol. MTT-16, no. 10, Oct. 1968, pp. 889–891.
- [39] G.E. Forsythe and W.R. Wasow, *Finite Difference Methods for Partial Differential Equations*. New York: John Wiley, 1960.
- [40] M.L. James et al., *Applied Numerical Methods for Digital Computation*, 3rd ed. New York: Harper & Row, 1985, pp. 203–274.
- [41] Y. Naiheng and R.F. Harrington, "Characteristic impedance of transmission lines with arbitrary dielectrics under the TEM approximation," *IEEE Trans. Micro. Theo. Tech.*, vol. MTT-34, no. 4, April 1986, pp. 472–475.
- [42] K.S. Yee, "Numerical solution of initial boundary-value problems involving Maxwell's equations in isotropic media," *IEEE Trans. Ant. Prop.*, vol. AP-14, May 1966, pp. 302–307.

- [43] A. Taflove and M.E. Brodwin, "Numerical solution of steady-state electromagnetic scattering problems using the time-dependent Maxwell's equations," *IEEE Micro. Theo. Tech.*, vol. MTT-23, no. 8, Aug. 1975, pp. 623–630.
- [44] A. Taflove and K. Umashankar, "A hybrid moment method/finite-difference time-domain approach to electromagnetic coupling and aperture penetration into complex geometries," *IEEE Trans. Ant. Prop.*, vol. AP-30, no. 4, July 1982, pp. 617–627. Also in B. J. Strait (ed.), *Applications of the Method of Moments to Electromagnetic Fields*. Orlando, FL: SCEE Press, Feb. 1980, pp. 361–426.
- [45] M. Okoniewski, "Vector wave equation 2D-FDTD method for guided wave equation," *IEEE Micro. Guided Wave Lett.*, vol. 3, no. 9, Sept. 1993, pp. 307–309.
- [46] A. Taflove and K.R. Umashankar, "The finite-difference time-domain method for numerical modeling of electromagnetic wave interactions," *Electromagnetics*, vol. 10, 1990, pp. 105–126.
- [47] M.N.O. Sadiku, V. Bommel, and S. Agbo, "Stability criteria for finite-difference time-domain algorithm," *Proc. IEEE Southeastcon*, April 1990, pp. 48–50.
- [48] J.G. Blaschak and G.A. Kriegsmann, "A comparative study of absorbing boundary conditions," *J. Comp. Phys.*, vol. 77, 1988, pp. 109–139.
- [49] G. Mux, "Absorbing boundary conditions for the finite-difference approximation of the time-domain electromagnetic-field equations," *IEEE Trans. EM Comp.*, vol. EMC-23, no. 4, Nov. 1981, pp. 377–382.
- [50] R. Holland, "THREDE: A free-field EMP coupling and scattering code," *IEEE Trans. Nucl. Sci.*, vol. NS-24, no. 6, Dec. 1977, pp. 2416–2421.
- [51] R.W. Ziolkowski et al., "Three-dimensional computer modeling of electromagnetic fields: a global lookback lattice truncation scheme," *J. Comp. Phys.*, vol. 50, 1983, pp. 360–408.
- [52] E.R. Demarest, "A finite difference—time domain technique for modeling narrow apertures in conducting scatterers," *IEEE Trans. Ant. Prop.*, vol. AP-35, no. 7, July 1987, pp. 826–831.
- [53] A. Taflove et al., "Detailed FD-TD analysis of electromagnetic fields penetrating narrow slots and lapped joints in thick conducting screens," *IEEE Trans. Ant. Prop.*, vol. 36, no. 2, Feb. 1988, pp. 24–257.
- [54] H. Meskanen and O. Pekonen, "FDTD analysis of field distribution in an elevator car by using various antenna positions and orientations," *Elect. Lett.*, vol. 34, no. 6, March 1998, pp. 534–535.

- [55] J.G. Maloney, G.S. Smith, and W.R. Scott, "Accurate computation of the radiation from simple antennas using the finite-difference time-domain method," *IEEE Trans. Ant. Prog.*, vol. 38, no. 7, July 1990, pp. 1059–1068.
- [56] J.G. Maloney and Smith, "The efficient modeling of thin material sheets in the finite-difference time-domain (FDTD) method," *IEEE Trans. Ant. Prog.*, vol. 40, no. 3, March 1992, pp. 323–330.
- [57] P.A. Tirkas and C.A. Balanis, "Finite-difference time-domain method for antenna radiation," *IEEE Trans. Ant. Prog.*, vol. 40, no. 4, March 1992, pp. 334–340.
- [58] E. Thiele and A. Taflove, "FD-TD analysis of vivaldi flared horn antennas and arrays," *IEEE Trans. Ant. Prog.*, vol. 42, no. 5, May 1994, pp. 633–641.
- [59] J.S. Colburn and Y. Rahmat-Samii, "Human proximity effects on circular polarized handset antennas in personal satellite communications," *IEEE Trans. Ant. Prog.*, vol. 46, no. 6, June 1998, pp. 813–820.
- [60] K. Uehara and K. Kagoshima, "Rigorous analysis of microstrip phased array antennas using a new FDTD method," *Elect. Lett.*, vol. 30, no. 2, Jan. 1994, pp. 100–101.
- [61] H. Klingbell, K. Beilenhoff, and H.L. Hartnagel, "FDTD full-wave analysis and modeling of dielectric and metallic losses of CPW short circuits," *IEEE Trans. Micro. Theo. Tech.*, vol. 44, no. 3, March 1996, pp. 485–487.
- [62] C. Zhao and I. Awai, "Applications of the finite difference techniques to the compensated VIP 3 dB directional coupler," *IEEE Trans. Micro. Theo. Tech.*, vol. 44, no. 11, Nov. 1996, pp. 2045–2052.
- [63] T. Shibata et al., "Analysis of microstrip circuits using three-dimensional full-wave electromagnetic field analysis in the time-domain," *IEEE Trans. Micro. Theo. Tech.*, vol. 36, no. 6, June 1988, pp. 1064–1070.
- [64] W.K. Gwarek, "Analysis of arbitrarily shaped two-dimensional microwave circuits by finite-difference time-domain method," *IEEE Trans. Micro. Theo. Tech.*, vol. 36, no. 4, April 1988, pp. 738–744.
- [65] X. Zhang, et al., "Calculation of the dispersive characteristics of microstrips by the time-domain finite-difference method," *IEEE Trans. Micro. Theo. Tech.*, vol. 36, no. 2, Feb. 1988, pp. 263–267.
- [66] X. Zhang and K.K. Mei, "Time-domain finite-difference approach to the calculation of the frequency-dependent characteristics of microstrip discontinuities," *IEEE Trans. Micro. Theo. Tech.*, vol. 36, no. 12, Dec. 1988, pp. 1775–1787.
- [67] R.W. Larson, "Special purpose computers for the time domain advance of Maxwell's equations," *IEEE Trans. Magnetics*, vol. 25, no. 4, July 1989, pp. 2913–2915.

- [68] K.K. Mei, et al., "Conformal time domain finite difference method," *Radio Sci.*, vol. 19, no. 5, Sept./Oct. 1984, pp. 1145–1147.
- [69] D.H. Choi and W.J.R. Hofer, "The finite-difference time-domain method and its application to eigenvalue problems," *IEEE Trans. Micro. Theo. Tech.*, vol. MTT-36, no. 12, Dec. 1986, pp. 1464–1470.
- [70] D.M. Sullivan, et al., "Use of the finite-difference time-domain method in calculating EM absorption in human tissues," *IEEE Trans. Biomed. Engr.*, vol. BME-34, no. 2, Feb. 1987, pp. 148–157.
- [71] A.D. Tinniswood, C.M. Furse, and O.P. Gandhi, "Computations of SAR distributions for two anatomically based models of the human head using CAD files of commercial telephone and the parallelized FDTD code," *IEEE Trans. Ant. Prog.*, vol. 46, no. 6, June 1998, pp. 829–833.
- [72] D. Dunn, C.M. Rappaport and A.J. Terzuoli, "FDTD verification of deep-set brain tumor hyperthermia using a spherical microwave source distribution," *IEEE Trans. Micro. Theo. Tech.*, vol. 44, no. 10, Oct. 1996, pp. 1769–1777.
- [73] V. Hombach et al., "The dependence of EM energy absorption upon human head modeling at 900 MHz," *IEEE Trans. Micro. Theo. Tech.*, vol. 44, no. 10, Oct. 1996, pp. 1865–1873.
- [74] O. Fujiwara and A. Kato, "Computation of SAR inside eyeball for 1.5-GHz microwave exposure using finite-difference time-domain technique," *IEICE Trans. Comm.*, vol. E77-B, no. 6, June 1994, pp. 732–737.
- [75] A. Christ and H.L. Hartnagel, "Three-dimensional finite-difference method for the analysis of microwave-device embedding," *IEEE Trans. Micro. Theo. Tech.*, vol. MTT-35, no. 8, Aug. 1987, pp. 688–696.
- [76] J.H. Whealton, "A 3D analysis of Maxwell's equations for cavities of arbitrary shape," *J. Comp. Phys.*, vol. 75, 1988, pp. 168–189.
- [77] R. Luebbers et al., "A frequency-dependence finite-difference time-domain formulation for dispersive materials," *IEEE Trans. EMC*, vol. 32, no. 3, Aug. 1990, pp. 222–227.
- [78] R. Holland, "Finite-difference time-domain (FDTD) analysis of magnetic diffusion," *IEEE Trans. EMC*, vol. 36, no. 1, Feb. 1994, pp. 32–39.
- [79] A. Taflove and K.R. Umashankar, "Review of FD-TD numerical modeling of electromagnetic wave scattering and radar cross section," *Proc. IEEE*, vol. 77, no. 5, May 1989, pp. 682–699.
- [80] V. Bommel, "Time-domain finite-difference analysis of electromagnetic scattering and penetration problems," *M. Sc. Thesis*, Dept. of Electrical and Computer Engr., Florida Atlantic University, Boca Raton, Dec. 1987.
- [81] D.S. Jones, *The Theory of Electromagnetism*. New York: MacMillan, 1964, pp. 450–452.

- [82] J.A. Stratton, *Electromagnetic Theory*. New York: McGraw-Hill, 1941, pp. 563–573.
- [83] G.A. Kriegsmann, A. Taflove, and K.R. Umashankar, “A new formulation of electromagnetic wave scattering using an on-surface radiation boundary condition approach,” *IEEE Trans. Ant. Prop.*, vol. 35, no. 2, Feb. 1987, pp. 153–161.
- [84] B. Zhiqiang et al., “A new finite-difference time-domain algorithm for solving Maxwell’s equation,” *IEEE Micro. Guided Wave Lett.*, vol. 1, no. 12, Dec. 1991, pp. 382–384.
- [85] S.X.R. Vahldieck and H. Jin, “Full-wave analysis of guided wave structures using a novel 2-D FDTD,” *IEEE Micro. Guided Wave Lett.*, vol. 2, no. 5, May 1992, pp. 165–167.
- [86] R. Mittra and P.H. Harms, “A new finite-difference time-domain (FDTD) algorithm for efficient field computation in resonator narrow-band structures,” *IEEE Micro. Guided Wave Lett.*, vol. 3, no. 9, Sept. 1993, pp. 336–318.
- [87] J.B. Cole, “A high accuracy realization of the Yee algorithm using non-standard finite differences,” *IEEE Trans. Micro. Theo. Tech.*, vol. 45, no. 6, June 1997, pp. 991–996.
- [88] J.B. Cole, “A high accuracy FDTD algorithm to solve microwave propagation and scattering problems on a coarse grid,” *IEEE Trans. Micro. Theo. Tech.*, vol. 43, no. 9, Sept. 1995, pp. 2053–2058.
- [89] U. Oguz, L. Gurel, and O. Arkan, “An efficient and accurate technique for the incident-wave excitations in the FDTD method,” *IEEE Trans. Micro. Theo. Tech.*, vol. 46, no. 6, June 1998, pp. 869–882.
- [90] I.J. Craddock and C.J. Railton, “A new technique for the stable incorporation of static field solutions in the FDTD method for the analysis of thin wires and narrow strips,” *IEEE Trans. Micro. Theo. Tech.*, vol. 46, no. 8, Aug. 1998, pp. 1091–1096.
- [91] J.B. Cole et al., “Finite-difference time-domain simulations of wave propagation and scattering as a research and educational tool,” *Computer in Physics*, vol. 9, no. 2, March/April 1995, pp. 235–239.
- [92] P.H. Harms, J.F. Lee, and R. Mittra, “A study of the nonorthogonal FDTD method versus the conventional FDTD technique for computing resonant frequency of cylindrical cavities,” *IEEE Trans. Micro. Theo. Tech.*, vol. 40, no. 4, April 1992, pp. 741–746.
- [93] Y. Chen, R. Mittra, and P. Harms, “Finite-difference time-domain algorithm for solving Maxwell’s equations in rotationally symmetric geometries,” *IEEE Trans. Micro. Theo. Tech.*, vol. 44, no. 6, June 1996, pp. 832–839.

- [94] C. Wang, B.Q. Gao, and C.P. Deng, "Q factor of a resonator by the finite difference time-domain method incorporating perturbation techniques," *Elect. Lett.*, vol. 29, no. 21, Oct. 1993, pp. 1866–1867.
- [95] G. Cerri et al., "MoM-FDTD hybrid technique for analysing scattering problems," *Elect. Lett.*, vol. 34, no. 5, March 1998, pp. 438–440.
- [96] A.R. Bretones, R. Mittra, and R.G. Martin, "A hybrid technique combining the method of moments in the time domain and FDTD," *IEEE Micro. Guided Wave Lett.*, vol. 8, no. 8, Aug. 1998, pp. 281–283.
- [97] C.J. Railton, E.M. Daniel, and J.P. McGeehan, "Use of second order absorbing boundary conditions for the termination of planar waveguides in the FDTD method," *Elect. Lett.*, vol. 29, no. 10, May 1993, pp. 900–902.
- [98] P.Y. Wang et al., "Higher order formulation of absorbing boundary conditions for finite-difference time-domain method," *Elect. Lett.*, vol. 29, no. 23, Nov. 1993, pp. 2018–2019.
- [99] J.C. Olivier, "On the synthesis of exact free space absorbing boundary conditions for the finite-difference time-domain method," *IEEE Trans. Ant. Prop.*, vol. 40, no. 4, April 1992, pp. 456–460.
- [100] D.S. Katz, E.T. Thiele, and A. Taflove, "Validation and extension to three dimensions of the Berenger PML absorbing boundary conditions for FD-TD meshes," *IEEE Micro. Guided Wave Lett.*, vol. 4, no. 6, Aug. 1994, pp. 268–270.
- [101] J.P. Berenger, "A perfectly matched layer for the absorption of electromagnetic waves," *Jour. Comp. Phys.*, vol. 114, Aug. 1994, pp. 185–200.
- [102] J.P. Berenger, "Perfectly matched layer for the FDTD solution of wave-structure interaction problems," *IEEE Trans. Ant. Prop.*, vol. 44, no. 1, Jan. 1996, pp. 110–117.
- [103] D.T. Prescott and N.V. Shuley, "Reflection analysis of FDTD boundary conditions – Part I: Time-space absorbing boundaries," *IEEE Trans. Micro. Theo. Tech.*, vol. 45, no. 8, Aug. 1997, pp. 1162–1170. For Part II, see the same issue, pp. 1171–1178.
- [104] A. Taflove, *Computational Electrodynamics: The Finite-Difference Time-Domain Method*. Boston, MA: Artech House, 1995, pp. 145–202.
- [105] K.S. Kunz and R.J. Luebbers, *The Finite-Difference Time-Domain Method for Electromagnetic*. Boca Raton, FL: CRC Press, 1993, pp. 347–358.
- [106] A. Taflove and K.R. Umashankar, "The finite-difference time-domain method for numerical modeling of electromagnetic wave interactions with arbitrary structures," in M.A. Morgan (ed.), *Finite Element and Difference Methods in Electromagnetic Scattering*. New York: Elsevier, 1990, pp. 287–373.

- [107] K.K. Mei and J. Fang, "Superabsorption — a method to improve absorbing boundary conditions," *IEEE Trans. Ant. Prop.*, vol. 40, no. 9, Sept. 1992, pp. 1001–1010.
- [108] M. DiStasio and W.C. McHarris, "Electrostatic problems? Relax!," *Am. J. Phys.*, vol. 47, no. 5, May 1979, pp. 440–444.
- [109] M.N.O. Sadiku, "Finite difference solution of axisymmetric potential problems," *Int. J. Appl. Engr. Educ.*, vol. 6, no. 4, 1990, pp. 479–485.
- [110] H.E. Green, "The numerical solution of transmission line problems," in L. Young (ed.), *Advances in Microwaves*, vol. 2. New York: Academic Press, 1967, pp. 327–393.
- [111] C.D. Taylor, et al., "Electromagnetic pulse scattering in time varying inhomogeneous media," *IEEE Trans. Ant. Prop.*, vol. AP-17, no. 5, Sept. 1969, pp. 585–589.
- [112] P.J. Davis and P. Rabinowitz, *Methods of Numerical Integration*. New York: Academic Press, 1975.
- [113] R. Piessens, et al., *QUADPACK: A Subroutine Package for Automatic Integration*. Berlin: Springer-Verlag, 1980.
- [114] *Tables of Functions and Zeros of Functions*. Washington, DC: National Bureau of Standards, Applied Mathematical Series, no. 37, 1954.
- [115] M. Abramowitz and I.A. Stegun (eds.), *Handbook of Mathematical Functions*. Washington, DC: National Bureau of Standards, Applied Mathematical Series, no. 55, 1964.
- [116] L.G. Kelly, *Handbook of Numerical Methods and Applications*. Reading, MA: Addison-Wesley, 1967, pp. 57–61.
- [117] M.N.O. Sadiku and R. Jongakiem, "Newton-Cotes rules for triple integrals," *Proc. IEEE Southeastcon*, April 1990, pp. 471–475.
- [118] B.P. Rynne, "Instabilities in time marching methods for scattering problems," *Electromagnetics*, vol. 6, no. 2, 1986, pp. 129–144.
- [119] J.I. Steger and R.F. Warming, "On the convergence of certain finite-difference schemes by an inverse-matrix method," *J. Comp. Phys.*, vol. 17, 1975, pp. 103–121.
- [120] D.W. Kelly, et al., "A posteriori error estimates in finite difference techniques," *J. Comp. Phys.*, vol. 74, 1988, pp. 214–232.

Problems

3.1 Show that the following finite difference approximations for Φ_x are valid:

(a) forward difference,

$$\frac{-\Phi_{i+2} + 4\Phi_{i+1} - 3\Phi_i}{2\Delta x}$$

(b) backward difference,

$$\frac{3\Phi_i - 4\Phi_{i-1} + \Phi_{i-2}}{2\Delta x}$$

(c) central difference

$$\frac{-\Phi_{i+2} + 8\Phi_{i+1} - 8\Phi_{i-1} + \Phi_{i-2}}{12\Delta x}$$

3.2 Solve the equation $\Phi_t = \Phi_{xx}$, $0 \leq x \leq 1$, subject to initial and boundary conditions

$$\begin{aligned}\Phi(x, 0) &= \sin \pi x, \quad 0 \leq x \leq 1, \\ \Phi(0, t) &= 0 = \Phi(1, t) \quad t > 0\end{aligned}$$

Obtain the solution by hand calculation and use $\Delta x = 0.25$ and $r = 0.5$.

3.3 Derive the Crank-Nicholson implicit algorithm for the hyperbolic equation $\Phi_{xx} = a^2\Phi_{yy}$, $a^2 = \text{constant}$. Let $\Delta x = \Delta y = \Delta$.

3.4 Given a boundary-value problem defined by

$$\frac{d^2\Phi}{dx^2} = x + 1, \quad 0 < x < 1$$

subject to $\Phi(0) = 0$ and $\Phi(1) = 1$, use the finite difference method to find $\Phi(0.5)$. You may take $\Delta = 0.25$ and perform 5 iterations. Compare your result with the exact solution.

3.5 Prove that the fourth-order approximation of Laplace's equation $\Phi_{xx} + \Phi_{yy} = 0$ is

$$\begin{aligned}60\Phi(i, j) - 16[\Phi(i + 1, j) + \Phi(i - 1, j) + \Phi(i, j + 1) + \Phi(i, j - 1)] \\ + \Phi(i + 2, j) + \Phi(i - 2, j) + \Phi(i, j + 2) + \Phi(i, j - 2) = 0\end{aligned}$$

Draw the computational molecule for the finite difference scheme.

- 3.6 (a) If $\Delta x \neq \Delta y$, show that for the computational molecule in Fig. 3.48 (a), Eq. (3.49) becomes

$$V_o = \frac{V_1}{2(1 + \alpha)} + \frac{V_2}{2(1 + \alpha)} + \frac{V_3}{2(1 + 1/\alpha)} + \frac{V_4}{2(1 + 1/\alpha)}$$

where $\alpha = (\Delta x/\Delta y)^2$.

- (b) Show that for the molecule in Fig. 3.48 (b), Eq. (3.49) becomes

$$\begin{aligned} V_o = & \frac{V_1}{(1 + \Delta x_1/\Delta x_2)(1 + \Delta x_1 \Delta x_2/\Delta y_3 \Delta y_4)} \\ & + \frac{V_2}{(1 + \Delta x_2/\Delta x_1)(1 + \Delta x_1 \Delta x_2/\Delta y_3 \Delta y_4)} \\ & + \frac{V_3}{(1 + \Delta y_3/\Delta y_4)(1 + \Delta y_3 \Delta y_4/\Delta x_1 \Delta x_2)} \\ & + \frac{V_4}{(1 + \Delta y_4/\Delta y_3)(1 + \Delta y_3 \Delta y_4/\Delta x_1 \Delta x_2)} \end{aligned}$$

The molecule in Fig. 3.48 (b) is useful in treating irregular boundaries.

- (c) For the nine-point molecule in Fig. 3.48 (c), show that

$$V_o = \frac{1}{8} \sum_{i=1}^8 V_i$$

This is a more accurate difference equation than Eq. (3.49).

- 3.7 For a long hollow conductor with a uniform U-shape cross-section shown in Fig. 3.49, find the potential at points A, B, C, D, and E.
- 3.8 It is desired to solve

$$\frac{\partial^2 \Phi}{\partial x^2} + \frac{\partial^2 \Phi}{\partial y^2} + 50 = 0$$

in the square region $0 \leq x, y \leq 1$ subject to the boundary conditions $\Phi = 10$ at $x = 0, 1$, $\Phi_y = 40$ at $y = 0$, $\Phi_y = -20$ at $y = 1$.

- (a) Set up a system of finite difference equations which will allow the solution to be found at $x = y = 0.25$ using $\Delta x = \Delta y = h = 0.25$. Perform three iterations.
- (b) Develop a program to solve the same problem using $h = 0.05, 0.1$, and 0.2 .
- 3.9 Modify the FORTRAN code of Fig. 3.12 to solve the following three-dimensional problem:

$$\nabla^2 V = -\rho_v/\epsilon, \quad 0 \leq x, y, z \leq 1 \text{ meter},$$

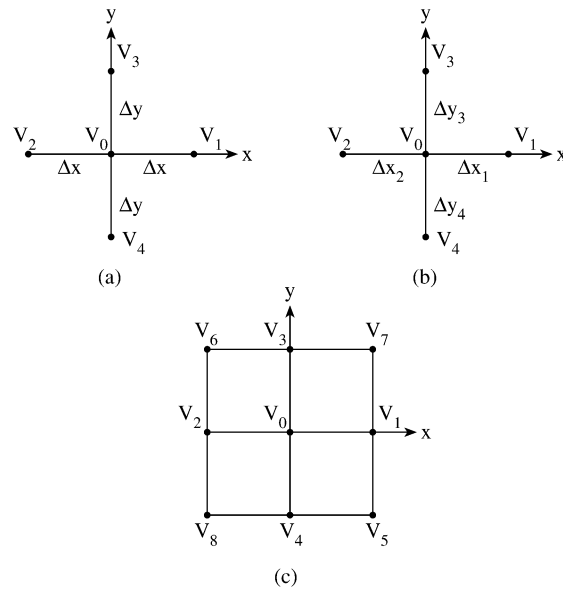


Figure 3.48
For Problem 3.6.

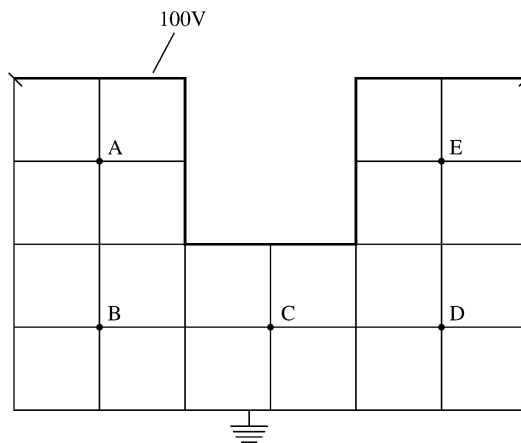


Figure 3.49
For Problem 3.7.

where $\rho_v = xyz^2 nC/m^2$ and $\epsilon = 2\epsilon_o$ subject to the boundary conditions

$$\begin{aligned} V(0, y, z) = 0 &= V(1, y, z) \\ V(x, 0, z) = 0 &= V(x, 1, z) \\ V(x, y, 0) = 0, & V(x, y, 1) = V_o \end{aligned}$$

Find the potential at the center of the cube and compare your result with the analytic solution. Take $V_o = 100$ volts.

3.10 Show that the leapfrog method applied to the parabolic equation (3.10) is unstable, whereas applying the DuFort-Frankel scheme yields an unconditionally stable solution.

3.11 The advective equation

$$\frac{\partial \Phi}{\partial t} + u \frac{\partial \Phi}{\partial x} = 0, \quad u > 0$$

can be discretized as

$$\Phi_i^{n+1} = \Phi_i^n - r(\Phi_{i+1}^n - \Phi_{i-1}^n),$$

where $r = u\Delta t/2\Delta x$. Show that the difference scheme is unstable. An alternative scheme is:

$$\Phi_{n+1} = \frac{1}{2}(\Phi_{i+1}^n + \Phi_{i-1}^n) - r(\Phi_{i+1}^n - \Phi_{i-1}^n)$$

Find the condition on r for which this scheme is stable.

3.12 The two-dimensional parabolic equation

$$\frac{\partial U}{\partial t} = \frac{\partial^2 U}{\partial x^2} + \frac{\partial^2 U}{\partial y^2}, \quad 0 \leq x, y \leq 1, \quad 1 > 0$$

is approximated by the finite difference methods:

$$(i) U_{i,j}^{n+1} = [1 + r(\delta_x^2 + \delta_y^2)]U_{i,j}^n$$

$$(ii) U_{i,j}^{n+1} = (1 + r\delta_x^2)(1 + r\delta_y^2)U_{i,j}^n \quad \text{where } r = \Delta t/h^2, h = \Delta x = \Delta y \text{ and}$$

$$\delta_x^2 U_{i,j}^n = U_{i-1,j}^n - 2U_{i,j}^n + U_{i+1,j}^n$$

$$\delta_y^2 U_{i,j}^n = U_{i,j-1}^n - 2U_{i,j}^n + U_{i,j+1}^n$$

Show that (i) is stable for $r \leq 1/4$ and (ii) is stable for $r \leq 1/2$

3.13 (a) The constitutive parameters of the earth allow the displacement currents to be negligibly small. In this type of medium, show that Maxwell's equations for two-dimensional TM mode, where

$$\mathbf{E}(x, y, t) = E_z \mathbf{a}_z$$

and

$$\mathbf{H}(x, y, t) = H_x \mathbf{a}_x + H_y \mathbf{a}_y,$$

reduce to the diffusion equation

$$\frac{\partial^2 E}{\partial x^2} + \frac{\partial^2 E}{\partial y^2} - \mu\sigma \frac{\partial E}{\partial t} = \mu \frac{\partial J_s}{\partial t}$$

where $E = E_z$ and J_s is the source current density in the z direction.

- (b) Taking $J_s = 0$, $\Delta x = \Delta y = \Delta$ and

$$\sum E_{i,j} = E_{i+1,j}^n + E_{i-1,j}^n + E_{i,j+1}^n + E_{i,j-1}^n,$$

show that applying Euler, leapfrog, and DuFort-Frankel difference methods to the diffusion equation gives:

Euler:

$$E_{i,j}^{n+1} = (1 - 4r)E_{i,j}^n + r \sum E_{i,j}^n,$$

Leapfrog:

$$E_{i,j}^{n+1} = E_{i,j}^{n-1} + 2r \left(\sum E_{i,j}^n - 4E_{i,j}^n \right),$$

DuFort-Frankel:

$$E_{i,j}^{n+1} = \frac{1 - 4r}{1 + 4r} E_{i,j}^{n-1} + \frac{2r}{1 + 4r} \sum E_{i,j}^n$$

where $r = \Delta t / (\sigma \mu \Delta^2)$.

- (c) Analyze the stability of these finite difference schemes by substituting for $E_{i,j}^n$ a Fourier mode of the form

$$E_{i,j}^n = E(x = i\Delta, y = j\Delta, t = n\Delta t) = A_n \cos(k_x i \Delta) \cos(k_y j \Delta)$$

3.14 Yee's FD-TD algorithm for one-dimensional wave problems is given by

$$H_y^{n+1/2}(k + 1/2) = H_y^{n-1/2}(k + 1/2) + \frac{\delta t}{\mu \delta} [E_x^n(k) - E_x^n(k + 1)]$$

Determine the stability criterion for the scheme by letting

$$E_x^n(k) = A^n e^{j\beta k \delta}, \quad H_y^n(k) = \frac{A^n}{\eta} e^{j\beta k \delta},$$

where $\eta = (\mu/\epsilon)^{1/2}$ is the intrinsic impedance of the medium.

- 3.15 (a) The potential system in Fig. 3.50 (a) is symmetric about the y -axis. Set the initial values at free nodes equal to zero and calculate (by hand) the potential at nodes 1 to 5 for 5 or more iterations.

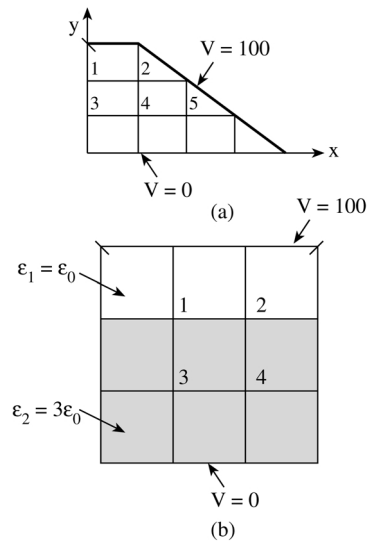


Figure 3.50
For Problem 3.15.

- (b) Consider the square mesh in Fig. 3.50(b). By setting initial values at the free nodes equal to zero, find (by hand calculation) the potential at nodes 1 to 4 for 5 or more iterations.
- 3.16 The potential system shown in Fig. 3.51 is a quarter section of a transmission line. Using hand calculation, find the potential at nodes 1, 2, 3, 4, and 5 after 5 iterations.

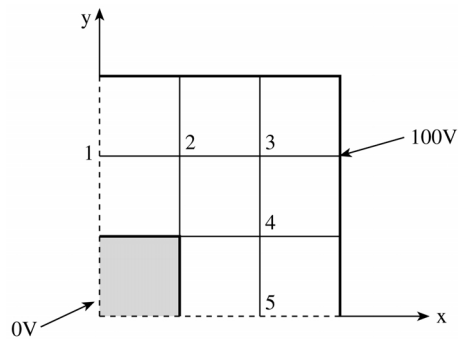


Figure 3.51
For Problem 3.16.

- 3.17 A transformer has its primary and secondary windings maintained at 100 and 0 V, respectively, as shown in Fig. 3.52. Assuming a square mesh of $h = 0.2$ cm,

determine the potential distribution between the windings. Find its value at (8 cm, 4 cm).

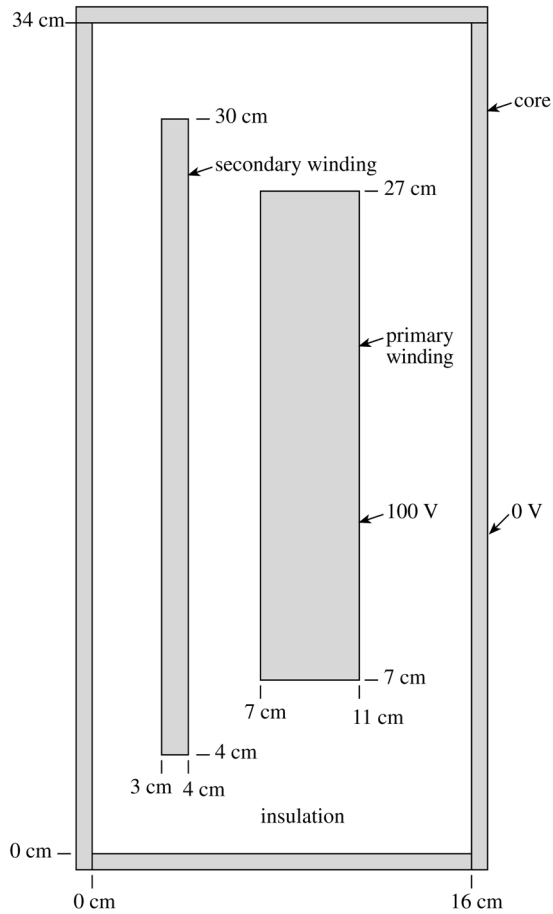


Figure 3.52

For Problem 3.17.

- 3.18 Modify the program in Fig. 3.21 or write your own program to calculate Z_o for the microstrip line shown in Fig. 3.53. Take $a = 2.02$, $b = 7.0$, $h = 1.0 = w$, $t = 0.01$, $\epsilon_1 = \epsilon_0$, $\epsilon_2 = 9.6\epsilon_0$.
- 3.19 Use the FDM to calculate the characteristic impedance of the high-frequency, air-filled rectangular transmission line shown in Fig. 3.54. Take advantage of the symmetry of the problem and consider cases for which:
- $B/A = 1.0$, $a/A = 1/3$, $b/B = 1/3$, $a = 1$,
 - $B/A = 1/2$, $a/A = 1/3$, $b/B = 1/3$, $a = 1$.

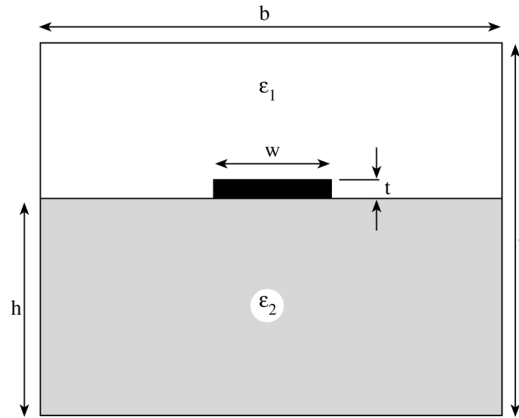


Figure 3.53
For Problem 3.18.

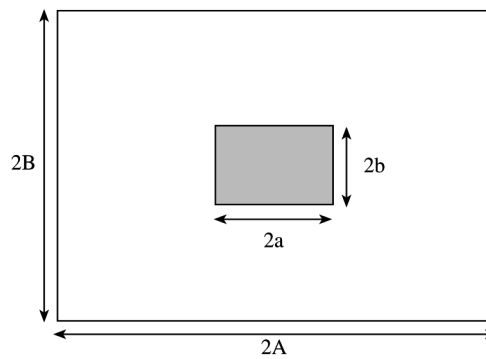


Figure 3.54
For Problem 3.19.

3.20 [Figure 3.55](#) shows a shield microstrip line. Write a program to calculate the potential distribution within the cross-section of the line. Take $\epsilon_1 = \epsilon_o$, $\epsilon_2 = 3.5\epsilon_o$ and $h = 0.5$ mm. Find the potential at the middle of the conducting plates.

3.21 Use the FDM to determine the lowest (or dominant) cut-off wave-number k_c of the TM_{11} mode in waveguides with square ($a \times a$) and rectangular ($a \times b$, $b = 2a$) crosssections. Compare your results with the exact solution

$$k_c = \sqrt{(m\pi/a)^2 + (n\pi/a)^2}$$

where $m = n = 1$. Take $a = 1$.

3.22 Instead of the 5-point scheme of Eq. (3.115), use a more accurate 5-point

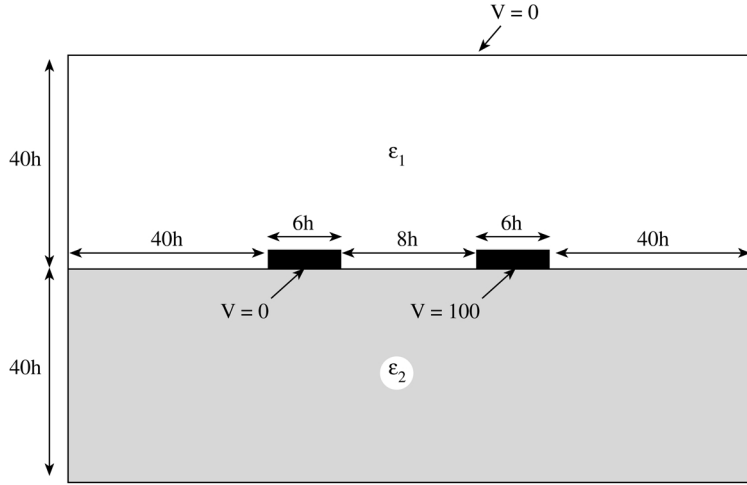


Figure 3.55
For Problem 3.20.

formula

$$\begin{aligned}
 2i(8i^2 - 5)V(i, j) &= (4i^3 + 2i^2 - 4i + 1)V(i + 1, j) \\
 &\quad + (4i^3 - 2i^2 - 4i - 1)V(i - 1, j) \\
 &\quad + i(4i^2 - 1)V(i, j + 1) + i(4i^2 - 1)V(i, j - 1)
 \end{aligned}$$

in Example 3.9 while other things remain the same.

3.23 For two-dimensional problems in which the field components do not vary with z coordinate ($\partial/\partial z = 0$), show that Yee's algorithm of Eqs. (3.84a)–(3.84f) becomes:

(a) for TE waves ($E_z = 0$)

$$\begin{aligned}
 H_z^{n+1/2}(i + 1/2, j + 1/2) &= H_z^{n-1/2}(i + 1/2, j + 1/2) \\
 &\quad - \alpha \left[E_y^n(i + 1, j + 1/2) - E_y^n(i, j + 1/2) \right] \\
 &\quad + \alpha \left[E_x^n(i + 1/2, j + 1) - E_x^n(i + 1/2, j) \right], \\
 E_x^{n+1}(i + 1/2, j) &= E_x^n(i + 1/2, j) + \beta \left[H_z^{n+1/2}(i + 1/2, j + 1/2) \right. \\
 &\quad \left. - H_z^{n+1/2}(i + 1/2, j - 1/2) \right], \\
 E_z^{n+1}(i, j + 1/2) &= \gamma E_y^n(i, j + 1/2) - \beta \left[H_z^{n+1/2}(i + 1/2, j + 1/2) \right. \\
 &\quad \left. - H_z^{n+1/2}(i - 1/2, j + 1/2) \right];
 \end{aligned}$$

(b) for TM waves ($H_z = 0$)

$$E_z^{n+1}(i, j) = \gamma E_z^n(i, j) + \beta \left[H_y^{n+1/2}(i + 1/2, j) - H_y^{n+1/2}(i - 1/2, j) \right] - \beta \left[H_x^{n+1/2}(i, j + 1/2) - H_x^{n+1/2}(i, j - 1/2) \right],$$

$$H_x^{n+1/2}(i, j + 1/2) = H_x^{n-1/2}(i, j + 1/2) - \alpha \left[E_z^n(i, j + 1) - E_z^n(i, j) \right],$$

$$H_y^{n+1/2}(i + 1/2, j) = H_y^{n-1/2}(i + 1/2, j) + \alpha \left[E_z^n(i + 1, j) - E_z^n(i, j) \right],$$

where

$$\alpha = \frac{\delta t}{\mu \delta}, \quad \beta = \frac{\delta t}{\epsilon \delta}, \quad \gamma = 1 - \frac{\sigma \delta t}{\epsilon},$$

and $\delta = \Delta x = \Delta y$.

3.24 Consider the diffraction/scattering of an incident TM wave by a perfectly conducting square of side $4a$. The conducting obstacle occupies $17 < i < 49$, $33 < j < 65$, while artificial boundaries are placed at $i = 1, 81$, $j = 0.5, 97.5$ as shown in Fig. 3.56. Assume an incident wave with only E_z and H_y components given by

$$E_z = \begin{cases} \sin \pi \theta, & 0 < \theta < 1 \\ 0, & \text{otherwise} \end{cases}$$

$$H_y = \frac{1}{\eta_o} E_z$$

where $\eta_o = 120\pi\Omega$, $\theta = \frac{(x-50a+ct)}{8a}$, $\Delta x = \Delta y = a/8$, $\Delta t = c\Delta x = a/16$. Write a program that applies the algorithm in Problem 3.23 (b). Assume “hard lattice truncation conditions” at the artificial boundaries shown in Fig. 3.56 and reproduce Yee’s result [42] in his figure 3.

3.25 Repeat the previous problem but assume “soft lattice truncation conditions” of Eqs. (3.87) to (3.89a)–(3.89l) at the artificial boundaries.

3.26 In cylindrical coordinates with the vector magnetic potential $\mathbf{A} = A_z(\rho, \phi)\mathbf{a}_z$, Laplace’s equation is

$$\nabla^2 A_z = -\mu J_z$$

Obtain the finite difference equivalent.

3.27 Consider the finite cylindrical conductor held at $V = 100$ volts and enclosed in a larger grounded cylinder as in Fig. 3.57. Such a deceptively simple

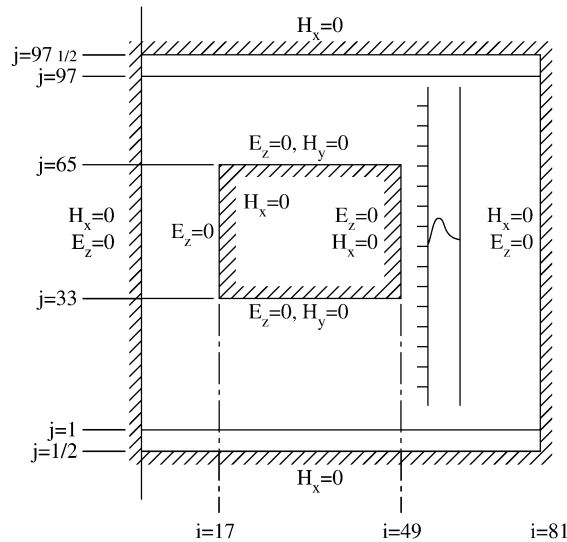


Figure 3.56
For Problem 3.24.

looking problem is beyond closed form solution, but by employing finite difference techniques, the problem can be solved without much effort. Using the finite difference method, write a program that determines the potential distribution in the axisymmetric solution region. Output the potential at $(\rho, z) = (2, 10), (5, 10), (8, 10), (5, 2),$ and $(5, 18)$.

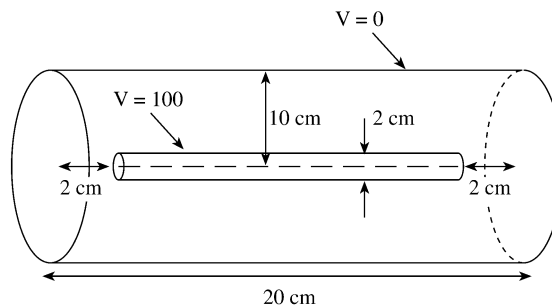


Figure 3.57
For Problem 3.27.

3.28 The problem in Fig. 3.58 is a prototype of an electrostatic particle focusing system which is employed in a recoil-mass time-of-flight spectrometer. Write a program to determine the potential distribution in the system. The problem is similar to the previous problem except that the outer conductor

abruptly expands radius by a factor of 2. Output the potential at $(\rho, z) = (5, 18), (5, 10), (5, 2), (10, 2),$ and $(15, 2)$.

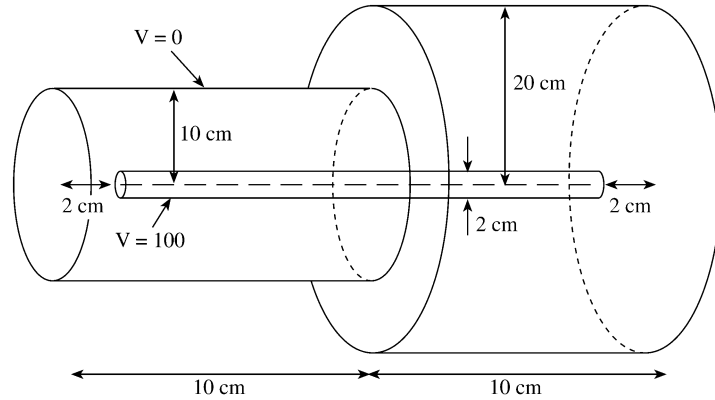


Figure 3.58
For Problem 3.28.

3.29 For axisymmetric problems (no variation with respect to ϕ), show that Yee's algorithm for TM waves can be written as

$$H_{\phi}^{n+1}(i, j) = H_{\phi}^n(i, j) + \alpha \left[E_z^{n+1/2}(i, j + 1/2) - E_z^{n+1/2}(i, j - 1/2) \right] - \alpha \left[E_{\rho}^{n+1/2}(i + 1/2, j) - E_{\rho}^{n+1/2}(i - 1/2, j) \right]$$

$$E_z^{n+3/2}(i, j + 1/2) = \gamma E_z^{n+1/2}(i, j + 1/2) + \beta \left[\frac{1}{j} H_{\phi}^{n+1}(i, j + 1/2) + H_{\phi}^{n+1}(i, j + 1) - H_{\phi}^{n+1}(i, j) \right],$$

$$E_{\rho}^{n+3/2}(i + 1/2, j) = \gamma E_{\rho}^{n+1/2}(i + 1/2, j) - \beta \left[H_{\phi}^{n+1}(i + 1, j) - H_{\phi}^{n+1}(i, j) \right],$$

where

$$\alpha = \frac{\delta t}{\mu \delta}, \quad \beta = \frac{\delta t}{\epsilon \delta}, \quad \gamma = 1 - \frac{\sigma \delta t}{\epsilon}, \quad \delta = \Delta \rho = \Delta z,$$

and $H_{\phi}(z, \rho, t) = H_{\phi}(z = i \Delta z, \rho = (j - 1/2) \Delta \rho, t = n \delta t) = H_{\phi}^n(i, j)$.

3.30 (a) Show that the finite difference discretization of Mur's ABC for two-dimensional problem

$$\frac{\partial E_z}{\partial x} - \frac{1}{c_o} \frac{\partial E_z}{\partial t} - \frac{c_o \mu_o}{2} \frac{\partial H_x}{\partial y} = 0$$

at the boundary $x = 0$ is

$$\begin{aligned} E_z^{n+1}(0, j) = & E_z^n(i, j) + \frac{c_o \delta t - \delta}{c_o \delta t + \delta} \left[E_z^{n+1}(i, j) - E_z^n(0, j) \right] \\ & - \frac{\mu_o c_o}{2(c_o \delta t + \delta)} \left[H_x^{n+1/2}(0, j + 1/2) - H_x^{n+1/2}(0, j - 1/2) \right. \\ & \left. + H_x^{n+1/2}(1, j + 1/2) - H_x^{n+1/2}(1, j - 1/2) \right] \end{aligned}$$

where c_o is the velocity of wave propagation.

- (b) Discretize the first-order boundary condition

$$\frac{\partial E_z}{\partial x} - \frac{1}{c_o} \frac{\partial E_z}{\partial t} = 0$$

at $x = 0$.

- 3.31 For a three-dimensional problem, the PML modification of Maxwell's equations yields 12 equations because all the six Cartesian field components split. Obtain the 12 resulting equations.

- 3.32 (a) In a PML region, E_z is split into E_{zx} and E_{zy} for the TM case. Show that Maxwell's equation becomes

$$\begin{aligned} \epsilon_o \frac{\partial E_{zx}}{\partial t} + \sigma_x E_{zx} &= \frac{\partial H_y}{\partial x} \\ \epsilon_o \frac{\partial E_{zy}}{\partial t} + \sigma_y E_{zy} &= -\frac{\partial H_x}{\partial y} \\ \mu_o \frac{\partial H_x}{\partial t} + \sigma_y^* H_x &= -\frac{\partial}{\partial y} (E_{zx} + E_{zy}) \\ \mu_o \frac{\partial H_y}{\partial t} + \sigma_x^* H_y &= \frac{\partial}{\partial x} (E_{zx} + E_{zy}) \end{aligned}$$

- 3.33 An FDTD equation for a PML region is given by

$$\begin{aligned} H_z^{n+1/2}(i + 1/2, k) = & H_z^{n-1/2}(i + 1/2, k) \\ & - \frac{\delta t}{\mu \delta} \left[E_{yx}^n(i + 1, k) + E_{yz}^n(i + 1, k) - E_{yx}(i, k) - E_{yz}^n(i, k) \right] \end{aligned}$$

where δ , δt , n , i , and k have their usual FDTD meanings. By substituting the harmonic dependence $e^{j\omega t} e^{-jk_z z}$, show that the impedance of the PML region is

$$Z_z = \frac{E_y}{H_z} = \frac{\mu_o \delta \sin(\omega \delta t / 2)}{\delta t \sin(k_o \delta / 2)}$$

- 3.34 The conventional 3-D FDTD lattice in cylindrical coordinates is shown in Fig. 3.59 (a) while its projection on the $\rho - z$ plane is in Fig. 3.59 (b). Show that by discretizing Maxwell's equation,

$$E_{\rho}^{n+1}(i, j) = \frac{(1 - \frac{\sigma\delta}{2\epsilon})}{(1 + \frac{\sigma\delta}{2\epsilon})} E_{\rho}^n(i, j) - \frac{\delta t}{\epsilon\delta} \frac{1}{(1 + \frac{\sigma\delta}{2\epsilon})} \cdot [H_{\phi}^{n+1/2}(i, j) - H_{\phi}^{n+1/2}(i, j - 1)]$$

where $\delta = \Delta z = \Delta\rho$. Obtain the FDTD equations for H_{ρ} and H_{ϕ} .

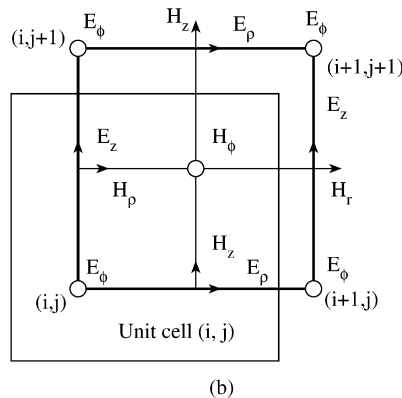
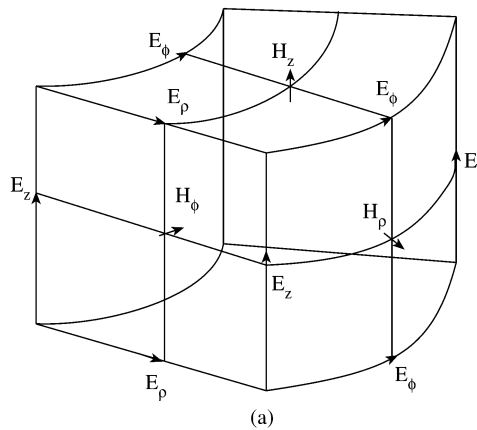


Figure 3.59

For Problem 3.34: (a) A conventional 3-D FDTD lattice in cylindrical coordinates, (b) projection of 3-D FDTD cell at $\rho - z$ plane.

- 3.35 Given the tabulated values of $y = \sin x$ for $x = 0.4$ to 0.52 radians in intervals of $\Delta x = 0.02$, find: (a) $\frac{dy}{dx}$ at $x = 0.44$, (b) $\int_{0.4}^{0.52} y dx$ using Simpson's rule.

x	$\sin x$
0.40	0.38942
0.42	0.40776
0.44	0.42594
0.46	0.44395
0.48	0.46178
0.50	0.47943
0.52	0.49688

- 3.36 (a) Use a pocket calculator to determine the approximate area under the curve $f(x) = 4 - x^2$, $0 < x < 1$ by the trapezoidal rule with $h = 0.2$.
- (b) Repeat part (a) using the Newton-Cotes rule with $n = 3$.
- 3.37 For a half-wave dipole, evaluating the integral

$$\int_0^{1/2} \frac{\cos^2(\frac{\pi}{2} \cos \theta)}{\sin \theta} d\theta$$

is usually required. Evaluate this integral numerically using any quadrature rule of your choice.

- 3.38 Compute

$$\int_0^1 e^{-x} dx$$

using the Newton-Cotes rule for cases $n = 2, 4$, and 6 . Compare your results with exact values.

- 3.39 Evaluate

$$\int_0^{2\pi} x \cos 10x \sin 20x dx$$

- (a) using the trapezoidal rule with $\Delta x = \pi/10$
- (b) using Simpson's $\frac{1}{3}$ -rule with $\Delta x = \pi/10$
- (c) using Gaussian quadrature.

- 3.40 The criterion for accuracy of the numerical approximation of an integral

$$I = \int_a^b f(x) dx \simeq \sum_{i=0}^{\infty} a_i f(x_i)$$

is that the formula is exact for all polynomials of degree less than or equal to n . If $a = 0$, $b = 4$, and the values of $f(x)$ are available at points $x_0 = 0$, $x_1 = 1$, $x_2 = 3$, $x_4 = 4$, find the values of the coefficients a_i for which the above requirement of accuracy is met.

3.41 The elliptic integral of the first type

$$F(k, \phi) = \int_0^{\phi} (1 - k^2 \sin^2 \theta)^{-1/2} d\theta$$

cannot be evaluated in a closed form. Write a program using Simpson's rule to determine $F(k, \phi)$ for $k = 0.5$ and $\phi = \pi/2$.

3.42 The following integral represents radiation from a circular aperture antenna with a constant current amplitude and phase distribution

$$I = \int_0^1 \int_0^{2\pi} e^{j\alpha\rho \cos\phi} \rho d\phi d\rho$$

Find I numerically for $\alpha = 5$ and compare your result with the exact result

$$I(\alpha) = \frac{2\pi J_1(\alpha)}{\alpha}$$

3.43 Evaluate the following double integral using the trapezoidal rule:

(a) $\int_0^{\pi/2} \int_0^{\pi/2} \sin(\sqrt{2xy}) dx dy,$

(b) $\int_1^5 \int_1^5 [x^2 + y^2]^{-1/2} dx dy,$

(c) $\int_2^4 \left[\int_4^6 \ln(xy^2) dx \right] dy$